

9-12-2014

# FUNCTIONAL NETWORK CONNECTIVITY IN HUMAN BRAIN AND ITS APPLICATIONS IN AUTOMATIC DIAGNOSIS OF BRAIN DISORDERS

Mohammad Arbabshirani

Follow this and additional works at: [https://digitalrepository.unm.edu/ece\\_etds](https://digitalrepository.unm.edu/ece_etds)

---

## Recommended Citation

Arbabshirani, Mohammad. "FUNCTIONAL NETWORK CONNECTIVITY IN HUMAN BRAIN AND ITS APPLICATIONS IN AUTOMATIC DIAGNOSIS OF BRAIN DISORDERS." (2014). [https://digitalrepository.unm.edu/ece\\_etds/18](https://digitalrepository.unm.edu/ece_etds/18)

This Dissertation is brought to you for free and open access by the Engineering ETDs at UNM Digital Repository. It has been accepted for inclusion in Electrical and Computer Engineering ETDs by an authorized administrator of UNM Digital Repository. For more information, please contact [disc@unm.edu](mailto:disc@unm.edu).

Mohammad Reza Arbabshirani

*Candidate*

---

Electrical and Computer Engineering

*Department*

---

This dissertation is approved, and it is acceptable in quality and form for publication:

*Approved by the Dissertation Committee:*

Vince D. Calhoun , Chairperson

---

Thomas P. Caudell

---

Erik B. Erhardt

---

Marios S. Pattichis

---

---

---

---

---

---

---

---

**FUNCTIONAL NETWORK CONNECTIVITY IN  
HUMAN BRAIN AND ITS APPLICATIONS IN  
AUTOMATIC DIAGNOSIS OF BRAIN DISORDERS**

**by**

**MOHAMMAD REZA ARBABSHIRANI**

B.S, Electrical Engineering, Isfahan University of technology, 2005

M.S., Electrical Engineering, Yazd University, 2008

M. S., Statistics, University of New Mexico, 2013

**DISSERTATION**

Submitted in Partial Fulfillment of the  
Requirements for the Degree of

**Doctor of Philosophy  
Engineering**

The University of New Mexico  
Albuquerque, New Mexico

**July, 2014**

## **DEDICATION**

To my parents for their unforgettable sacrifice and devotion

and

To my wife, Nassim, for her great support and inspiring encouragement

## **ACKNOWLEDGEMENTS**

I would like to thank all the wonderful colleagues at Mind Research network especially those in the Medical Image Analysis Laboratory (MIALab). Working and collaborating with all of them has been remarkable for me. Special thanks to Kent Kiehl and his group, Elena Allen, Sergey Plis and Eswar Damaraju for their contribution to this work. Also, I would like to thank all outside collaborators who contributed to the studies presented in this dissertation: Godfrey Pearlson from Yale University, Tülay Adalı and her group from University of Maryland Baltimore County and Martin Havlicek from Maastricht University in Netherland.

**FUNCTIONAL NETWORK CONNECTIVITY IN HUMAN BRAIN AND ITS  
APPLICATIONS IN AUTOMATIC DIAGNOSIS OF BRAIN DISORDERS**

by

**Mohammad Reza Arbabshirani**

**B.S., Electrical Engineering, Isfahan University of technology, 2005**

**M.S., Electrical Engineering, Yazd University, 2008**

**M. S., Statistics, University of New Mexico, 2013**

**PhD, Engineering, University of New Mexico, 2014**

**ABSTRACT**

The human brain is one of the most complex systems known to the mankind. Over the past 3500 years, mankind has constantly investigated this remarkable system in order to understand its structure and function. Emerging of neuroimaging techniques such as functional magnetic resonance imaging (fMRI) have opened a non-invasive in-vivo window into brain function. Moreover, fMRI has made it possible to study brain disorders such as schizophrenia from a different angle unknown to researchers before. Human brain function can be divided into two categories: functional segregation and integration. It is well-understood that each region in the brain is specialized in certain cognitive or motor tasks. The information processed in these specialized regions in different temporal and spatial scales must be integrated in order to form a unified cognition or behavior.

One way to assess functional integration is by measuring functional connectivity (FC) among specialized regions in the brain. Recently, there is growing interest in studying the FC among brain functional networks. This type of connectivity, which can

be considered as a higher level of FC, is termed functional network connectivity (FNC) and measures the statistical dependencies among brain functional networks. Each functional network may consist of multiple remote brain regions.

Four studies related to FNC are presented in this work. First FNC is compared during the resting-state and auditory oddball task (AOD). Most previous FNC studies have been focused on either resting-state or task-based data but have not directly compared these two. Secondly we propose an automatic diagnosis framework based on resting-state FNC features for mental disorders such as schizophrenia. Then, we investigate the proper preprocessing for fMRI time-series in order to conduct FNC studies. Specifically the impact of autocorrelated time-series on FNC will be comprehensively assessed in theory, simulation and real fMRI data. At the end, the notion of autoconnectivity as a new perspective on human brain functionality will be proposed. It will be shown that autoconnectivity is cognitive-state and mental-state dependent and we discuss how this source of information, previously believed to originate from physical and physiological noise, can be used to discriminate schizophrenia patients with high accuracy.

# Table of Contents

Chapter 1: Introduction.....	1
1.1 Human Brain .....	2
1.2 Functional Segregation and Integration .....	2
1.3 Functional Neuroimaging.....	3
1.4 fMRI Experiment .....	6
1.5 Functional Connectivity .....	8
1.6 Functional Network Connectivity .....	10
1.7 Independent Component Analysis .....	12
1.8 Resting-state fMRI.....	14
1.9 Functional Network Connectivity during Rest and Task.....	15
1.10 Automatic Diagnosis of Mental Disorders .....	17
1.11 Preprocessing of fMRI Time-Series for Functional Connectivity Studies.....	18
1.12 Notion of Autoconnectivity .....	19
1.13 Organization of the Dissertation.....	20
1.14 Datasets.....	21
1.14.1 Hartford Dataset.....	22
1.14.2 FBRIN Dataset.....	24
Chapter 2: Functional Network Connectivity during Rest and Task.....	28
2.1 Motivation .....	29
2.2 Proposed Approach .....	30
2.2.1 Preprocessing .....	30
2.2.2 Group ICA and Back Reconstruction .....	30
2.2.3 Component Selection .....	32
2.2.4 Functional Network Connectivity.....	32
2.2.5 Statistical Analysis.....	34
2.2.6 Functional Network Volumes .....	34
2.2.7 Maximum Activation.....	35
2.2.8 Validation.....	35
2.3 Results .....	36
2.4 Discussion .....	43
Chapter 3: Automatic Classification of Schizophrenia patients based on Resting-state FNC Features .....	48
3.1 Introduction .....	49



3.2	What is Schizophrenia? .....	50
3.3	Previous Studies based on Structural Biomarkers.....	50
3.4	Previous Studies based on Functional Biomarkers .....	53
3.5	Motivation and Objective.....	57
3.6	Proposed Approach .....	57
3.6.1	Classification.....	59
3.6.2	Parameter Selection .....	66
3.6.3	Effect of Medication .....	66
3.7	Results .....	67
3.8	Discussion .....	74
Chapter 4:	Impact of Autocorrelation of Functional connectivity.....	81
4.1	Introduction and Motivation.....	82
4.2	Theoretical Background .....	84
4.2.1	Pearson Correlation Coefficient.....	84
4.3	Pearson Correlation Coefficient of Two Autocorrelated Time-Series.....	86
4.3.1	Modeling the Time-Series with Autoregressive Process of Model Order One: AR(1).....	87
4.3.2	Autoregressive Process in the Frequency Domain .....	90
4.4	Methods.....	92
4.4.1	Simulated Data.....	92
4.4.2	Real fMRI Data.....	92
4.4.3	Group Independent Component Analysis.....	92
4.4.4	Post ICA Processing .....	93
4.4.5	Functional Network Connectivity.....	94
4.4.6	Autocorrelation Correction .....	94
4.5	Results .....	95
4.5.1	Simulated Data.....	95
4.5.2	Real fMRI Data.....	97
4.6	Discussion .....	105
4.6.1	Autocorrelation Correction and Frequency Filtering.....	108
4.6.2	Model Order for Autocorrelation Correction.....	110
4.6.3	Impact of Autocorrelation on FC: Hyperconnectivity, Hypoconnectivity or No Impact?.....	111
4.6.4	Limitations and Future Studies .....	114
4.7	Conclusion.....	115

Chapter 5: Autoconnectivity, a New Perspective on Human Brain's Functionality ..	117
5.1 Introduction and Motivation.....	118
5.2 Methods .....	120
5.2.1 Time-Series Preprocessing.....	120
5.2.2 Autoregressive Modeling.....	120
5.2.3 Classification.....	120
5.2.4 Hemodynamic Response Function Estimation .....	121
5.3 Results .....	121
5.3.1 Mapping Autocorrelation Coefficient to the Brain during the Resting-State	121
5.3.2 Mapping Autocorrelation Coefficient to the Brain during the AOD Task	123
5.3.3 Relationship Between AR(1) during Rest and Task .....	124
5.3.4 Classification of Schizophrenia Patients Based on Autoconnectivity	
Features	126
5.4 Discussion .....	127
5.5 Classification of Schizophrenia Patients based on Combination of Resting-State	
FNC and Autoconnectivity Features.....	130
5.5.1 Feature Selection.....	130
5.5.2 Classification.....	131
Chapter 6: Conclusion and Future Works .....	132
6.1 Summary .....	133
6.2 Future Works.....	134
References.....	136

## List of Figures

Figure 1-1: An example of functional segregation and integration. A: Parcellation of brain into 116 specialized regions. Structure of functional integration during resting-state in 3 groups: B: Control group, C: Yoga practitioner and D: Mediator group. Figure courtesy of (Gard et al., 2014). ..... 4

Figure 1-2: Voxel as a cubic element of a 3D image. Image on the left is sampled with a 3D grid and represented by voxels on the right. Figure courtesy of (Smith, 2004)..... 6

Figure 1-3: Typical fMRI experiment equipment. Figure courtesy of (<http://culhamlab.ssc.uwo.ca/fmri4newbies/>) ..... 7

Figure 1-4: Two typical designs in fMRI experimental: block-design and event-related design. .... 8

Figure 1-5: Illustration of functional connectivity. Figure courtesy of (Dosenbach et al., 2010) ..... 9

Figure 1-6: Example of functional network connectivity. Figure courtesy of (Jafri et al., 2008). ..... 11

Figure 1-7: Illustration of two types of ICA on fMRI data: SICA and TICA. Figure courtesy of (Calhoun et al., 2001b)..... 13

Figure 1-8: Spatial ICA for fMRI data. Data matrix,  $\mathbf{X}$  is decomposed into independent sources that are rows of matrix  $\mathbf{S}$  and corresponding time-courses that are columns of the mixing matrix,  $\mathbf{A}$ . Figure is courtesy of (Ylipavalniemi and Vigario, 2008) ..... 13

Figure 1-9: Simplified group ICA and back –reconstruction. Figure courtesy of (Erhardt et al., 2011). ..... 14

Figure 1-10: The AOD task used to collect the Hardford dataset. Subject should press the button just upon hearing target tones. Figure courtesy of (Kiehl and Liddle, 2001). ..... 23

Figure 2-1: Block diagram of the proposed approach ..... 30

Figure 2-2: Spatial maps of the ten selected IC components. The time-course of each component during AOD task was regressed against task paradigms (see section 2.3.3). The p-value for the regression coefficients corresponding to novel and target stimulations are color-coded in the bottom left and right corners of each component respectively. Reference color bar is shown on the right side of the figure. .... 37

Figure 2-3: Top row: mean of maximum lagged correlation pairs for rest and AOD. Bottom row: T-value of each correlation pair resulted from Student t-test. Left column: unfiltered components. Right column: filtered components. Black circles indicate the pairs surviving the t-test with a FDR corrected p-value threshold of 0.05. .... 39

Figure 2-4: Left: mean maximum lagged correlation difference between rest and AOD (rest-AOD) for filtered and unfiltered components. Right: T-value resulting from paired t-test with FDR corrected p-value threshold of 0.05 for filtered and unfiltered components. Stars: pairs surviving the paired t-test..... 40

Figure 2-5: Volume of each functional network during rest and task averaged over subjects. Each black error bar is symmetric and twice the standard error of the mean long. Red stars show components surviving paired t-test at FDR corrected 0.05 level between the volumes in the two states. .... 42

Figure 2-6: Peak activation for each component during rest and task. A voxel-wise one sample t-test on each component (each subject is an observation) for each state was

performend. Then the highest T-value of the test is illustrated in this Figure. The highest activated voxel is not necessarily the same for rest and task. .... 42

Figure 3-1: The Proposed Approach. The pink blocks on the top show the feature extraction steps. The statistical analysis box (green) is not part of the classification approach. The light green blocks describe the classification stage. .... 58

Figure 3-2: Spatial maps of the nine selected IC components..... 67

Figure 3-3: Left: Mean of correlation pairs for controls and patients. Right: T-value of each correlation pair resulted from Student t-test with p-value threshold of 0.05 corrected for FDR. Black circles indicate the pairs surviving the t-test. .... 68

Figure 3-4: Left: Mean correlation difference between control subjects and patients(control-patient). Right: T-value resulting from two sample t-test with p-value threshold of 0.05 corrected for FDR. Stars show pairs that survived the paired t-test. .... 69

Figure 3-5: Fisher’s decision tree using full set of features. This tree includes 8 features in 10 nodes. The number on each branch is FNC between the two networks preceding the branch..... 73

Figure 3-6: Information gain decision tree using full set of features. This tree includes 6 features in 6 nodes. The number on each branch is FNC between the two networks preceding the branch. .... 73

Figure 4-1: Autoregressive process modeled as a linear time-invariant system with the input of a white time-series ( $\mathbf{wt}$ ) and output of a autocorrelated time-series ( $\mathbf{xt}$ ). .... 90

Figure 4-2: AR(1) as a frequency filter: Magnitude of the frequency response function for AR(1) model for different  $\alpha$  values (Eq. (4-21)). Note that  $\pi$  corresponds to the highest

frequency possible in the signal. Positive and negative values of  $\alpha$  results in low and high pass filters respectively. .... 91

Figure 4-3: Empirical bias and standard deviation of estimation of true  $\rho_{w, z} = +0.5$  based on  $r_{x, y}$  and  $r_{w, z}$  for different combination of AR(1) coefficients ( $\alpha$  and  $\beta$  in Eq. (4-8) and (4-9) for time-series  $x$  and  $y$  and different sample sizes (length of time-series  $x$  and  $y$ ) of (64, 256, 1024) obtained from 10,000 simulations. The empirical results are compared with theoretical bias and standard deviation of  $r_{w, z}$  and  $r_{x, y}$  derived in Eq. (4-5) & (4-6) and Eq. (4-16) & (4-19) respectively. The whiskers show standard error of the estimation of the mean (square root of variance of the estimator). It is evident that theoretical and empirical results agree with each other. For equal coefficients, estimation of  $\rho_{w, z}$  based on  $r_{x, y}$  is unbiased. For different AR(1) coefficients, estimation is biased. The variance of the estimator increases as the product of AR(1) coefficients if  $xt$  and  $yt$  increases. .... 96

Figure 4-4: Top row: Histogram of corrected and uncorrected empirical Pearson cross correlation coefficients ( $r_{w, z}$  and  $r_{x, y}$ ) obtained from 10,000 simulations based on (4-8) and (4-9) with sample size of 256 and true correlation of +0.5 for 3 different combination of  $\alpha$  and  $\beta$  ((4-8) & (4-9)). Bottom Row: Scatter plot of uncorrected correlation coefficients,  $r_{x, y}$ , against corrected correlation coefficients  $r_{w, z}$ . Correlation coefficient between  $r_{w, z}$  and  $r_{x, y}$  is provided in the bottom row scatter plots ( $r$ ). .... 97

Figure 4-5: Spatial maps of selected 47 independent components grouped based on functionality into 7 categories: subcortical (5 components), auditory (2 components),

visual (11 components), sensorimotor (6 components), attention/cognitive control (13 components), default-mode network (8 components) and cerebellar (2 components). .... 98

Figure 4-6: Durbin-Watson statistics histogram for A: Uncorrected IC time-series for healthy controls B: Uncorrected IC time-series for schizophrenia patients C: Corrected IC time-series for healthy controls D: Corrected IC time-series for schizophrenia patients. Autocorrelation correction could successfully concentrate DW statistics around 2 which is a sign for absence of autocorrelation..... 99

Figure 4-7: A,B: Mean and standard deviation of FNC grouped by functionality of brain networks (Figure 2) for healthy controls before and after autocorrelation correction. C:  $-\log(p\text{-value}) \times \text{sign of } t\text{-statics}$  after subject-wise 1-sample t-test on each FNC pair before and after autocorrelation correction. Although the FNC values alter noticeably before and after autocorrelation correction, p-values remain very similar. .... 101

Figure 4-8: A,B: Mean and standard deviation of FNC grouped by functionality of brain networks (Figure 2) for schizophrenia patients before and after autocorrelation correction. C:  $-\log(p\text{-value}) \times \text{sign of } t\text{-statics}$  after subject-wise 1-sample t-test on each FNC pair before and after autocorrelation correction. Although the FNC values alter noticeably before and after autocorrelation correction, p-values remain very similar. .... 102

Figure 4-9: A: Difference in mean of FNC between healthy controls and schizophrenia patients (healthy-patients) grouped by functionality of brain networks (Figure 1) before and after autocorrelation correction. B:  $-\log(p\text{-value}) \times \text{sign of } t\text{-statics}$  after subject-wise 2-sample t-test between controls and patients before and after autocorrelation correction. Although the differences in FNC values between healthy controls and patients alter

noticeably before and after autocorrelation correction, p-values of 2-sample t-test remain very similar. .... 103

Figure 4-10: A: Histogram of corrected and uncorrected FNC values (pooled all subjects and pairs) for healthy controls and schizophrenia patients. B: Scatter plot of uncorrected FNC values against corrected FNC values for healthy controls and schizophrenia patients. Correlation coefficient between corrected and uncorrected FNC values is high for both groups ( $r = +0.89$ ). Compare these results with simulation results in Figure 4-4 (especially for  $\alpha = \beta = 0.5$ ). C: Scatter plot of  $-\log(p\_value) \times \text{sign}(T\_Statistics)$  before and after autocorrelation correction for healthy controls and schizophrenia patients (these are scatter plots of color-coded values in Figure 4-7C and Figure 4-8C). .... 104

Figure 4-11: Histogram of AR coefficient for pooled IC time-series for all subject for healthy controls and schizophrenia patients if all time-series are corrected with AR(1). .... 105

Figure 4-12: Autocorrelation function with 95% confidence interval lines and amplitude of frequency spectra for two fMRI time-series,  $x(t)$ ,  $y(t)$  before autocorrelation correction (left column), after autocorrelation correction with AR(4) model (middle column) and after frequency filtering with a order 6 Butterworth passband filter with cutoff frequencies of 0.01 Hz and 0.10 Hz (right column). While autocorrelation correction improves the autocorrelation function (all values are inside 95% confidence interval), frequency filtering introduce back the autocorrelation in a more severe and complicated manner. .... 109



Figure 4-13: A: Canonical HRF function B: Best model order based on AIC for correcting autocorrelation of samples taken with different **TR** (repetition time) from the HRF function. Best model order increases exponentially as **TR** decreases..... 111

Figure 4-14: A: Two correlated low frequency time-series (200 time-points) B: After adding high frequency noise to the original time-series in part A (**SNR = 20db**) C: Time-series in part B passed through AR(1) process with coefficients of +0.6. Autocorrelation acts as a low pass filter and enhances the correlation between two noisy signals in part B close to the original level in part A..... 113

Figure 5-1: A: Resting-state AR(1) coefficient estimated for each voxel for both healthy control and schizophrenia patients. B: T-maps resulted from group-wise one-sample t-test on each voxel for both healthy control and schizophrenia C: T-maps resulted from two sample t-test between healthy controls and schizophrenia patients..... 123

Figure 5-2: A: AOD task AR(1) coefficient estimated for each voxel for both healthy control and schizophrenia patients. B: T-maps resulted from group-wise one-sample t-test on each voxel for both healthy control and schizophrenia ..... 124

Figure 5-3: A: Group-wise correlation between average AR(1) coefficients during rest and AOD task for healthy controls (HC) and schizophrenia patients (SZ) B: Group-wise correlation between AR(1) coefficients during rest and task for each region in AAL atlas. The 116 regions are divided into eight groups based on the correlation pattern. .... 125

Figure 5-4: Scatterplot of peak HRF during AOD task vs. AR(1) during the resting-state for the auditory network..... 127

## List of Tables

Table 2-1: Brain regions, corresponding Brodmann areas, volumes, maximum t-values and spatial coordinates of each component in Talairach space. ....	38
Table 2-2: Detailed information about significant pairs. Left: means of correlation, standard deviation and p-values resulting from the t-test for each pair in rest. Middle: mean of correlation, standard deviation and p-value resulting from the t-test for each corresponding pair in the AOD task. Right: mean correlation difference (rest-AOD) along with p-value resulting from paired t-test. Bolded p-values survived t-test or paired t-test with 0.05 threshold corrected for FDR. ....	41
Table 2-3: Mean, standard deviation (Std), absolute (Abs) mean and standard deviation of absolute mean for all 45 correlation pairs averaged over all subjects. ....	43
Table 3-1: Summary of neuroimaging-based automatic diagnosis of schizophrenia studies. OV: Overall accuracy, Schiz.: schizophrenia, DMN: Default mode network, SNP: single nucleotide polymorphism.....	56
Table 3-2: Testing classification results using full set of features. Overall Acc.: overall accuracy, Sens: sensitivity, Spec: Specificity, PPV: positive predictive value, NPV: negative predictive value, CI: Wilson’s binomial confidence interval. Bold classifiers perform above the chance (lower bound of confidence interval is greater than 50%). ....	71
Table 3-3: Testing classification results using reduced set of features (27 features). Overall Acc.: overall accuracy, Sens: sensitivity, Spec: Specificity, PPV: positive predictive value, NPV: negative predictive value, CI: Wilson’s binomial confidence	

interval. Bold classifiers perform above the chance (lower bound of confidence interval is greater than 50%)...... 72

Table 5-1: Classification Results ..... 131

## **Chapter 1: Introduction**

## **1.1 Human Brain**

The human brain is one of the most complex systems known to mankind. This central nervous system organ weighs about 1400g (about 2% of body weight) but consumes about 20% of the body's energy. This complex multilayer structure consists of more than 100 billion neurons interconnected with about 100 trillion synaptic connections (Azevedo et al., 2009; Williams and Herrup, 1988). From more than 3500 years ago, the brain has been under constant investigation of different disciplines ranging from philosophy to modern neuroscience. While Aristotle believed that blood cooling was the only function of the brain (Finger, 1994), today the key functionalities of the brain such as information processing, perception, motor control, learning and memory are well studied and confirmed (Kandel et al., 2000).

Anatomically, brain consists of gray matter, white matter and cerebrospinal fluid (CSF). Gray matter consists mostly of neuron body cells and is responsible for most of the higher level functionalities of the brain. White matter mostly consists of long myelinated axons and is responsible to transfer information among different gray matter regions. CSF is a clear liquid in the brain and spinal cord.

## **1.2 Functional Segregation and Integration**

There are two key principles which can be used to describe brain function: functional segregation and functional integration (Friston, 2011; Tononi et al., 1998). Functional segregation refers to the fact that each brain region is specialized in specific tasks. Functional segregation has been demonstrated on multiple spatial scales ranging from brain networks to neuronal columns. For example, each region in the visual cortex is specialized in a distinct aspect of visual perception such shape, motion and color (Zeki,

1990; Zeki et al., 1991). The information processed by different specialized regions at different spatial and temporal scales should be functionally integrated to form unified cognition and behavior. The process of functional integration is harder to assess compared to functional segregation. Functional integration similar to functional segregation occurs at multiple spatial and temporal scales. In the visual system, for example, at the lower level elements such as dots and edges must group together to form shapes (Kanizsa, 1979). In the next level, different attributes such as shape. Color and size are grouped together to form objects. Finally objects should combine together to form a unified visual image (Treisman, 1996). This is a simplified scheme in just the visual system. In higher level, visual information must integrate with other sources of information processed in other brain regions such as auditory, somatosensory and memory networks to form a conscious scene (Tononi and Edelman, 1998). Figure 1-1 illustrates an example of functional segregation and integration during resting-state in three groups.

### **1.3 Functional Neuroimaging**

Advances in neuroimaging techniques such as electroencephalography (EEG), magnetoencephalography (MEG), positron emission tomography (PET), single-photon emission computed tomography (SPECT), structural magnetic resonance imaging (sMRI), functional magnetic resonance imaging (fMRI), diffusion tensor imaging (DTI) and diffusion spectrum imaging (DSI) in the past few decades have opened up a non-invasive window into human brain's structure and function. These tools have made it possible to study the brain with high relative temporal and spatial resolution.

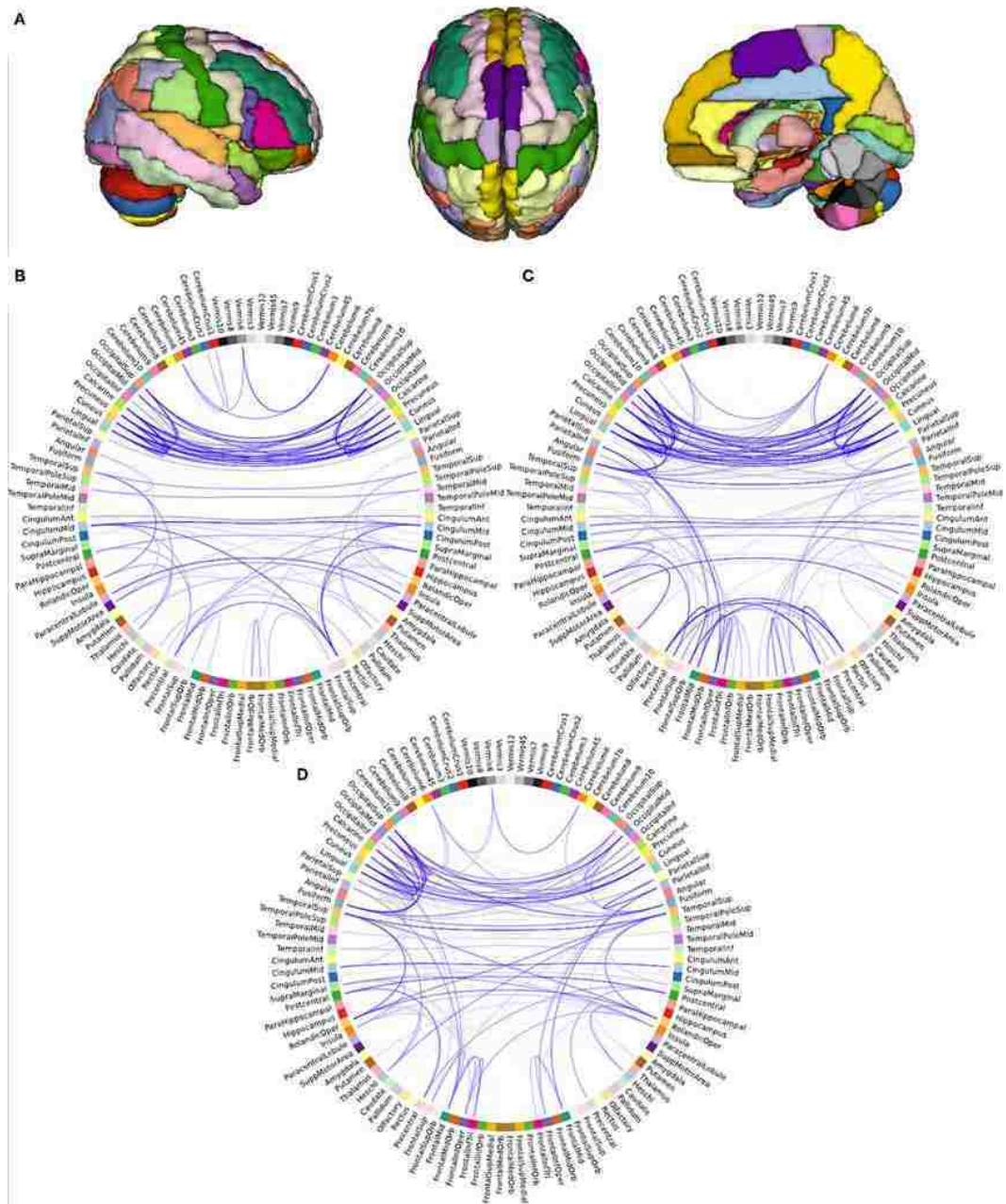


**Figure 1-1:** An example of functional segregation and integration. **A:** Parcellation of brain into 116 specialized regions. Structure of functional integration during resting-state in 3 groups: **B:** Control group, **C:** Yoga practitioner and **D:** Mediator group. Figure courtesy of (Gard et al., 2014).

Specifically MRI-related techniques such as sMRI, fMRI, and DTI, have the benefit of providing localized spatial information. These MRI-related techniques have

provided new insight into the human brain and have brought hope to researchers trying to unravel the secrets of one of the most complex systems in the universe, the human brain.

SMRI has made it possible to visualize the brain noninvasively at relatively high spatial resolution (1 mm<sup>3</sup> or less). SMRI high-resolution images of the brain are useful for studying various brain structures as well as detecting physical abnormalities, lesions, and damages. DTI allows mapping the diffusion process of water in biological tissues. In brain imaging, DTI at each voxel is represented by a symmetrical 3×3 matrix, called diffusion tensor. In the white matter regions of the brain, there is a higher rate of diffusion along the direction of the fibers. This property enables this imaging technique to visualize anatomical connections between different brain regions.

Among all neuroimaging tools, fMRI has been used extensively to study functionality of the brain in the past 2 decades. FMRI which is an indirect measure of neuronal activity, tracks blood oxygenation which is linked to neuronal activity. Upon activation of a brain region, blood flow and volume increases in that area to provide oxygen and glucose. MRI is sensitive to this increase in blood oxygenation since oxygenated blood has different magnetic properties compared to deoxygenated blood. FMRI uses this phenomenon better known as blood-oxygenation-level dependent (BOLD) to measure the underlying neuronal activity (Ogawa et al., 1990). Neuronal activity is linked to blood flow via hemodynamic response function. FMRI has a temporal resolution of about one second (recent imaging techniques have increased the temporal resolution to about 200mS) and spatial resolution of 1-3mm<sup>3</sup>. This modality also has been used to measure functional connectivity in the brain.



Since MRI can take three dimensional images of the brain, the term voxel is used as the smallest cubic element of the 3D image similar to pixel which is the smallest element in a 2D image. This is depicted in Figure 1-2.

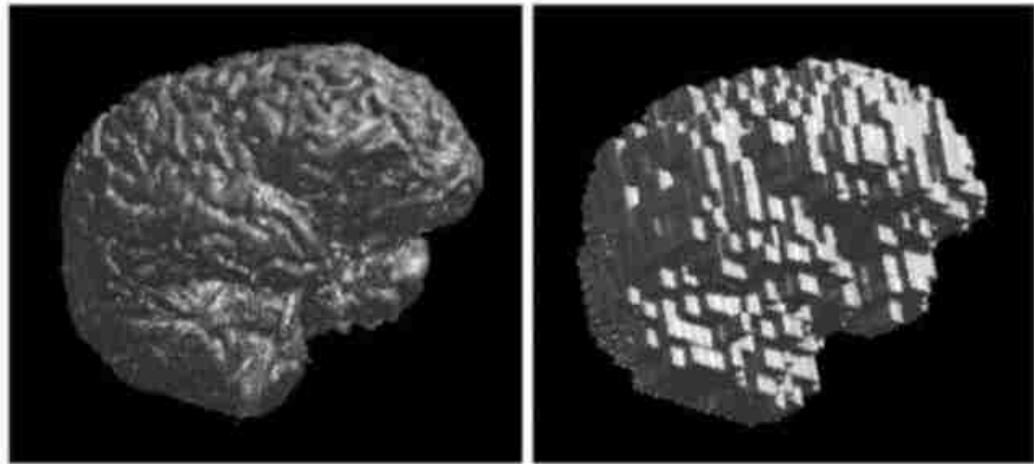


**Figure 1-2:** Voxel as a cubic element of a 3D image. Image on the left is sampled with a 3D grid and represented by voxels on the right. Figure courtesy of (Smith, 2004).

## 1.4 fMRI Experiment

In an fMRI experiment, Subject lies in a MRI machine. MRI machine consist of a main coil making high steady magnetic field (typically 1.5T or 3T but also at 7T and higher) in the chamber of the scanner, three gradient coils that make small changes in the steady magnetic field and radio frequency coil that emits radio frequency signals to excite the protons that are spinning at a certain frequency according to Larmor law.

The research participant is instructed to not move his/her head since motion is one of the main artifacts in an fMRI experiment. Depending on the type of the task, the MR machine may be equipped with special tools such as projector, speaker, headphones, microphone and button boxes. In a typical task-based experiment, subject need to attend to a task and respond if it is required. For example auditory oddball task, different sounds

with different frequencies are played and the subject is supposed to respond to certain frequencies by pressing a button. Figure 1-3 illustrates a typical fMRI experiment.

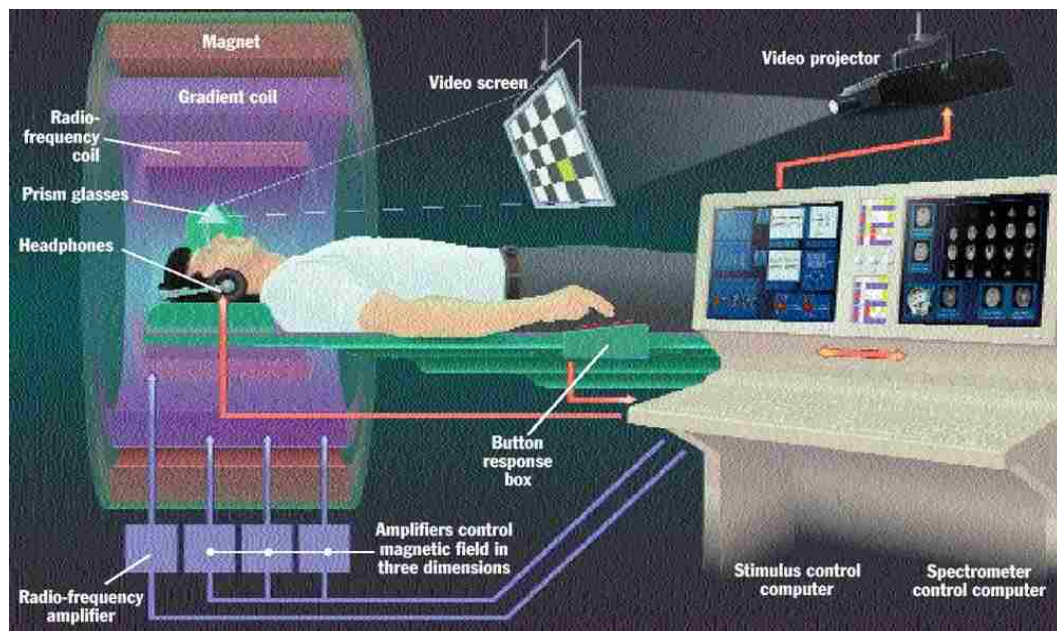


**Figure 1-3:** Typical fMRI experiment equipment. Figure courtesy of (<http://culhamlab.ssc.uwo.ca/fmri4newbies/>)

There are two main types of task-based fMRI designs: block design and event-related design. In block design experiment, two or more different conditions are alternated in order to determine the differences among them. Each block have duration in the order of tens of seconds and only one condition is presented in each block. Conditions should be designed in such a way that the fMRI signal can differentiate the cognitive process of interest. Alternation of a block of task with a block of resting-state is a typical block design experiment. This type of experiment design has more statistical power.

Event-related is another type popular fMRI experiment design. In this type of design the stimuli is not presented in blocks, but is randomized throughout the course of the experiment. The duration between two consecutive stimuli can vary to make it less predictable by the subject. Event-related design allows more real world testing despite its

lower statistical power compared to block design experiment. These two designs are illustrated in Figure 1-4.

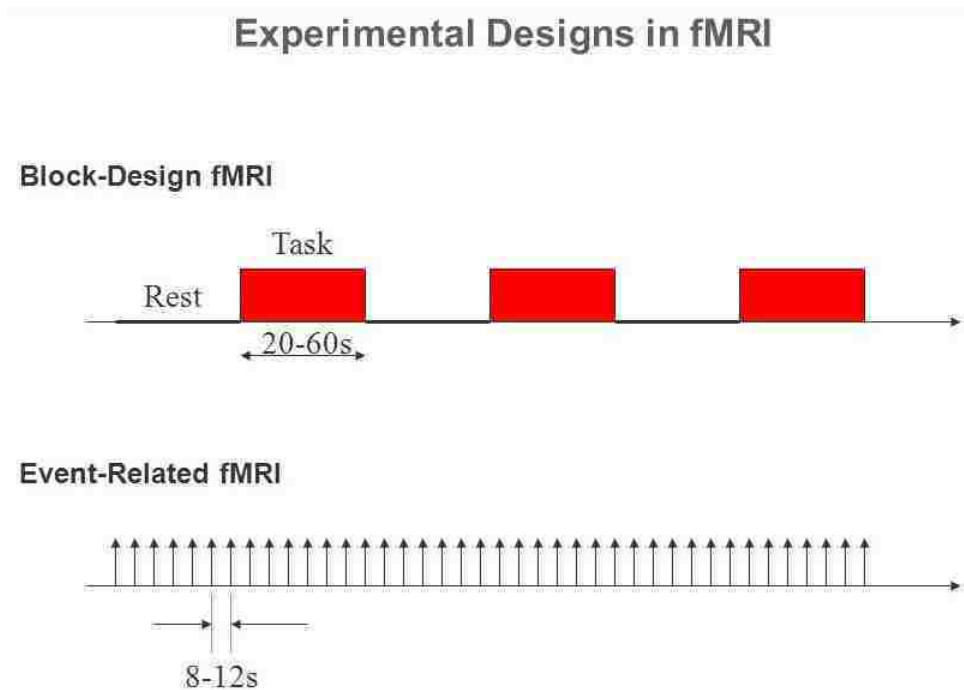


**Figure 1-4:** Two typical designs in fMRI experimental: block-design and event-related design.

## 1.5 Functional Connectivity

As discussed earlier, function can be described via two key principles: functional segregation and functional integration. While the evidence for functional segregation or specialization is overwhelming, functional integration of specialized regions is more difficult to assess. The usual way to study functional integration is by measuring statistical dependency mostly in the form of correlation among activity of different brain areas. Functional connectivity (FC) is defined as the cross-correlation between activity of two specialized brain regions (Friston, 2002). fMRI is a powerful tool to study FC since it makes it possible to find the specialized regions with high spatial resolution and then

assessing FC by calculating correlation between the activities of those regions. FC analysis documents interactions among brain regions during a task as well as during resting state scans. FC is believed to characterize large-scale integrity in human brain (Van Dijk et al., 2010). Figure 1-5 illustrates an example of functional connectivity.

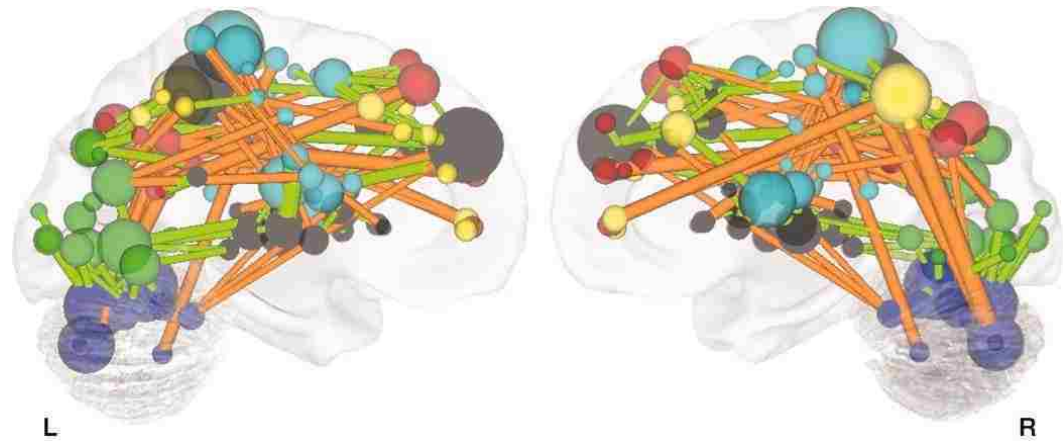


**Figure 1-5:** Illustration of functional connectivity. Figure courtesy of (Dosenbach et al., 2010)

Two widely used FC approaches are: (a) seed-based analysis (Biswal et al., 1995b; Biswal et al., 1997; Cordes et al., 2002; Cordes et al., 2000; Fox et al., 2005; Lowe et al., 1998; Stein et al., 2000) and (b) spatial independent component analysis (ICA) (Calhoun et al., 2001b; Esposito et al., 2005; Garrity et al., 2007a; McKeown et al., 1998; van de Ven et al., 2004). In the seed-based approach, individual seed voxels from predefined brain regions of interest (ROI) are chosen and the cross correlation of other voxels' time courses with the selected seeds then computed, to derive a correlation map. This map can then be thresholded to identify voxels showing significant FC with the seed voxels.

An alternative approach is based on ICA, a multivariate data-driven method which as a blind source separation method, can recover a set of signals from their linear mixtures and has yielded fruitful results with fMRI data (Calhoun et al., 2009b). ICA

estimates maximally independent components using independence measures based on higher-order statistics. ICA requires no specific temporal model (task-based design matrix), making it ideal for analyzing resting state data. Spatial ICA (sICA) is the predominant ICA approach used for fMRI data (Calhoun et al., 2001b; McKeown et al., 1998).

sICA decomposes fMRI data into a set of maximally spatially independent maps and their corresponding time-courses. Each thresholded sICA map may consist of several remote brain regions forming a brain functional network. Spatial ICA generates consistent spatial maps while modeling complex fMRI data collected during a task or in the resting-state (Turner and Twieg, 2005) although the task can result in a subtle modulation of the spatial patterns (Calhoun et al., 2008a). The dynamics of the BOLD signal within a single component is described by that component's time course. Regions contributing significantly within a given component are strongly functionally connected to each other.

## **1.6 Functional Network Connectivity**

It has been shown that a collection of remote specialized regions collaborate on performing a specific motor or cognitive task. The regions within this collection exhibit strong functional connectivity with each other and form a functional network. Recently, there is growing interest in studying FC among brain functional networks. This type of connectivity, which can be considered as a higher level of FC, is termed functional network connectivity (FNC) (Jafri et al., 2008) and measures the statistical dependencies among brain functional networks. Each functional network may consist of multiple remote brain regions. Spatial components resulting from sICA are maximally spatially

independent but their corresponding time-courses can show a considerable amount of temporal dependency. This property of sICA makes it an excellent choice for studying FNC, which can be studied by analyzing these weaker dependencies among sICA time courses. These dependencies can be analyzed by correlation methods (Jafri et al., 2008) or algorithms such as dynamic causal modeling (Stevens et al., 2007) or Granger causality (Allen et al., 2012; Havlicek et al., 2010; Stevens et al., 2009). Figure 1-6 illustrates an example of functional network connectivity among seven brain networks.

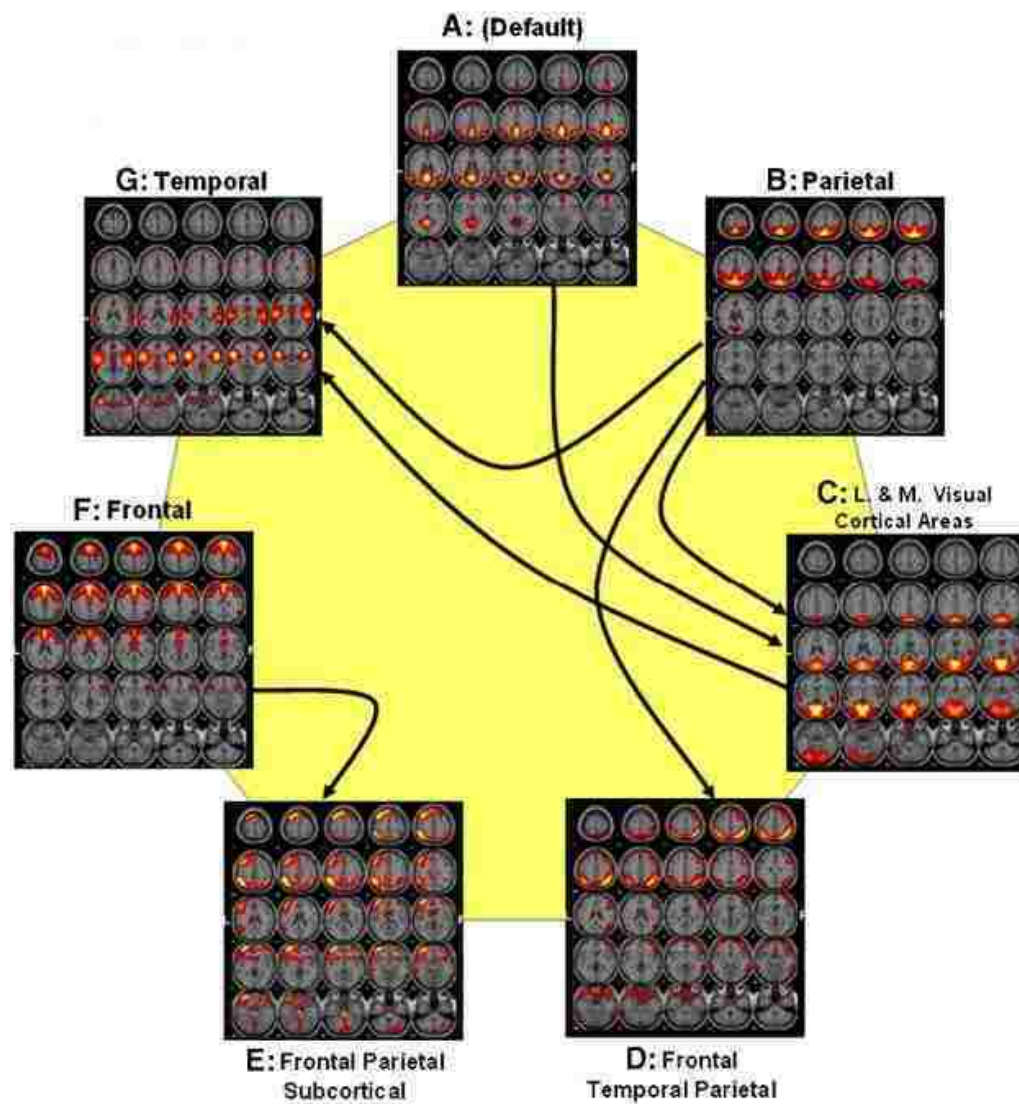


**Figure 1-6:** Example of functional network connectivity. Figure courtesy of (Jafri et al., 2008).

## 1.7 Independent Component Analysis

Independent component analysis is mathematical method to separate multivariate signals into statistically independent components. ICA assumes a generative model where observations are linear mixture of independent sources. In a typical ICA setting, it is assumed that the both the sources and the linear mixing process are unknown. Mathematically ICA formulation can be written as:

$$\mathbf{X} = \mathbf{A}\mathbf{S} \quad (1-1)$$

where  $\mathbf{X} = (x_1, x_2, \dots, x_M)^T$  is an M-dimensional observed vector and  $\mathbf{S} = (s_1, s_2, \dots, s_N)^T$  is an N-dimensional vector whose elements are independent sources.  $\mathbf{A}_{M \times N}$  is the unknown mixing matrix. The goal of ICA is recover the unmixing matrix,  $\mathbf{W}_{N \times M}$  so that the sources can be approximated with  $\mathbf{Y}$  in the following equation:

$$\mathbf{Y} = \mathbf{W}\mathbf{X} \quad (1-2)$$

It has been shown that the problem is solvable with some assumptions and constraints (Hyvarinen and Oja, 2000). ICA assumes that the sources are independent and their distribution is non-Gaussian.

There are several methods for solving the ICA problem based on criteria such as mutual information, kurtosis and negentropy and as a result there are several practical algorithms for ICA. The most popular methods are Infomax (Bell and Sejnowski, 1995), FastICA (Hyvarinen and Oja, 1997) and joint diagonalization of eigen-matrices (JADE) (Cardoso and Souloumiac, 1993).

Real fMRI data consists of two main dimensions, time and space. Depending on formation of the data matrix, two types of ICA can be performed on fMRI data. Temporal ICA (TICA) decomposes the fMRI data into independent time-series and spatial ICA

decomposes the data into independent spatial maps. These two methods are illustrated in Figure 1-7. Spatial ICA is more popular for fMRI data since it recovers independent specialized networks in the brain as well as their corresponding time-courses. Figure 1-8 illustrates SICA.

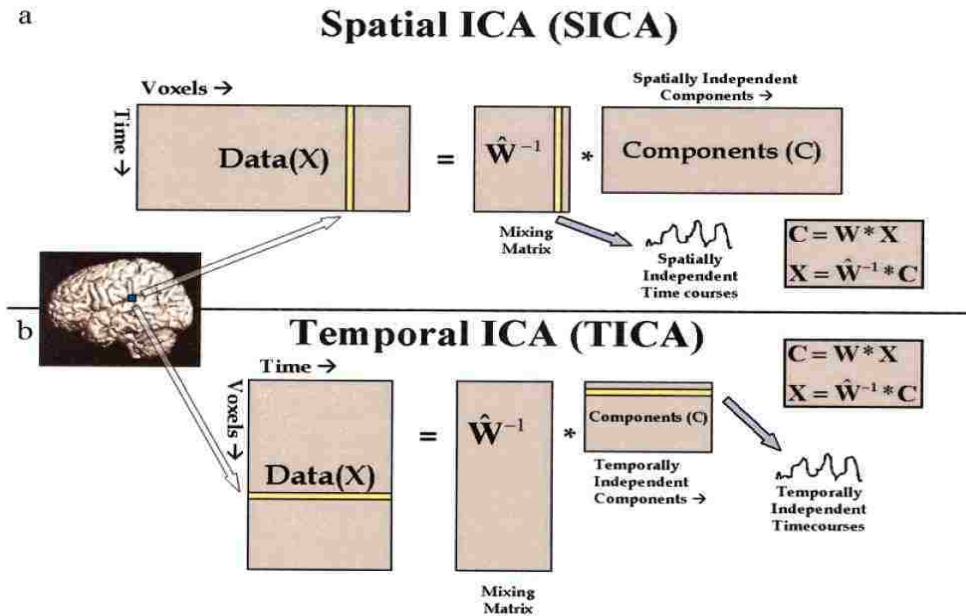


**Figure 1-7:** Illustration of two types of ICA on fMRI data: SICA and TICA. Figure courtesy of (Calhoun et al., 2001b)

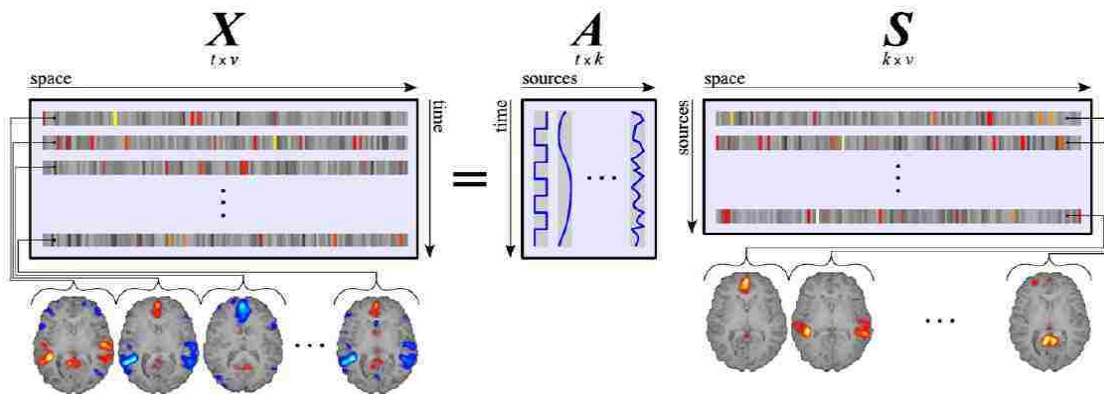


**Figure 1-8:** Spatial ICA for fMRI data. Data matrix,  $X$  is decomposed into independent sources that are rows of matrix  $S$  and corresponding time-courses that are columns of the mixing matrix,  $A$ . Figure is courtesy of (Ylipavalniemi and Vigario, 2008)



It is also possible to extend ICA to group level analysis. Usually the dimensionality of each subject's data matrix is reduced with principal component analysis (PCA). Then all the reduced matrices are concatenated and another PCA is performed. Finally ICA is performed and the common components among the subjects are estimated. In order to recover subject specific spatial maps additional step named back-reconstruction is required. Group ICA and back-reconstruction are illustrated in Figure 1-9.

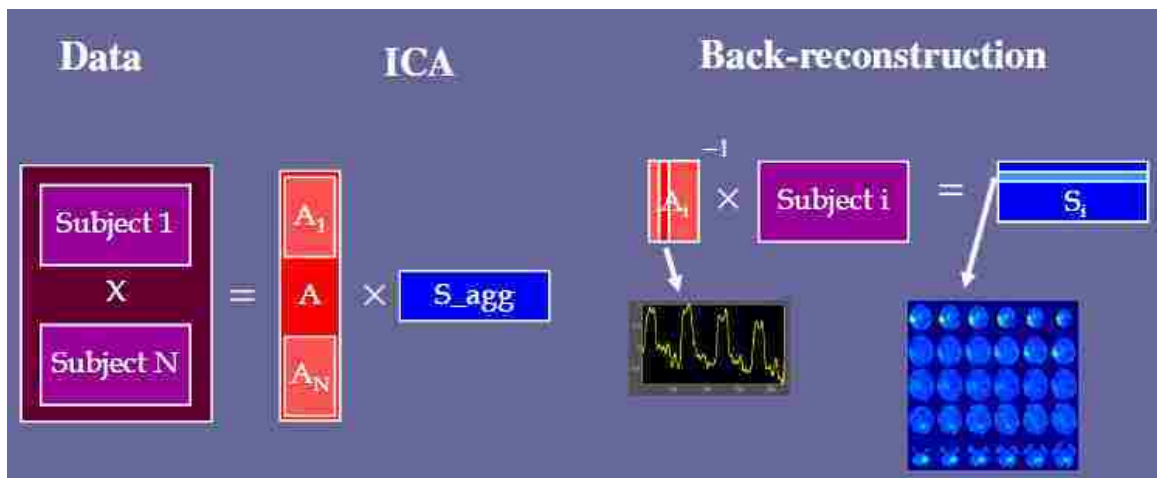


**Figure 1-9:** Simplified group ICA and back –reconstruction. Figure courtesy of (Erhardt et al., 2011).

## 1.8 Resting-state fMRI

Hans Berger, inventor of the electroencephalogram stated in his seminal paper in 1929: “We have to assume that the central nervous system is always, and not only during wakefulness, in a state of considerable activity” (Berger, 1929). But this brilliant finding was ignored for several decades and spontaneous fluctuations in the brain were mostly attributed to noise since brain was considered to be shut down during the resting-state. About 2 decades ago, it was shown that fMRI time-series of one part of the motor cortex is correlated with fMRI signals from other parts of the motor network during the resting-

state (Biswal et al., 1995b). Since then, several other brain networks with correlated temporal patterns have been identified as resting-state networks (RSN). These networks have been identified even in other cognitive states such as during sleep (Fukunaga et al., 2006) and even anesthesia (Vincent et al., 2007). One interesting RSN discovered about 15 years ago is called default-mode network (DMN) which is a collection of brain regions that tend to be more active during the resting-state (Raichle et al., 2001; Raichle and Snyder, 2007). The activity of this network suppresses during a cognitive or motor task.

Most of the RSNs are consistently present during the resting-state as well as during performance of a task (Calhoun et al., 2008a; Harrison et al., 2008; Laird et al., 2009; Smith et al., 2009a) and exhibit high reproducibility and reliability (Allen et al., 2011; Franco et al., 2009; Shehzad et al., 2009; Zuo et al., 2010).

In recent years, spontaneous modulation of BOLD signal during the resting condition has found fruitful clinical applications (Fox and Greicius, 2010). Resting-state fMRI (rfMRI) experiments are less prone to multi-site variability, allow a wider range of patients to be scanned and make it possible to study multiple cortical systems from one dataset (Fox and Greicius, 2010). Moreover, more accurate connectivity maps can be detected using rfMRI data compared to task-based fMRI data (Xiong et al., 1999).

## **1.9 Functional Network Connectivity during Rest and Task**

Most FNC research has been focused on either resting-state or task-based data but has not compared these two. Studying the differences between rest and task to explore changes in the interaction among functional networks in these two states can clarify how the brain responds to a given task in the network level. The relatively small amount of

research on comparison of brain connectivity in the resting state and during a particular task is limited mostly to seed-based approaches to measure the FC. Arfanakis et al. (Arfanakis et al., 2000) compared FC during rest, during simple tasks (bilateral finger tapping, passive listening to narrated text and looking at an alternating checkerboard) and also when the effect of task was removed using ICA. Hampson et al. (Hampson et al., 2002) compared FC during rest and during continuous listening to speech and showed strengthened connectivity among the language related brain regions during task. Another study by Hampson et al. (Hampson et al., 2004) compared FC in the resting state and during viewing moving concentric circles. They reported decreased FC between middle temporal (MT/V5) and dorsal cuneus, lingual gyrus and thalamus and increased FC between MT/V5 and middle occipital gyrus during viewing continuous motion task. Bartels et al. (Bartels and Zeki, 2005) showed that, natural viewing specifically increases correlations between anatomically connected regions while it decreases correlations between non-connected regions compared to rest. Nir et al. (Nir et al., 2006) compared brain's visual system during rest and visual stimulation. They reported robust organized slow BOLD signal fluctuations and widespread FC in the visual cortex during complete darkness with eyes closed. Fransson and Marrelec (Fransson and Marrelec, 2008) studied FC within the default-mode network during rest and during continuous working memory task using the partial correlation method. They found global reduction in FC within the default mode network (DMN) during the memory task. Hasson et al. (Hasson et al., 2009) reported stronger FC during rest compared to continuous listening, between DMN and brain regions showing differential connectivity during listening. Shirer et al. (Shirer et al., 2012) used whole brain connectivity patterns for cognitive state decoding in healthy

subjects. The found increased FC during memory and subtraction tasks among task-related regions compared to rest.

As part of this dissertation, we compare FNC during resting-state and during performance of an auditory task. This study can clarify more how large-scale functional integration differs during resting-state compared to other cognitive states. We devote Chapter 2 of this manuscript to this subject.

## **1.10 Automatic Diagnosis of Mental Disorders**

In this section, we review the importance of accurate diagnosis of mental disorders using neuroimaging data. Later we discuss how abnormalities in functional network connectivity that were introduced in section 1.6, can be used as biomarker for mental disorders such as schizophrenia.

Population studies show that lifetime prevalence of all psychotic disorders is as high as 4%<sup>1</sup>. These disorders can impair normal life significantly and impose huge societal cost (Rice, 1999). Clinically, the patient's self-reported experiences and observed behavior over the longitudinal course of the illness constitute the basis for diagnosis. The overlapping symptoms of mental disorders and the absence of standard biologically-based clinical tests make differential diagnosis a challenging task. Early diagnosis of these diseases can significantly improve treatment response and reduce associated costs (McGlashan, 1998).

Advances in neuroimaging technologies in the past two decades have opened a new window into the structure and function of the healthy human brain as well as illuminating many brain disorders such as schizophrenia. Schizophrenia is among the most prevalent

---

<sup>1</sup> [http://www.nimh.nih.gov/statistics/SML\\_AASR.shtml](http://www.nimh.nih.gov/statistics/SML_AASR.shtml)

mental disorders affecting about 1% of the population worldwide (Bhugra, 2005; Wyatt et al., 1995). This devastating, chronic heterogeneous disease is usually characterized by disintegration in perception of reality, cognitive problems and chronic course with lasting impairment (Heinrichs and Zakzanis, 1998). Multiple structural and functional brain abnormalities are widely reported in patients with schizophrenia (Calhoun et al., 2009a; Karlsgodt et al., 2010; Shenton et al., 2001). Most neuroimaging-based studies of schizophrenia focus on showing aberrations of some features (structural or functional) in a patient group by comparing them to a control group. While many of these findings are statistically significant in the average sense, discrimination ability of those features is under question for classification purposes on a case-by-case basis. Since classification provides information for each individual subject, it is considered a much harder task than reporting group differences. In the case of classifying schizophrenia patients, a small number of training samples (subjects) and high dimensional data make it a challenging task to design an accurate, robust classifier for such a heterogeneous brain disorder.

In Chapter 3, we propose a framework for automatic diagnosis of mental disorders such as schizophrenia based on resting-state functional network connectivity features. The proposed framework can discriminate subjects with schizophrenia from healthy controls using just 5 minutes of resting-state fMRI data.

### **1.11 Preprocessing of fMRI Time-Series for Functional Connectivity Studies**

While FC studies are pervasive, there has been little attention to the assumptions linked to these studies. In recent years, there has been a debate in the neuroimaging community regarding the possible impact of intrinsic autocorrelation in fMRI time-courses on functional connectivity analysis outcome. Some researchers have even

questioned the validity of previous connectivity studies by arguing that not correcting for autocorrelation in fMRI time-series may result in spurious high correlation values (Christova et al., 2011; Georgopoulos and Mahan, 2013). These subject-level studies have confirmed that fMRI time-series are autocorrelated through the use of the Durbin-Watson statistic and have suggested to reduce the autocorrelation by using an autoregressive integrated moving average (ARIMA) model which is called prewhitening (Granger and Morris, 1976; Haugh, 1976).

Autocorrelation in fMRI data is assumed to originate from colored physical and physiological noise (Aguirre et al., 1997; Bullmore et al., 2001; Friston et al., 2000; Lenoski et al., 2008; Lund et al., 2006; Purdon and Weisskoff, 1998; Rajapakse et al., 1998; Zarahn et al., 1997). Several methods have been proposed to deal with autocorrelation in the general linear modeling framework (Friston et al., 2000; Gautama and Van Hulle, 2004; Lund et al., 2006; Woolrich et al., 2001). While some studies have suggested that intrinsic fMRI time-series autocorrelation is negligible compared to smoothing induced autocorrelation (Friston et al., 1995), others found it to be a significant confound (Christova et al., 2011; Lenoski et al., 2008; Zarahn et al., 1997).

In Chapter 4, the problem of autocorrelation on FC is discussed. We investigate Pearson correlation coefficient between two autocorrelated time-series. Furthermore, we discuss characteristics of fMRI time-series and propose a preprocessing pipeline for connectivity studies.

## **1.12 Notion of Autoconnectivity**

In the past two decades, the main focus of the neuroimaging community in the context of autocorrelation in fMRI time-series has been on methods to remove or

compensate for it. Methods such as prewhitening and precoloring have been widely adopted by researcher to eliminate or reduce the effect of autocorrelation on fMRI data analysis.

The neuronal process can be decomposed into evoked transients and intrinsic activity (Friston et al., 1995). If we assume that smooth hemodynamic response is the main source of autocorrelation in fMRI time-series, then it can be decomposed similar to the neuronal process into an evoked component which is phased-lock to the task and an intrinsic component (Friston et al., 1995). Worsley et al. (Worsley et al., 2002) showed that autocorrelation is mostly local to the gray matter.

The sources of autocorrelation and exact connection between autocorrelation and neuronal process have been open questions with very limited amount of research. Also to the best of our knowledge no one has investigated the autocorrelation in fMRI time-series as a potential source of information about functionality of human brain and for clinical use.

In Chapter 5 we introduce a new concept called autoconnectivity. Autoconnectivity is complementary to functional connectivity as it captures the connectivity of a voxel/region/network to itself. Properties of autoconnectivity during rest and task will be discussed and it will be shown how autoconnectivity is cognitive-state dependent (for example resting-state vs. task) and mental state dependent (for example in schizophrenia patients vs. healthy controls).

### **1.13 Organization of the Dissertation**

Four main studies are discussed in this dissertation. While the main focus is on functional connectivity and functional network connectivity, each chapter is devoted to

one aspect of functional connectivity in the human brain. In chapter 2, comparison of FNC during resting-state and during auditory oddball task is presented. We also discuss FNC during rest and task in schizophrenia patients and compare it to healthy controls. Chapter 3 discusses an emerging field of neuroimaging-based automatic diagnostic of mental disorders. It will be shown that functional network connectivity pattern during resting-state fMRI can be used as a biomarker for schizophrenia. A classification framework will be proposed based on resting-state FNC features that discriminates schizophrenia patients from healthy controls with high accuracy. The problem of autocorrelation in functional connectivity studies will be investigated in chapter 4. This problem will be discussed in theory, simulation and real fMRI data. Specifically, the hypothesis testing on FNC values will be investigated when the corresponding time-courses are autocorrelated. Autocorrelation is mostly attributed to noise in fMRI time-series. In chapter 5, the concept of autoconnectivity as a new perspective of human brain functionality will be introduced. Autoconnectivity captures connectivity of a brain voxel/region/network with itself as can be considered as a complement to functional connectivity. Autoconnectivity during rest and task and between healthy controls and schizophrenia patients will be investigated. It will be shown that combining FNC features with autoconnectivity feature can increase the accuracy of automatic diagnosis systems for mental disorders.

## **1.14 Datasets**

There are two main datasets used in the studies described in the following chapters. For convenience we call them “Hartford” dataset and “FBIRN” dataset hereafter.



### **1.14.1 Hartford Dataset**

Three sessions of fMRI data were collected from 28 healthy volunteers, two sessions of an AOD task and one session of resting state in the same day. All subjects gave written, informed, IRB approved consent at Hartford Hospital and were compensated for their participation. Exclusion criteria included having an axis I disorder on DSM IV-TR (First et al., 1995) as revealed by structured interview with the SCID, mental retardation (estimated full-scale IQ <70), history of major central nervous system injury or disease, family history of psychotic illness in a first-degree relative, past history of alcohol or drug dependence, or positive urine toxicologic screen for common drugs of abuse. Women were excluded for a positive urine pregnancy test. All subjects were screened for implanted ferromagnetic material. During practice prior to the scanning session, all participants were able to perform the oddball task successfully. All participants were scanned during both an auditory oddball task and at rest with eyes open while fixating on a cross hair.

The auditory oddball task consists of detecting an infrequent target sound within a series of regular and different sounds. The task consisted of two runs of auditory stimuli presented to each participant by a computer stimulus presentation system (<http://nilab.psychiatry.ubc.ca/vapp>) via insert earphones embedded within 30-dB sound attenuating MR compatible headphones. The standard stimulus was a 500-Hz tone, the target stimulus was a 1,000-Hz tone, and the novel stimuli consisted of nonrepeating random digital noises (e.g., tone sweeps, whistles). The target and novel stimuli each occurred with a probability of 0.10; the standard stimuli occurred with a probability of

0.80. The stimulus duration was 200 ms with a 1,000, 1,500, or 2,000 ms interstimulus interval. Figure 1-10 illustrates the AOD task.

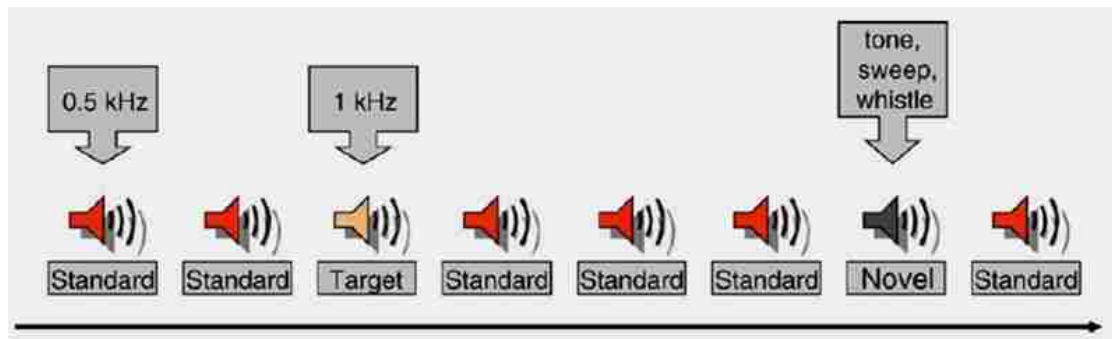


**Figure 1-10:** The AOD task used to collect the Hardford dataset. Subject should press the button just upon hearing target tones. Figure courtesy of (Kiehl and Liddle, 2001).

All stimuli were presented at 80 dB above the standard threshold of hearing. All participants reported that they could hear the stimuli and discriminate them from the background scanner noise. Prior to entry into the scanning room, each participant performed a practice block of 10 trials to ensure understanding of the instructions. The participants were instructed to respond as quickly and accurately as possible with their right index finger every time they heard the target stimulus and not to respond to the nontarget stimuli or the novel stimuli. An MRI compatible fiber-optic response device (Lightwave Medical, Vancouver, BC) was used to acquire behavioral responses for both tasks.

The stimulus paradigm data acquisition techniques and previously found stimulus-related activation are described more fully elsewhere (Kiehl and Liddle, 2001; Kiehl et al., 2005). Participants also performed a 5 min resting state scan (rest) and were instructed to rest quietly without falling asleep with their eyes open (eyes were open to avoid the possibility that participants would fall asleep).

### **1.14.1.1 Image Acquisition**

Scans were acquired at the Olin Neuropsychiatry Research Center at the Institute of Living/Hartford Hospital on a Siemens Allegra 3T dedicated head scanner equipped with 40 mT/m gradients and a standard quadrature head coil. The transaxial functional scans were acquired using gradient-echo echo-planar-imaging with the following parameters (repeat time (TR) = 1.50 s, echo time (TE) = 27 ms, field of view = 24 cm, acquisition matrix =  $64 \times 64$ , flip angle =  $70^\circ$ , voxel size =  $3.75 \times 3.75 \times 4 \text{ mm}^3$ , slice thickness = 4 mm, gap = 1 mm, 29 slices, ascending acquisition). Six “dummy” scans were performed at the beginning to allow for longitudinal equilibrium, after which the paradigm was automatically triggered to start by the scanner. auditory oddball task and resting state scans consisted of 8 and 5 minute run respectively.

### **1.14.2 FBRIN Dataset**

FBRIN data set consist of 195 patients with schizophrenia and 175 healthy volunteers that were matched for age, gender, handedness, and race distributions. The subjects were recruited across seven different sites in the United States as a part of the Functional Imaging Biomedical Informatics Research Network (FBIRN) (Potkin & Ford, 2009). All patients included in the study had been diagnosed with schizophrenia based on the Structured Clinical Interview for DSM-IV-TR Axis I Disorders (SCID-I/P)(First, Spitzer, Gibbon, & Williams, 2002a). All patients were clinically stable on antipsychotic medication for at least two months prior to scanning. Exclusion criteria for both schizophrenia patients and healthy volunteers included a history of major medical illness, contraindications for MRI, poor vision even with MRI compatible corrective lenses, an IQ less than 75, a history of drug dependence in last 5 years or a current substance abuse

disorder. Additionally patients with extrapyramidal symptoms and healthy volunteers with a current or past history of major neurological or psychiatric illness (SCIS-I/NP)(First, Spitzer, Gibbon, & Williams, 2002b) or with a first-degree relative with Axis-I psychotic disorder diagnosis were also excluded.

All subjects gave written informed consent to share their de-identified data between centers and the study was approved by the Institutional Review Boards of the following participating data collection sites for the subjects included: University of California Irvine, the University of California Los Angeles, the University of California San Francisco, Duke University, University of North Carolina, University of New Mexico, University of Iowa, and University of Minnesota.

#### **1.14.2.1 Imaging Parameters**

Imaging data for six of the seven sites was collected on a 3T Siemens Tim® Trio System and on a 3T General Electric Discovery MR750 scanner at one site. Resting state fMRI scans were acquired using a standard gradient-echo echo planar imaging paradigm: FOV of 220x220 mm (64x64 matrix), TR = 2 sec, TE = 30 ms, FA = 77<sup>0</sup>, 162 volumes, 32 sequential ascending axial slices of 4 mm thickness and 1 mm skip. Subjects had their eyes closed during the resting state scan.

#### **1.14.2.2 Data preprocessing and quality control**

First we computed signal-fluctuation-to-noise (SFNR)(Friedman & Glover, 2006) for all 370 subjects' EPI data sets as implemented in *dataQuality* matlab package<sup>1</sup>. SFNR is defined as the ratio of mean signal intensity across time and space to the average standard deviation of the same voxels' time series in a ROI in the center of brain. Data

---

<sup>1</sup> <http://cbi.nyu.edu/software/dataQuality.php>

processing was performed using a combination of toolboxes (AFNI<sup>1</sup>, SPM<sup>2</sup>, GIFT<sup>3</sup>) and custom code written in Matlab<sup>4</sup>. We performed rigid body motion correction using the INRIAlign(Freire & Mangin, 2001) toolbox in SPM to correct for subject head motion. All subjects that had SFNR < 150 and a maximum root mean squared translation > 4 mm were excluded from further analysis. Maximum root mean squared translation is defined as  $\{\sqrt{\sum(x^2 + y^2 + z^2)}\}$ , where  $x$ ,  $y$  and  $z$  are the estimated motion (in mm) in X, Y, and Z directions. This excluded a total of 56 subjects, resulting in 314 subjects (163 HC and 151 SZ) for subsequent analysis. Similar stringent inclusion procedures have been shown to minimize the influence of head motion on the subsequent functional connectivity measures (Power, Barnes, Snyder, Schlaggar, & Petersen, 2012; Satterthwaite et al., 2012; Van Dijk, Sabuncu, & Buckner, 2012). The maximum translation as well as root mean square translation of the retained subjects did not differ between groups. Average framewise displacement (FD)(Power et al., 2012), i.e. the average across frames of the absolute sum of instantaneous head motion in each direction from the previous frame, was slightly higher in the patient group than healthy controls (mean FD for each group,  $t = X$ ,  $p = X$ ).

For the retained subjects, we performed slice-timing correction to account for timing differences in slice acquisition. Then the fMRI data were despiked using AFNI's 3dDespike algorithm to mitigate the impact of outliers. The fMRI data were subsequently warped to a Montreal Neurological Institute (MNI) template and resampled to 3 mm<sup>3</sup> isotropic voxels. Instead of Gaussian smoothing, we smoothed the data to 6 mm full

---

<sup>1</sup> <http://afni.nimh.nih.gov/>

<sup>2</sup> <http://www.fil.ion.ucl.ac.uk/spm/>

<sup>3</sup> <http://mialab.mrn.org/software/gift/index.html>

<sup>4</sup> <http://www.mathworks.com/products/matlab>

width at half maximum (FWHM) using AFNI's BlurToFWHM algorithm which performs smoothing by a conservative finite difference approximation to the diffusion equation. This approach has been shown to reduce scanner specific variability in smoothness providing "smoothness equivalence" to data across sites (Friedman, Glover, Krenz, & Magnotta, 2006). Since the mean signal (and therefore signal variance) at one site (GE scanner) was much higher than rest of the site data, data were variance normalized. This step removed site specific differences in signal fluctuation.

## **Chapter 2: Functional Network Connectivity during Rest and Task**

## 2.1 Motivation

Studying the differences between rest and task to explore changes in the interaction among functional networks in these two states can clarify how the brain responds to a given task. Most of the studies mentioned in section 1.9 used constant or block design tasks in order to steadily engage parts of the brain in that particular task and make the comparison more meaningful. However, a main drawback of the constant task is the possibility that the subject loses his/her concentration during the course of the paradigm. Also, predictability of block design tasks may affect brain connectivity. In contrast, the auditory oddball (AOD) task requires continuous attention throughout the experiment. A passive listening task is a combination of listening, attention and active responding and likely some resting as well. Moreover most of the mentioned studies used a small cohort.

The motivation for this study is to comprehensively compare FNC among relevant (non-artifactual) functional networks during the resting state and during and event-related task such as AOD task in healthy subjects. The main question we addressed is how FNC differs during rest versus during task performance in healthy subjects. We predicted that DMN and task-related networks would play key roles in our findings. The default-mode network is a set of brain regions showing activation during the rest and deactivation during most cognitive tasks (Buckner et al., 2008; Raichle et al., 2001). This network is not only relevant to understanding brain's intrinsic functional activity but is also important in studying a number of neurological disorders (Broyd et al., 2009; Garrity et al., 2007a; Greicius, 2008).



## 2.2 Proposed Approach

The block diagram in Figure 2-1 shows our approach. For this study we used the Hartford dataset. The raw fMRI data was first preprocessed. Then preprocessed resting state and AOD data were analyzed with group ICA. Subject specific spatial maps and time-courses were computed for rest and AOD conditions using back reconstruction. Next, FNC analysis was performed on the subject specific ICA time-courses. Finally by using a paired t-test, significant differences in FNC during rest versus task are highlighted. Since filtering ICA time-courses prior to FNC analysis can impact the results, we also report and discuss the results on both strongly filtered and weakly filtered time courses. Each of these steps is described in more detail in the next sections.

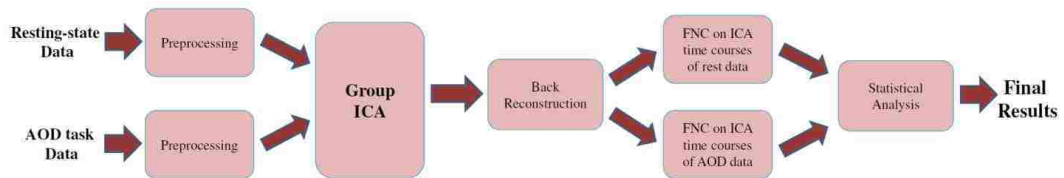


**Figure 2-1:** Block diagram of the proposed approach

### 2.2.1 Preprocessing

Data were preprocessed using SPM5 software (<http://fil.ion.ucl.ac.uk/spm/software/spm5>). Data were motion corrected, spatially normalized into standard MNI space and slightly subsampled to voxel size  $3 \times 3 \times 3 \text{ mm}^3$ , resulting in  $53 \times 63 \times 46$  voxels. Next, spatial smoothing with a  $10 \times 10 \times 10 \text{ mm}^3$  FWHM Gaussian kernel was performed.

### 2.2.2 Group ICA and Back Reconstruction

Prior to the ICA, dimensionality of data was reduced at two levels using principal component analysis (PCA). First at the subject level, dimensionality was reduced to 80.

Then reduced data from all subjects and all sessions were concatenated together and put through another reduction step. The number of components for the second level reduction was estimated to be 20 by minimum description length (MDL) criterion (Li et al., 2007). This is also the number of IC components. Note the MDL is a data driven approach, so it is not dependent on whether data are collected at rest or during a task.

Infomax group sICA (Calhoun et al., 2001a) was conducted to decompose the aggregated data into components using GIFT software (<http://icatb.sourceforge.net/>). SICA applied to fMRI data identifies temporally-coherent networks (TCNs) by estimating maximally independent spatial sources, referred to as spatial maps (SMs) and their corresponding time-courses (TCs). Rest and AOD data were analyzed in one group ICA instead of two separate ICAs so that a tighter comparison between rest and task could be performed without additional variability induced due to trying to match components from separate ICA analyses. As mentioned before, compared to rest the AOD task also modulates some of the spatial maps as discussed by Calhoun et al. (Calhoun et al., 2008a). But, the change is subtle and the spatial maps of the components for rest and task are highly spatially correlated. Moreover, each ICA component is a temporally coherent network since the ICA model constrains the fluctuations of each voxel in a given component to have the same time course. So, considering the fact that these components were matched by the group ICA approach, it is relevant and meaningful to compare the time-courses of TCNs in the resting state and during a task.

In order to validate the number of ICA components chosen by MDL and also measure the robustness of each of them, ICA was repeated 10 times using ICASSO<sup>1</sup>. Each time ICA algorithm was started from a different initial point and the resulting components were

---

<sup>1</sup> <http://www.cis.hut.fi/projects/ica/icasso>

clustered to estimate the reliability of the decomposition (Himberg et al., 2004). Robustness and reliability of components were well validated by ICASSO results showing compact clusters.

In order to estimate subject-specific SMs and TCs, the recently developed GICA3 back-reconstruction method based on PCA compression and projection was used (Calhoun et al., 2001a; Erhardt et al., 2011). Subject-specific TCs were reconstructed separately for rest and task.

### **2.2.3 Component Selection**

Spatial maps were reconstructed and converted to Z values for each of the subjects. All of the components were visually inspected and the non-artifactual components were selected. To compute the degree of task-relatedness of the components, regression analysis of ICA TCs was conducted. Target, novel and standard stimulations were modeled by convolving each of their corresponding paradigms with canonical hemodynamic response function using SPM5. These three regressors along with their first derivative, 6 cosine signals for noise removal and a constant term were put together to form a regressor matrix. After performing regression analysis, t-tests were computed on the beta values corresponding to the target and novel stimulations.

### **2.2.4 Functional Network Connectivity**

The functional network connectivity toolbox (<http://icatb.sourceforge.net/fnc/software/FncVer2.2.zip>) was used for the FNC analysis. As mentioned before, significant temporal correlation can exist among the sICA TCs. The FNC toolbox computes maximum lagged correlation among the components. The maximum lagged correlation was computed as in (Jafri et al., 2008). First the TCs of the ICA components were

interpolated to allow us detection of any delays less than the TR of the scanner (Calhoun et al., 2000; Ford et al., 2005). We assume  $\rho$  for the correlation between two TCs named  $\bar{X}$  and  $\bar{Y}$  of dimension  $T \times 1$  where  $T$  is the number of time points in TCs. Starting reference point of the TCs is named  $i_0$  and  $\Delta i$  represents the non-integer change in time.  $\rho_{\Delta i}$  represents the correlation between  $\bar{X}_{i_0}$  which is vector  $\bar{X}$  at the reference time point  $i_0$  and  $\bar{Y}_{i_0+\Delta i}$  which is vector  $\bar{Y}$  shifted  $\Delta i$  from the reference time point. This correlation between the overlapping points of  $\bar{X}_{i_0}$  and  $\bar{Y}_{i_0+\Delta i}$  can be computed as follows:

$$\rho_{\Delta i} = \frac{(\bar{X}_{i_0}^T)(\bar{Y}_{i_0+\Delta i})}{\sqrt{\bar{X}_{i_0}^T \bar{X}_{i_0}} \times \sqrt{\bar{Y}_{i_0+\Delta i}^T \bar{Y}_{i_0+\Delta i}}} \quad (2-1)$$

The  $\rho_{\Delta i}$  vector is calculated for each pair of TCs when one of TCs is shifted  $\Delta i$  units from -3 to +3 seconds (i.e.  $\pm 2$  TR). The maximum correlation and the corresponding lag is calculated and saved for each of the subjects and separately for rest and task. Allowing lag between signals is important to account for variations in hemodynamic response shapes among brain regions as well as among subjects. Although the lag can give an idea of temporal order of fMRI TCs, but the source of the lag is not completely understood and could be due to mixture of functional and physiological effects. For these reasons, we will not report any analysis on the lag parameter in this study. The lag corresponding to the maximum correlation was checked to be distributed in  $\pm 3$  seconds interval and often away from its maximum or minimum.

Prior to computing correlations, ICA TCs were filtered. There are reports that show task-related and other interesting information resides in lower frequencies while noise and artifacts contributes mostly to the higher frequency contents of the TCs (Cordes et al., 2001a). We performed FNC analysis both on strongly filtered and weakly filtered

components to further explore the filtering effects. In the weak filtering approach, a band pass Butterworth filter with cut-off frequencies at 0.017 Hz and 0.32 Hz was used to suppress the very low and very high frequencies, respectively. In the strong filtering approach, the cut-off frequencies were set at 0.017 Hz and 0.15 Hz. In the remainder of the paper we call the weakly filtered and strongly filtered TCs, unfiltered and filtered TCs, respectively.

### **2.2.5 Statistical Analysis**

For all FNC analyses, correlations were transformed to z-scores using Fisher's transformation ( $z = \text{arctanh}(r)$ ). Then, robustness of maximum lagged correlation between each pair of TCs was tested separately for rest and task using t-tests. Finally, to determine the significant differences of rest versus task, paired t-tests were conducted on the two groups. The cut-off p-value for all of the tests was set at  $p < 0.05$  and was corrected for multiple comparisons using the false discovery rate (FDR) method (Benjamini and Hochberg, 1995; Genovese et al., 2002).

### **2.2.6 Functional Network Volumes**

We found it interesting to compare functional network volumes during rest and task. So, we thresholded each back reconstructed IC component at  $\text{mean} + 3 \times \text{standard deviation}$  level for each subject. Then we counted number of voxels survived the threshold for each subject in each state. We compared the volumes by means of paired-t-test at .05 level corrected for multiple comparisons (FDR method).

### **2.2.7 Maximum Activation**

As the volume of functional networks may change between the states, the level of activation can change too. To measure this, we performed a voxel-wise one sample t-test on each component (each subject is an observation) for each state. Then the highest T-value of the test was saved. Note that the highest activated voxel is not necessarily the same for rest and task.

### **2.2.8 Validation**

After the whole experiment, we tried to identify the points of concern in our analysis and address them with additional validation steps. Specifically, we focused on two issues which are: one group ICA instead of two separate ones and effect of ICA on FNC analysis. Validation steps are described in this subsection.

As shown in Figure 2-1, one group ICA was done on aggregated rest and AOD data for the reasons mentioned before. To show that this has not affected the results in an undesirable way, we repeated the FNC analysis with two separate ICA on rest and task. The results were compared with the one group ICA results using paired t-test and no effect was found ( $p$ -value threshold of 0.05 corrected for FDR).

FNC was computed on ICA TCs as defined in section 2.2.4. We compared the results with a hybrid ICA seed-based approach (Kelly et al., 2010). In the hybrid approach, first we created network masks by thresholding ICA SMs and then used them to extract original fMRI time courses for each subject. After detrending and filtering, the TCs of voxels within each map (network) were averaged together and the maximum lagged correlation coefficients were computed among the networks separately for rest and task. The same statistical tests mentioned in section 2.2.5 were conducted on the

outcomes. Again paired-t test was used to compare the FNC results with our method and no effect was found (p-value threshold of 0.05 corrected for FDR). This validates FNC analysis on ICA TCs. For clarity and due to lack of space, we only report results from the proposed approach.

### **2.3 Results**

From the 20 ICA components, 10 components were selected as non-artifactual, relevant networks. Figure 2-2 illustrates the spatial maps of the selected IC components. These networks are: frontal-parietal networks (IC #6 and 7), visual network (IC #4), parietal network (IC #14), auditory network (IC #12), motor network (IC #16), cerebellum network (IC #15) and default-mode networks (IC #18, 5, 3). In order to determine task-relatedness of each IC, we regressed the corresponding time-courses against task paradigms (see section 2.2.3 for more details). The p-value for the regression coefficients corresponding to novel and target stimulations are color-coded in the bottom left and right corners of each component in Figure 2-2 respectively (reference color bar shown on the right side of the figure). As expected, auditory component (IC #12) is the most task-related component. Parietal component (IC #14) is significantly more active during novel stimulations of the task compared to target stimulations. Detailed information of each spatial map such as regions of activation, Brodmann area, volume and peak activation t-value and coordinates are provided in Table 2-1.

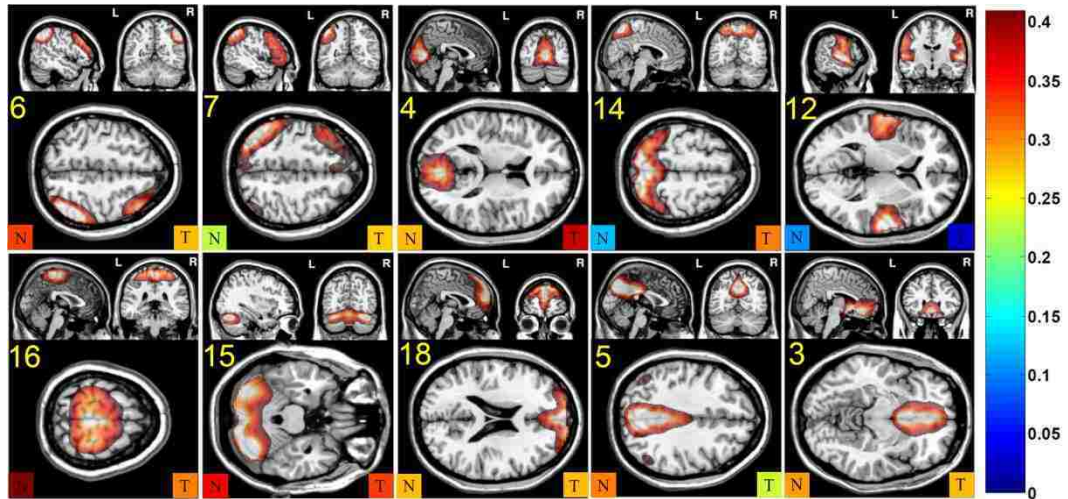


**Figure 2-2:** Spatial maps of the ten selected IC components. The time-course of each component during AOD task was regressed against task paradigms (see section 2.3.3). The p-value for the regression coefficients corresponding to novel and target stimulations are color-coded in the bottom left and right corners of each component respectively. Reference color bar is shown on the right side of the figure.

The maximum lagged correlation was computed for each of the subjects and for rest and AOD separately. For each of the correlation pairs, student t-test was conducted at 0.05 level corrected for FDR. This process was repeated for filtered components. In Figure 2-3 the average correlation and the corresponding t-values are shown for rest and AOD. The black circles determine the correlation pairs that survived the t-test.

To determine which correlation pairs are significantly different between rest and task, paired t-tests were conducted at FDR corrected 0.05 level. Also a mean correlation difference between rest and AOD (rest-aod) was computed for each correlation pair. The results are shown in Figure 2-4. Starred pairs indicate those surviving the paired t-test.

Table 2-2 summarizes the information about the significant pairs surviving the paired t-test (pairs with black stars in Figure 2-4). Mean correlation, t-test results, mean correlation difference and paired t-test values are included in the table for both filtered and unfiltered components.



**Table 2-1:** Brain regions, corresponding Brodmann areas, volumes, maximum t-values and spatial

coordinates of each component in Talairach space.

<b>Attentional Networks</b>	BA	Vol.	T <sub>max</sub>	X-Y-Z Coordinate
<b>IC 6</b>				
R Middle Frontal Gyrus	8	26.7	52.2	(42,20, 43)
R Inferior Parietal Lobule	40	21.2	26.2	(53, -44, 49)
R Inferior Frontal Gyrus	44, 45	25.5	19.9	(53, 27, 21)
R Superior Frontal Gyrus	6, 8, 9	23.4	24.5	(36, 20, 52)
<b>IC 7</b>				
L Middle Frontal Gyrus	8	43.5	24.0	(-50, 25, 26)
L Inferior Parietal Lobule	40	21.7	25.3	(-50,-44,49)
L Inferior Frontal Gyrus	44, 45	32.4	20.8	(-50, 24, 21)
L Superior Frontal Gyrus	6,8,9	29.3	17.5	(-6, 31, 43)
<b>Default-Mode Networks</b>	BA	Vol.	T <sub>max</sub>	X-Y-Z Coordinate
<b>IC 5</b>				
R/L Precuneus	7	28.0/ 27.0	43.1/ 47.3	(6, -51, 33)/ (-3, -54, 33)
R/L Cingulate Gyrus	23, 24, 31	14.5/ 15.7	45.3/ 47.3	(6, -48, 27)/ (-6, -42, 35)
<b>IC 3</b>				
R/L Anterior Cingulate Cortex	32	10.8/ 10.6	30.8/ 30.4	(15, 14, -8)/ (-9, 5, -10)
R/ L Medial Frontal Gyrus	9, 10	14.4/ 13.2	26.7/ 27.0	(3, 34, -12)/ (-3, 43, -7)
<b>Frontal Network</b>	BA	Vol.	T <sub>max</sub>	X-Y-Z Coordinate
<b>IC 18</b>				
R/L Superior Frontal Gyrus	6,8, 9	33.1/ 35.6	27.8/ 24.6	(3, 11, 49)/ (0, 8, 49)
R/L Medial Frontal Gyrus	8,9, 10	21.8/ 21.8	29.7/ 30.4	(3, 17, 43)/ (-3, 44, 14)
<b>Visual Network</b>	BA	Vol.	T <sub>max</sub>	X-Y-Z Coordinate
<b>IC 4</b>				
L/R Cuneus	7, 19	15.0/ 18.4	33.3/ 36.9	(9, -61, 9)/ (-12, -64, 4)
L/R Lingual Gyrus	18, 19	12.1/ 14.9	33.7/ 35.7	(3, -73, 1)/ (-12, -61, 3)
<b>Parietal Network</b>	BA	Vol.	T <sub>max</sub>	X-Y-Z Coordinate
<b>IC 14</b>				
R/L Superior Parietal Lobule	5, 7	6.8/ 6.5	36.4/ 31.2	(21, -67, 56)/ (-24, -82, 4)
R/L Precuneus	7	29.0/ 27.6	32.5/ 35.4	(3, -52, 61)/ (-3, -52, 6)
R/L Cuneus	7, 19	8.5/ 7.3	10.9/ 16.3	(30, -83, 37)/ (-27, -77, 3)
<b>Motor Network</b>	BA	Vol.	T <sub>max</sub>	X-Y-Z Coordinate
<b>IC 16</b>				
R/L Precentral Gyrus	4, 6	26.4/ 22.8	33.7/ 31.8	(30, -29, 56)/ (-27, -23, 5)
R/L Medial Frontal Gyrus	6, 32	15.7/ 17.1	38.8/ 34.1	(3, -9, 58)/ (-3, -12, 5)
R/L Postcentral Gyrus	1, 2, 3	21.7/ 28.1	30.9/ 29.8	(30, -32, 66)/ (-21, -35, 63)
<b>Auditory Network</b>	BA	Vol.	T <sub>max</sub>	X-Y-Z Coordinate
<b>IC 12</b>				
R/L Superior Temporal Gyrus	22	25.5/ 24.8	28.9/ 29.6	(50, 3, -3)/ (-56, -9, 3)
R/L Postcentral Gyrus	1, 2, 3	13.2/ 16.2	27.2/ 25.1	(59, -20, 15)/ (-48, -17, 1)
R/L Insula	13, 47	16.9/ 17.0	29.1/ 26.4	(45, 0, 0)/ (-42, -6, 0)
<b>Cerebellum Network</b>	BA	Vol.	T <sub>max</sub>	X-Y-Z Coordinates
<b>IC 15</b>				
R/L Declive	*	17.3/ 15.0	28.6/ 29.2	(30, -68, -19)/ (-39, -62, -2)
R/L Culmen	*	15.4/ 15.3	24.4/ 25.8	(30, -62, -25)/ (-36, -56, -2)

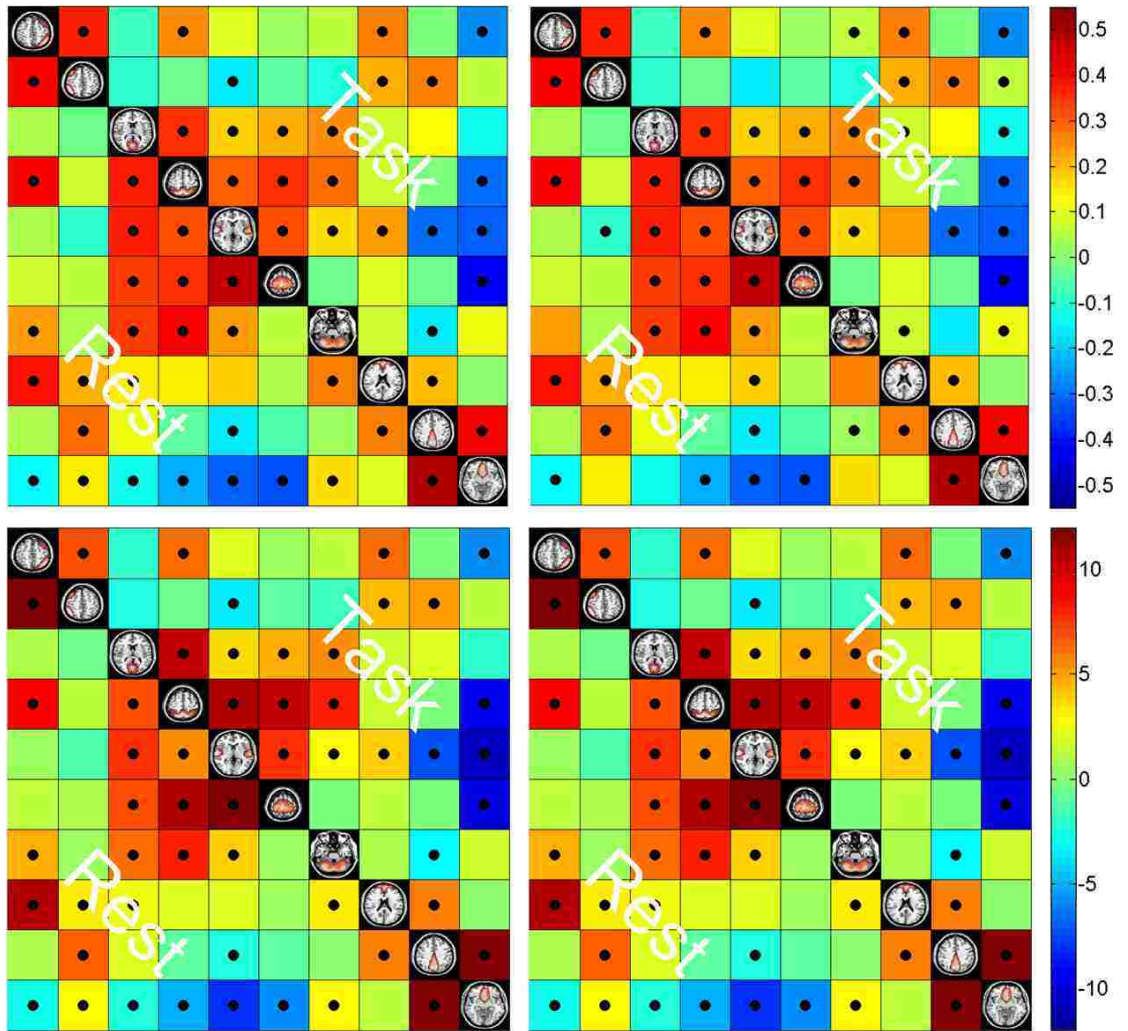


**Figure 2-3:** Top row: mean of maximum lagged correlation pairs for rest and AOD. Bottom row: T-value of each correlation pair resulted from Student t-test. Left column: unfiltered components. Right column: filtered components. Black circles indicate the pairs surviving the t-test with a FDR corrected p-value threshold of 0.05.

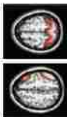


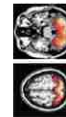






**Figure 2-4:** Left: mean maximum lagged correlation difference between rest and AOD (rest-AOD) for filtered and unfiltered components. Right: T-value resulting from paired t-test with FDR corrected p-value threshold of 0.05 for filtered and unfiltered components. Stars: pairs surviving the paired t-test

As described in 2.2.6 and 2.2.7, we also calculated network volumes and peak activation in each network during rest and task. The results are illustrated in Figure 2-5 and Figure 2-6 respectively.

Also the mean of all 45 correlation pairs, standard deviation, absolute mean and standard deviation for absolute mean values were computed for each subject. The results are averaged over subjects and are shown in Table 2-3. We conducted a t-test on the mean correlation and it survived the test at 0.05 level (p-value of 0.010 and 0.014 for unfiltered and filtered schemes respectively).

**Table 2-2:** Detailed information about significant pairs. Left: means of correlation, standard deviation and p-values resulting from the t-test for each pair in rest. Middle: mean of correlation, standard deviation and p-value resulting from the t-test for each corresponding pair in the AOD task. Right: mean correlation difference (rest-AOD) along with p-value resulting from paired t-test. Bolded p-values survived t-test or paired t-test with 0.05 threshold corrected for FDR.

Components	Rest			AOD			Paired t-test		
	Cor. (unfiltered/filtered)	Std. (unfiltered/filtered)	P-value (unfiltered/filtered)	Cor. (unfiltered/filtered)	Std. (unfiltered/filtered)	P-value (unfiltered/filtered)	Cor. diff (unfiltered/filtered)	P-value (unfiltered/filtered)	
	+0.396/+0.411	0.216/0.229	8.88E-09/1.39E-08	+0.256/+0.237	0.213/0.221	2.23E-05/1.18E-04	+0.140/+0.174	6.02E-03/4.41E-04	
	+0.238/+0.223	0.260/0.305	6.25E-04/5.04E-03	+0.065/0.104	0.284/0.289	7.38E-01/2.96E-01	+0.173/+0.119	1.39E-02/1.02E-01	
	+0.374/+0.418	0.232/0.258	9.35E-08/5.45E-08	+0.173/+0.192	0.247/0.281	1.09E-02/9.91E-03	+0.200/+0.226	1.71E-03/4.79E-03	
	+0.412/+0.460	0.239/0.250	3.07E-08/1.11E-08	+0.280/+0.295	0.175/0.189	2.37E-07/4.56E-07	+0.132/+0.165	3.06E-02/1.95E-03	
	+0.466/+0.541	0.155/0.180	5.46E-12/1.65E-11	+0.320/+0.362	0.203/0.249	2.28E-07/8.08E-07	+0.146/+0.179	2.09E-03/3.19E-03	
	+0.269/+0.365	0.385/0.355	4.54E-03/7.28E-05	+0.081/+0.143	0.365/0.393	6.13E-01/1.97E-01	+0.188/+0.222	4.33E-02/5.65E-03	
	+0.018/+0.063	0.318/0.331	6.49E-01/7.42E-01	-0.164/-0.139	0.271/0.283	3.56E-04/1.84E-03	+0.181/+0.203	1.30E-02/1.23E-03	
	+0.498/+0.545	0.145/0.161	2.35E-13/8.65E-13	+0.398/+0.383	0.119/0.198	9.85E-14/4.78E-09	+0.100/+0.162	1.52E-02/1.79E-03	

Left: means of correlation, standard deviation, and P-values resulting from the t-test for each pair in rest. Middle: mean of correlation, standard deviation, and P-value resulting from the t-test for each corresponding pair in the AOD task. Right: mean correlation difference (rest-AOD) along with P-value resulting from paired t-test. P-values survived paired t-test at FDR corrected 0.05 level.

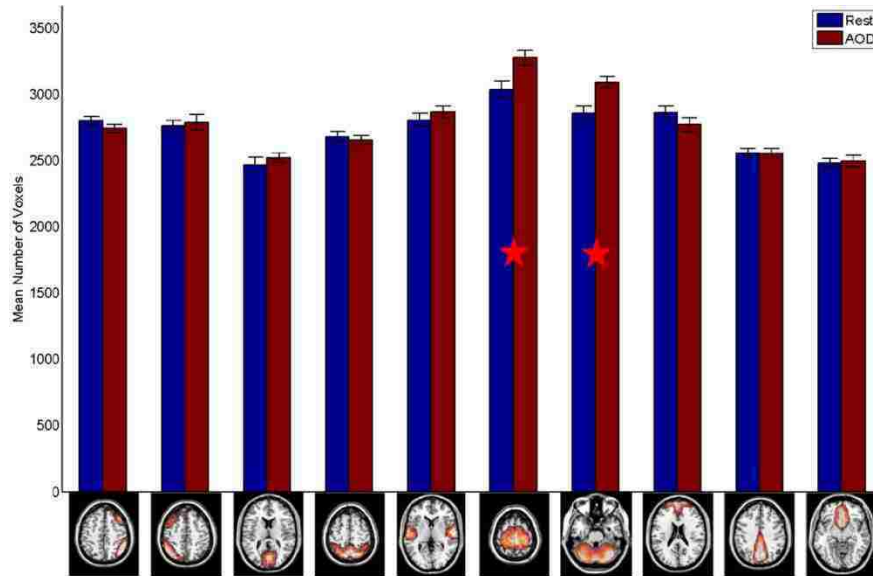


**Figure 2-5:** Volume of each functional network during rest and task averaged over subjects. Each black error bar is symmetric and twice the standard error of the mean long. Red stars show components surviving paired t-test at FDR corrected 0.05 level between the volumes in the two states.

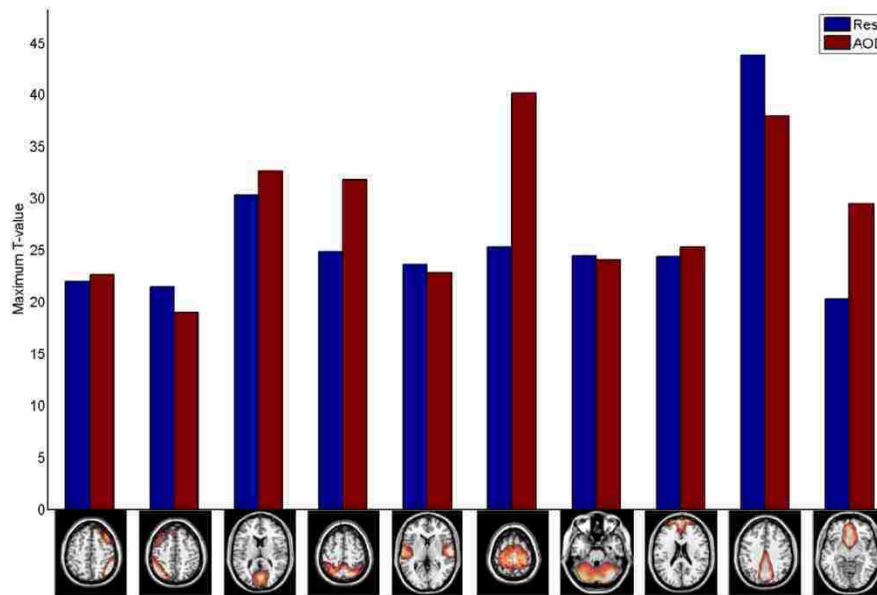


**Figure 2-6:** Peak activation for each component during rest and task. A voxel-wise one sample t-test on each component (each subject is an observation) for each state was performed. Then the highest T-value of the test is illustrated in this Figure. The highest activated voxel is not necessarily the same for rest and task.

**Table 2-3:** Mean, standard deviation (Std), absolute (Abs) mean and standard deviation of absolute mean for all 45 correlation pairs averaged over all subjects.

	Mean	Abs. Mean	Std	Abs. Std
Rest	0.136/	0.345/	0.326/	0.138/
(unfiltered/filtered)	0.147	0.361	0.344	0.155
AOD	0.066/	0.301/	0.314/	0.122/
(unfiltered/filtered)	0.074	0.302	0.319	0.138

## 2.4 Discussion

We compared functional network connectivity in both the resting-state and during performance of an AOD task in healthy subjects. ICA was successfully applied to aggregated resting and AOD data and was capable of extracting most relevant networks. Maximum lagged correlation was computed on back-reconstructed subject-specific time-courses of the selected networks. Statistical analysis showed several pairs of networks which differed significantly between rest and task in terms of correlation and robustness. Several interesting points can be inferred from the results.

FNC is weaker than intra-network connectivity. The correlation between each pair of networks is limited to the  $[-0.55, +0.55]$  range. The maximum correlation was between two default mode networks (IC #3 and #5) (Rest: +0.498/ AOD: +0.398). The maximum negative correlation was between IC #16 and IC #3 (Rest: -0.339/ AOD: -0.426). IC #16 is the motor network and IC #3 is the anterior node of DMN. As seen in Figure 2-3, most of the correlations are positive in both rest and AOD.

Black circles in Figure 2-3 show the pairs surviving the t-test. At rest 27 and during AOD, 24 pairs of 45 are consistent for unfiltered components. For filtered components these numbers are 24 and 26 respectively. Most of the difference comes from the pairs associated with IC #12 (auditory network), IC #15 (cerebellum) and IC #3 (anterior node of DMN).

Starred pairs in Figure 2-4 differed significantly between rest and task. Detailed information regarding these pairs is presented in Table 2-2. There are 5 and 7 significant differences for unfiltered and filtered components respectively. Most the differences coming from pairs including temporal (IC #12), cerebellum (IC #15) and DMN networks (IC #3 and #5). It is evident that FNC is higher during rest compared to task in most of the pairs. This suggests that FC at network level is consistent with most the findings at region level reported higher connectivity during rest compared to task (Fransson, 2006; Hasson et al., 2009; Nir et al., 2006). For example, FNC between anterior and posterior nodes of DMN (IC #3 and #5) decreased significantly during AOD task consistent with work by Fransson (Fransson, 2006).

We used t-test to compared FNC during rest and task. Our aim was to get very specific about the differences so we used this univariate test. But, there are well-developed multivariate methods such as PCA (Damaraju et al., 2010) and canonical correlation analysis (CCA) that can be applied to the connectivity matrices in each state.

We also examined the volume and peak activation of functional network during rest and task. As shown in Figure 2-5, just cerebellum and motor networks (IC #15 and #16) increased in volume significantly during task compared to rest. It has been previously shown that AOD task modulates brain functional networks (Calhoun et al.,

2008a). The peak activation in Figure 2-6 shows significant increase in parietal (IC #14), motor (IC #16) and anterior node of DMN (IC #3) during task compared to rest. Posterior node of DMN (IC #5) demonstrates reduce peak activation during task. Other networks show similar level of peak activation in both states.

Table 2-3 provides a summary of global decrease in FNC during the performance of AOD task compared to the resting state. The source of these phenomena is not well-studied yet but our results accord well with the results of Nir et al. (2006) reported strong slow coherence activation patterns during the resting-state. It has also been proposed that performing demanding tasks requires full attention which can suppress spontaneous thoughts (Fransson, 2006). Our results also suggests that performing an active task like AOD, may be facilitated by using more neurons (larger functional network) and higher activation in specialized networks rather than collaboration of different brain networks. All pairs except one that show significant differential connectivity between rest and task (Table 2-2), includes networks with significant change in size or peak activation. Larger volume of selected networks along with reduction in connectivity during the performance of AOD task consolidates previously suggested idea that recruitment of neurons for performing cognitive task may reduce the hemodynamic coupling between the brain regions (Morgan and Price, 2004).

Since contradicting results have been reported previously, it is plausible to accept that FNC during the task is task dependent. Some studies have reported stronger connectivity during the performance of the task (Aguirre et al., 1997; Harrison et al., 2008; Shirer et al., 2012). Type, length and design of the task may change the results.



Our results extend previous works demonstrating that global FC reduction is present not only among specific brain regions but also among different functional networks. Most of the previous studies were limited to few preselected brain regions using seed-based approach while we used ICA to extract all non-artifactual brain networks. ICA methodology doesn't require selecting seed voxels. The main advantage of using ICA in this experiment is its ability to decompose the fMRI data into independent spatial maps and corresponding time-courses. Since we want to measure the functional connectivity among networks (FNC) and not functional connectivity among regions (FC), ICA is an ideal choice. This is not trivial using seed-based or atlas-based methods. Moreover, ICA is a multivariate data driven method which does not require a specific temporal model. Some previous studies have used ICA but just for defining regions of interests (ROIs) and selecting the seed voxels and not for FNC analysis (Shirer et al., 2012). To our knowledge, this is the first study comparing FNC between rest and task.

We examined both unfiltered and highly filtered IC time courses in the FNC analysis. A major observation is that FNC results are not significantly dependent on specific filtering choice. Figure 2-3 reveals that only three change in consistent pairs between unfiltered and filtered components at rest and two such changes in AOD. The  $t$ -value is higher for most of the pairs for unfiltered components compared to filtered ones. Figure 2-4 demonstrates that are two more significant pairs for filtered components that are not seen for the unfiltered components. Only one pair for the unfiltered components is missing for the filtered components. The correlation is higher for filtered than unfiltered components in most pairs. We conclude that FNC fluctuations appear to be focused in a

narrow frequency range as weak and strong filtering of ICA time-courses did not alter the results significantly. This is in line with previous findings (Cordes et al., 2001a; Sun et al., 2004).

The present study (Arbabshirani et al., 2013a) is a step toward better understanding how the brain responds during rest versus a straightforward constrained cognitive task. We show several interesting results. In summary, we found that FNC is stronger during rest compared to AOD task. A global drop in FNC was observed during the performance of AOD task. We also showed that motor and cerebellum networks are significantly larger during the performance of the task. Also, parietal (IC #14), motor (IC #16) and anterior node of DMN (IC #3) demonstrated significantly higher peak activation during task compared to rest. This suggests that performing an active task like AOD requires larger and more active brain networks and not necessarily higher collaboration among networks. Generalization of these results can be accomplished by evaluating additional task types, as well exploring different subjects (e.g., patients with brain-based disorders may show different changes than healthy control subjects).

**Chapter 3: Automatic Classification of Schizophrenia patients based on  
Resting-state FNC Features**

### 3.1 Introduction

Recently, there is a growing interest in designing objective prognostic/diagnostic tools based on neuroimaging and other data that display high accuracy and robustness. The relatively small amount of research on MRI-based classification of schizophrenia patients can be divided into three categories based on the type of discriminating features used: structural-based (Ardekani et al., 2011; Caan et al., 2006b; Caprihan et al., 2008; Csernansky et al., 2004; Davatzikos et al., 2005; Fan et al., 2005; Fan et al., 2007b; Kawasaki et al., 2007; Nakamura et al., 2004; Pardo et al., 2006; Sun et al., 2009; Takayanagi et al., 2010; Takayanagi et al., 2011; Yoon et al., 2007), functional-based (Arribas et al., 2010; Calhoun et al., 2008b; Demirci et al., 2008a; Georgopoulos et al., 2007; Michael et al., 2008; Shen et al., 2010) or combination of structural and functional features (Fan et al., 2007a; Ford et al., 2002).

There are several biological markers (so-called biomarkers) that can be extracted from each of these complementary imaging techniques. These biomarkers have the potential to explain effects of psychiatric disorders on the brain. Promising results of these studies in detecting and predicting mental disorders such as schizophrenia suggest potential clinical utility of neuroimaging data. In this chapter, we focus on automatic diagnosis of schizophrenia as a good example of heterogeneous mental. However, most of the methods are applicable to other disorders, such as Alzheimer's disease, mild cognitive impairment, bipolar disorder, and even disorders such as psychopathy.

### **3.2 What is Schizophrenia?**

Schizophrenia is among the most prevalent mental disorders, affecting about 1 percent of the population worldwide (Bhugra, 2005; Wyatt et al., 1995). This devastating, chronic heterogeneous disease is usually characterized by disintegration in perception of reality, cognitive problems, and a chronic course with lasting impairment (Heinrichs and Zakzanis, 1998). Social isolation, paranoia, and difficulties in memory (both working and long-term) are other common symptoms of schizophrenia. The average age of onset of schizophrenia is 18 and 25 for men and women respectively. Schizophrenia is thought to be related to a combination of genetic and environmental factors, although the exact cause is still unknown. Several psychological and neurological mechanisms have been associated with schizophrenia. Unfortunately, there is no clinical test for schizophrenia, and the diagnosis is based on either the American Psychiatric Association's *Diagnostic and Statistical Manual of Mental Disorders* (DSM-IV) or the World Health Organization's *International Statistical Classification of Diseases and Related Health Problems*. The criteria for diagnosis are usually based on self-reported symptoms and abnormalities in behavior.

### **3.3 Previous Studies based on Structural Biomarkers**

Volumetric structural abnormalities measured by MRI are the main category of structural studies (Fan et al., 2007a; Kawasaki et al., 2007; Nakamura et al., 2004; Sun et al., 2009; Takayanagi et al., 2011). Neuroimaging studies using MRI have documented reductions in gray matter (GM) volume accompanied by proportionate increases in ventricular cerebrospinal fluid (CSF) volume. Also, some studies showed volumetric abnormalities in subcortical structures such as thalamus and hippocampus (Csernansky et

al., 2004; Honea et al., 2005). Various methods such as voxel-based morphometry (VBM) (Davatzikos et al., 2005; Fan et al., 2007b), cortical pattern matching (Sun et al., 2009), cortical thickness surface based approach (Yoon et al., 2007), and manually selected regions of interest (ROIs) (Nakamura et al., 2004; Takayanagi et al., 2010) have been used to differentiate schizophrenia patients from healthy controls.

Davatzikos et al. (2005) extracted GM, white matter, and CSF volumes in number of brain regions as features and trained and tested a classifier on a cohort of 69 patients and 79 healthy controls. They reported 81.1 percent mean classification accuracy. Fan et al. (2007) used a combination of deformation-based morphometry and machine learning methods to distinguish schizophrenia patients from healthy controls. First they computed local tissue volumes based on extracted tissue density maps. By using support vector machine (SVM), they selected the most important features, and then they trained and tested the SVM classifier using the leave-one-out strategy. Their method demonstrated high classification accuracy (91.8 percent for female and 90.8 percent for male subjects), which is very promising.

Yoon et al. (2007) proposed pattern classification based on cortical thickness. They computed the cortical thickness based on Euclidean distance between linked vertices on inner and outer cortical surfaces. They demonstrated that the thickness of several brain regions, such as precentral, postcentral, superior frontal and temporal, cingulate and parahippocampal gyri, have high discriminative power between the patient and control groups. They reported 88 to 94 percent accuracy for the automatic classification based on these cortical thicknesses.

Sun et al. (2009) used cortical pattern matching method to differentiate patients from controls. This method is able to capture correspondence between brain surfaces. It was shown that patients show lower gray matter density especially in lateral surface of the prefrontal and temporal lobes, limbic regions, cingulate sulci and parieto-occipital fissures. By using multinomial logistic regression classifier, they reported 86.1% of accuracy for automatic classification of patients from controls using gray matter densities as features.

Takayanagi et al. (2010) used volumes of 19 ROIs for differentiating first-episode schizophrenia patients from healthy controls. They reported 75.6% and 82.9% accuracy for male and female subjects respectively. Takayanagi et al. (2010) combined regional brain volumes with cortical thickness features and achieved above 80% accuracy in automatic classification of first-episode schizophrenia patients. They reported cortical thinning and volume reductions in prefrontal and temporal cortices of the patients.

Another major category of structural studies is based on DTI technique. There are number of parameters that can be computed based on tensor matrices of each brain voxel in DTI imaging. One of these measures is called fractional anisotropy (FA) which shows the anisotropy of the self-diffusion of water molecules (Kingsley, 2006). Since in the white matter of the brain, water tends have higher rate of diffusion along the direction of fibers, it is anisotropic. So, FA can reflect white matter fiber integrity which has been shown to be associated with number of brain disorders such as schizophrenia (Kubicki et al., 2007; Szeszko et al., 2008). Another measure calculated from tensor matrices is mean diffusivity (MA) which shows the magnitude of self-diffusion of water molecules. MA abnormality has been reported in schizophrenia patients in number of studies (Ardekani

et al., 2005; Lee et al., 2009; Narr et al., 2009). FA and MA features have been used in automatic classification of schizophrenia patients in several studies (Ardekani et al., 2011; Caan et al., 2006a; Caprihan et al., 2008).

Caprihan et al. (2008) proposed applying discriminant principal component analysis (DPCA) to FA images of DTI of healthy controls and schizophrenia patients. They reported 80% accuracy using FA features for automated classification of patients. Ardekani et al. (2011) used both FA and MD maps to discriminate patients for controls. Using linear discriminant analysis they achieved very promising classification accuracy of 94%.

### **3.4 Previous Studies based on Functional Biomarkers**

Using functional connectivity methods, researchers have shown disrupted functional integration in schizophrenia patients (Bokde et al., 2006; Jafri et al., 2008; Liang et al., 2006; Meyer-Lindenberg et al., 2005b; Mikula and Niebur, 2006; Salvador et al., 2010). Liang et al. reported decreased functional connectivity among insula, prefrontal lobe and temporal lobe and increase connectivity between cerebellum and several other brain regions (Liang et al., 2006). Meyer-Lindenberg et al. (2001) reported abnormal functional connectivity in fronto-temporal interactions in schizophrenia in selected regions of interest (ROIs) using positron emission tomography (PET) brain scans on working memory task (Meyer-Lindenberg et al., 2005b). Salvador et al., (2010) reported hyper-connectivity within medial and orbital structures of the frontal lobe and hyper-connectivity between these regions and several cortical and sub-cortical structures in schizophrenia patients.



Automatic diagnosis of schizophrenia based on functional biomarkers is a relatively new. These studies fall into two main groups based on the functional biomarker features they used; activation pattern of functional regions and networks of the brain and functional connectivity among brain regions and networks. (Arribas et al., 2010; Calhoun et al., 2008b; Demirci et al., 2008a; Georgopoulos et al., 2007; Michael et al., 2008; Shen et al., 2010).

Calhoun et al. (2008b) extracted temporal and default mode networks from fMRI data during the performance of an auditory oddball task using independent component analysis method. These networks were selected based on previous studies suggesting alteration of activation pattern of these networks in schizophrenia patients (Bluhm et al., 2007; Calhoun et al., 2004; Garrity et al., 2007b). They used the combined maps of these two networks as the feature set to differentiate schizophrenia patients, bipolar disorder patients and healthy controls from each other. They reported an average sensitivity and specificity of 90% and 95% which is very significant taking into account the highly overlapping symptoms of bipolar and schizophrenia patients.

Demirci et al. (2008) proposed applying projection pursuit algorithm on several ICA component of fMRI data obtained during auditory oddball task. 80%~90% was the reported accuracy of their automatic classification method for differentiating schizophrenia patients from healthy controls.

Shen et al. (2010) used an atlas-based method to extract mean time-courses of 116 brain regions in the resting-state for both healthy controls and schizophrenia subjects. The correlation between these features made the feature vector for each subject. By using feature selection and dimensionality reduction techniques, they reduced the

dimensionality down to three where they classified patients from controls with a high accuracy (93% for patients and 75% for healthy controls).

Table 3-1 summarizes the previous studies on MRI-based automatic diagnosis of schizophrenia (Calhoun and Arbabshirani, 2013).

**Table 3-1:** Summary of neuroimaging-based automatic diagnosis of schizophrenia studies. OV: Overall accuracy, Schiz.: schizophrenia, DMN: Default mode network, SNP: single nucleotide polymorphism

	<b>Modality</b>	<b>Features</b>	<b>Disorder</b>	<b>Results</b>	<b>References</b>
1	DTI	FA, MD	Schiz.	98% OV accuracy	(Ardekani et al., 2011)
2	DTI	FA	Schiz.	75% OV accuracy	(Caan et al., 2006a)
3	DTI	FA	Schiz.	80% OV accuracy	(Caprihan et al., 2008)
4	Structural MRI	Thalamic and Hippocampal Shape and volume	Schiz.	78% OV Error	(Csernansky et al., 2004)
5	Structural MRI	Gray matter, white matter, and ventricular cerebrospinal fluid volumes	Schiz.	81% OV accuracy	(Davatzikos et al., 2005)
6	Structural MRI	gray matter (GM), white matter (WM) and cerebrospinal fluid (CSF)	Schiz.	92% OV accuracy	(Fan et al., 2005)
7	Structural MRI	Distribution of Gray Matter	Schiz.	80-90% OV accuracy	(Kawasaki et al., 2007)
8	Structural MRI	22 neuropsychological test scores and 23 structural brain measurements	Schiz. & Bipolar	100% OV accuracy	(Pardo et al., 2006)
9	Structural MRI	principal components of cortical thickness	Schiz.	88%-93% OV accuracy	(Yoon et al., 2007)
10	Structural MRI	Regional brain volume and cortical thickness	first-episode Schiz.	80% OV accuracy	(Takayanagi et al., 2011)
11	Structural MRI	Structural brain measurements	Schiz.	~80% OV accuracy	(Nakamura et al., 2004)
12	Structural MRI	Volume of 29 ROIs	first-episode Schiz.	75%~83% OV accuracy	(Takayanagi et al., 2010)
13	Structural MRI	gray matter (GM), white matter (WM), and cerebrospinal fluid (CSF) density maps	Schiz.	91% OV accuracy	(Fan et al., 2007b)
14	Structural MRI	Gray matter density	schizophrenia, schizophreniform, or schizoaffective disorder	86.1% OV accuracy	(Sun et al., 2009)
15	Functional MRI	Activated voxels in DMN and temporal network during AOD task	Schiz. & Bipolar	70%–72%	(Arribas et al., 2010)
16	Functional MRI	Activated voxels in DMN and temporal network during AOD task	Schiz. & Bipolar	90%~95%	(Calhoun et al., 2008b)
17	Functional MRI	Functional Connectivity during the resting-state	Schiz.	93.75% for schizophrenic patients, 75.0% for healthy controls	(Shen et al., 2010)
18	Functional MRI	Functional Network Connectivity	Schiz.	67%~100% OV accuracy	(Arbabshirani et al., 2012)
19	Functional MRI	DMN and temporal network from ICA and GLM activation map	Schiz.	95% OV accuracy	(Castro et al., 2011)
20	Functional MRI	ICA Components	Schiz.	98% OV accuracy	(Du et al., 2012)
21	Functional MRI and Genetic	fMRI activation maps and SNP	Schiz.	87% OV accuracy	(Yang et al., 2010)

### **3.5 Motivation and Objective**

It has been shown that there are significant FNC differences between schizophrenic patients and the control group in the resting-state possibly showing deficiencies in the brain functional processing in the patients (Jafri et al., 2008). Jafri et al. (2008) reported increased FNC among frontal, temporal, visual and default-mode networks and decreased FNC between temporal and parietal networks. We hypothesized that disrupted functional integration in schizophrenia patients as captured by FNC analysis entail valuable information that can be used to discriminate patients automatically.

### **3.6 Proposed Approach**

For this study we used the resting state data from the Hartford dataset (see section 1.14.1 for more information). The block diagram in Figure 3-1 shows our approach. We divided the data into separate training (16 healthy subjects + 16 patients) and testing (12 healthy subjects + 12 patients) randomly. The raw fMRI data was first preprocessed. Then the training data were analyzed with group ICA. Subject specific spatial maps and time-courses were computed using back reconstruction. Next, FNC analysis was performed on the subject specific ICA time-courses. FNC was calculated between each pair of selected components.

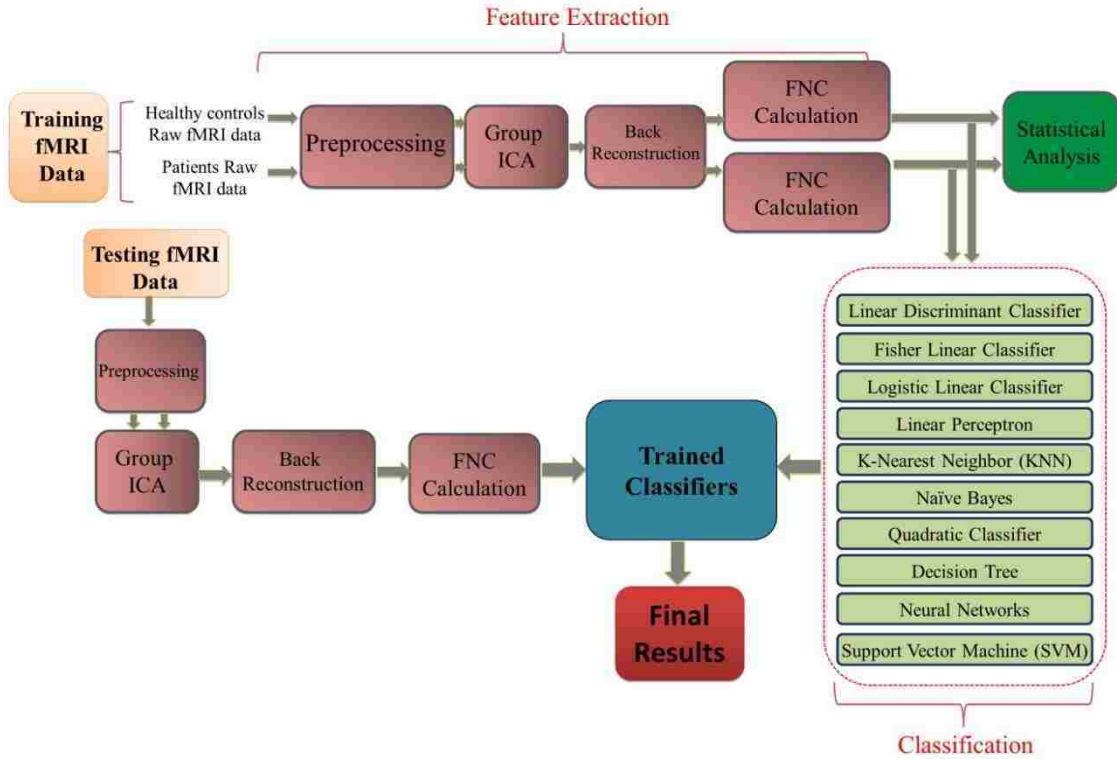


**Figure 3-1:** The Proposed Approach. The pink blocks on the top show the feature extraction steps. The statistical analysis box (green) is not part of the classification approach. The light green blocks describe the classification stage.

Several classifiers were trained using the training data and were evaluate using the testing data. Leave-one-out cross validation (LOOCV) inside the training set was used to select the hyperparameters for the classifiers. The optimum parameters for relevant classifiers were selected based on the averaged validation error over 32 validation iterations. In the testing phase, a separate ICA was performed on the testing dataset and the extracted brain networks where matched with those of training ICA based on maximum Pearson correlation coefficient. Finally, performances of trained classifiers were evaluated using the testing features.

As a supplementary study, the FNC features were statistically analyzed within each group of subjects using one sample t-tests and between groups using two-sample t-tests

on the training dataset. The statistical tests within each group test the null hypothesis that each feature has a mean of zero. Features surviving the test have non-zero mean which is statistically significant (which tells us there is a significant correlation between the pair of components). Two-sample t-tests between groups test the null hypothesis that corresponding FNC features in the two groups (controls and patients) have the same mean. Features surviving this test are the ones significantly (from a statistical point of view) different between control and patient groups (and tell us that the correlation between the pair of components is greater in one group compared to the other group). Note that these results are presented for descriptive purposes but were not used for feature selection or at all in the classification process. Preprocessing, group ICA, component selection, functional network connectivity calculations and statistical analysis are similar to those described in 2.2.1, 2.2.2, 2.2.3 and 2.2.4 respectively.

### **3.6.1 Classification**

We evaluated the performance of several well-known linear and non-linear classifiers. This will give us a better view of the complexity of the features. If simpler classifiers (such as linear classifiers) classify the data successfully, it means that the features have a simple structure (classes are almost linearly separable). However, if just complicated non-linear classifiers classify the data successfully, it is an indication that data has a more complex structure. The decision boundary in a linear classifier is a hyperplane while in a non-linear classifier the boundary can take any shape. In another sense, the classifiers can be divided into generative and discriminative. In generative classifiers, the probability density functions (pdf) of all classes are modeled and the Bayes theorem gives the posterior probabilities. On the other hand, discriminative

classifiers try to estimate the posterior probability directly or skip the challenging step of pdf estimation and determine the decision boundary based on the observed data (discriminant methods). Generative methods are often simpler and more computationally efficient but require estimation of pdf which require substantial amount of data. For complex data sets with few training samples, discriminative methods yield a better performance. It should be noted that in this study we computed the prior probabilities for the two classes from the data (which is equal) since the distribution of the data is very different from the real prevalence of schizophrenia (around 1%). All classifiers were implemented using Matlab (MathWorks, Inc.). Naïve Bayes, logistic linear and quadratic classifiers along with decision trees were implemented using PRTools<sup>1</sup> which is a Matlab-based pattern recognition toolbox (Duin et al., 2007). In this section, these methods will be briefly reviewed.

### **3.6.1.1 Linear Methods**

#### **3.6.1.1.1 Linear Bayes Normal Classifier**

This simple classifier assumes Gaussian pdf for both classes with equal covariance matrices but different means. The joint covariance matrix is the weighted average of class covariance matrices (weighted by prior probabilities). Using the Bayes rule, these assumptions lead to a linear decision boundary. This classifier is also called linear discriminant classifier (LDC) (Duda et al., 2001).

#### **3.6.1.1.2 Fisher Linear Classifier (FLC)**

Fisher's linear discriminant views classification as a dimensionality reduction task. Fisher formulation tries to maximize class mean separation while minimizing class overlap during linear dimension reduction. This choice of direction for projection can be

---

<sup>1</sup> <http://www.prtools.org>

used as a linear classifier in a two class problem. Fisher' linear classifier is special case of minimum least square linear classifier (Bishop, 2006).

### 3.6.1.1.3 Logistic Linear Classifier (LLC)

Logistic regression in method of learning functions from  $f: X \rightarrow Y$ .  $X = [X_1 X_2 \dots X_n]$  is the training vector with  $n$  variables and  $Y$  is the target value (class). Logistic regression assumes a parametric for the distribution  $P(Y|X)$ . The parameters are estimated from the training data. Assuming that  $Y$  is binary (two class problem), the logistic regression can be formulated as below:

$$P(Y = 0|X) = \frac{\exp(w_0 + \sum_{i=1}^n w_i X_i)}{1 + \exp(w_0 + \sum_{i=1}^n w_i X_i)} \quad (3-1)$$

$$P(Y = 1|X) = \frac{1}{1 + \exp(w_0 + \sum_{i=1}^n w_i X_i)} \quad (3-2)$$

One of the nice properties of the logistic regression is its ability to provide a linear discriminant between the two classes. Each new object is assigned to a class that has a larger probability for that object. Simplifying this rule results in a classification rule:

$$\text{if } w_0 + \sum_{i=1}^n w_i X_i > 0 \rightarrow Y = 0 \text{ Otherwise } Y = 1 \quad (3-3)$$

LLC also provides the weight for each feature so it can be used to rank the features.

### 3.6.1.1.4 Linear Perceptron Classifier

This classic linear discriminant tries to minimize the error function which is the number of misclassifications. This classifier can be considered as simple feed forward artificial neural network (Rosenblatt, 1958). First the input vector is transformed using a non-linear transformation to give a feature vector. The algorithm then tries to change the weight vector of the neural network using gradient stochastic descent algorithm to minimize the error in an iterative manner. At each iteration, the weight vector of the



network is manipulated by perceptron learning rule. The perceptron convergence theorem guarantees that the perceptron learning algorithm can find the solution in finite number of steps if such a solution (data is linearly separable) exists (Block et al., 1962).

#### **3.6.1.1.5 Linear Support Vector Machine (SVM)**

Over the last 15 years following the work by Cortes et al. (Cortes and Vapnik, 1995), SVM has proven useful in many machine learning and pattern recognition analysis problems. Moreover, when data classes are heterogeneous with few training samples, SVMs appear to be especially beneficial (Melgani and Bruzzone, 2004). This binary classifier aims at finding a hyperplane that maximizes the margin between the two classes. The training samples closest to the decision boundary are called support vectors. By allowing a margin (called soft margin) that allows for misclassification of some noisy samples, SVMs avoid the overfitting problem.

#### **3.6.1.2 Non-Linear Methods**

##### **3.6.1.2.1 K-Nearest Neighbor**

K-nearest neighbor (KNN) is a method of classifying objects based on proximity to the training samples (Cover and Hart, 1967). This instance-based learning method is among the simplest machine learning approaches. Each object is classified by the majority voting of the training samples in the neighborhood. The most common class among the  $k$  nearest neighbors is determined and is assigned to the object (Bremner et al., 2005). KNN can result in complex decision boundaries. The optimum  $k$  is determined by cross validation. Different distance metrics such as Euclidean, city block, cosine and correlation can be used to measure the proximity of the samples. KNN is fast, simple and

guarantees an error rate no worse than twice the Bayes error if the amount of data approach infinity. We used just Euclidean distance metric in our analysis.

#### **3.6.1.2.2 Naïve Bayes Classifier (NBC)**

The naïve Bayes classifier is a simple generative classifier based on Bayes theorem. The naïve assumption of NBC is that it assumes independence among the features. Although this over-simplified assumption is violated in most of the machine learning problems, this approach worked very well for many complex problems even when the independence assumption is not valid (Domingos and Pazzani, 1997; Rish, 2001). One of the main advantages of NBC is that it requires small amount of data to estimate the parameters of pdf function for each feature. Since the features are assumed to be independent, the joint pdf of the features is simply the multiplication of individual pdfs of each feature. When dealing with continuous data, typically Gaussian distribution is assumed for each feature. The pdf parameters are estimated from the training data. NBC works quite well in anti-spam filtering problems (Seewald, 2007).

#### **3.6.1.2.3 Quadratic Bayes Normal Classifier**

Quadratic discriminant analysis (QDC) is closely related to linear discriminant analysis. It assumes that the data is normally distributed with different mean and covariance matrices. This results in a quadratic decision boundary (Duda et al., 2001).

#### **3.6.1.2.4 Binary Decision Tree**

Decision trees (DT) find use in a wide range of applications. DT partitions the input space into cubic regions. In classification a class label is assigned to each region in the input space. Interpretability of the DT makes them very popular specially in medical diagnosis (Bishop, 2006). Each decision is a result of a sequence of binary decisions. In

order to learn a model from the training samples, the structure of the tree and the threshold value for each node should be determined. There are many variations of DT but most of them rely on the top-down greedy search in the space of possible trees called ID3 algorithm (Quinlan, 1987) and its successor C4.5 (Quinlan, 1993). Selecting optimal tree structure is usually infeasible due to large number possibilities. Usually the tree is started with a single root node and then at each step one node is added to the tree. This is called greedy strategy for growing the tree. At each node an attribute (feature) should be selected to be tested.

There are several criteria to measure the worth of each feature such as information gain, diversity index, Fisher's criterion (the same used in Fisher discriminant analysis) and gain ratio. The threshold values and structure of the tree is chosen so that the classification error is minimized. A criterion to stop growing the tree (pruning) should also be devised. Often the tree is fully grown and then the tree is pruned back to find the best tree for that structure. Graphical representation and human interpretability of the DT makes them very popular. However, since the edges of the decision regions are aligned with the axis of the feature space they are very suboptimal (Bishop, 2006). One of the main advantages of decision trees is interpretability. Moreover, they show the importance of each feature for classification in a graphical illustration.

#### **3.6.1.2.5 Artificial Neural Network**

Multilayer ANN is the extension of linear perceptron classifier. These networks can result in complex non-linear decision boundaries. A well-known structure for a tree layer structure: Input layer, hidden layer and output layer. Each neuron in each layer has connections to other neurons of the subsequent layers. Non-linear transfer function of the

neurons in the hidden layer can take any form such as sigmoid. The weights of the nodes are changed using a technique called backpropagation (Werbos, 1990). At each iteration, the output of the network is compared to correct answers and based on a predefined error function, an error value is computed. This error is fed back to the network and the weights of each node are adjusted to minimize this error. This can be done by gradient descent technique if the activation function is differentiable. Other method of minimizing the error is using Levenberg-Marquardt algorithm (Levenberg, 1944).

Another class of ANN uses radial basis activation function in the hidden layer (Chen et al., 1991). Usually this kind of network requires more neurons than standard feed forward back-propagation network but can be trained much faster. Topology of ANN used in this study can be found in the results section.

#### **3.6.1.2.6 Non-Linear Support Vector Machine**

By using the kernel trick, SVM can map the not-linearly separable data into a higher dimensional space where the samples are hopefully lineally separable. This mapping to higher dimensional space is difficult, but since SVM formulation depends on the inner product of each of training samples with the support vectors, the kernel is defined as this inner product so the problem is solved in the same fashion as the linear case. There are many kernel functions but the most widely used ones are Gaussian radial basis function (RBF) and polynomial kernel. There is at least one parameter in a kernel (except for the linear kernel) which should be optimized along with the soft margin usually by grid search over reasonable values of that parameter. RBF and polynomial kernels are defined as below:

$$K(X_i, X) = \exp\left(-\frac{\|x_i - x\|}{\sigma}\right) K(x_i, x) = \exp\left(-\frac{\|x_i - x\|}{\sigma}\right) \quad (3-4)$$

$$K(X_i, X) = [x_i \cdot x + 1]^p \quad (3-5)$$

In the above equations, support vectors are denoted by  $x_i$  and each training point is denoted by  $x$ .  $\sigma$  is a parameter proportional to the width of the RBF kernel.  $p$  is the degree of the polynomial kernel. A detailed mathematical formulation of SVM can be found in (Burges, 1998).

### **3.6.2 Parameter Selection**

The parameters for each classifier were selected by grid search. Unfortunately, there is no exact theoretical solution for the optimum value for most of the parameter. The parameters were selected based on the average validation error.

### **3.6.3 Effect of Medication**

One limitation of this study is the fact that patients are medicated. It is highly desirable to evaluate the performance of the proposed method on diagnosed but not yet medicated schizophrenia patients. It has been shown that antipsychotic medications have a normalizing effect on the functionality of the schizophrenia patients' brain (Davis et al., 2005). Moreover, prior fMRI and EEG studies on not medicated schizophrenia patients have reported altered functional connectivity (Meyer-Lindenberg et al., 2005a; Omori et al., 1995).

It has been shown that the main targets of antipsychotic treatments in schizophrenia patients are cortical and subcortical motor networks (Abbott et al., 2011; Muller et al., 2003; Rogowska et al., 2004; Wenz et al., 1994). Recently the effect of antipsychotic treatment on resting-state functional network connectivity was studied (Lui et al., 2010) and it was shown that after treatment patients showed 3 connectivity changes compared to healthy controls. From these 3 changes only one (FNC between the temporal

and parietal network) was present in this study. To further reduce the effect of medication on classification results, we repeated the classification with all described methods on reduced set of features where the motor network related features along with temporal-parietal FNC feature were excluded.

### 3.7 Results

From the 20 ICA components, 9 components were selected as non-artifactual, relevant networks. Since we selected nine IC components and we were interested in connectivity between each pair of networks, we ended up with 36 FNC features for each subject ( $\binom{9}{2}$ ). Figure 3-2 illustrates the spatial maps of the selected IC components. These networks are: auditory network (IC #2), frontal-parietal networks (IC #6 and 9), default-mode networks (IC #12,13, 19), visual networks (IC #15 and 20) and motor network (IC # 18).

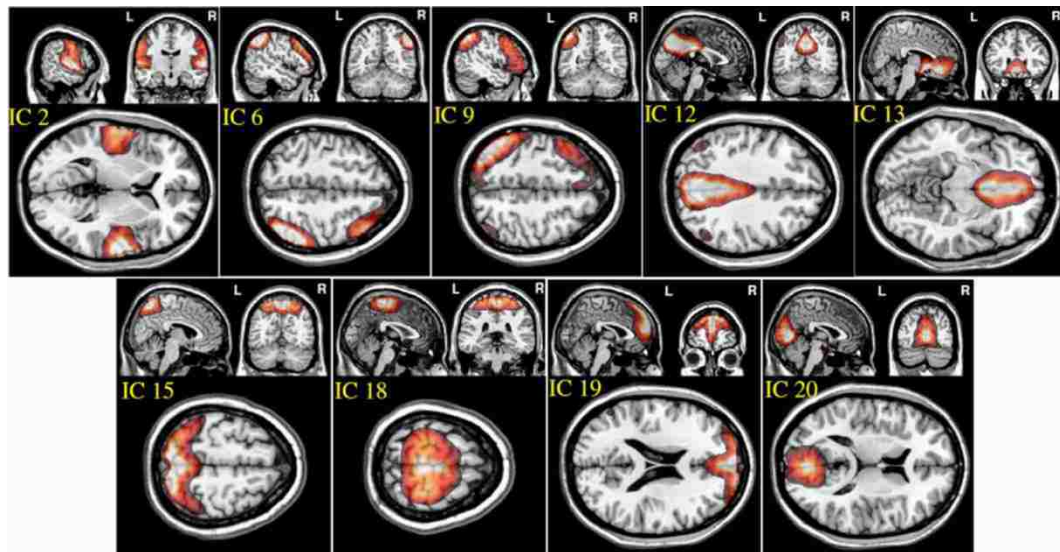


**Figure 3-2:** Spatial maps of the nine selected IC components

The maximum lagged correlation was computed for each of the subjects in each group. For each of the correlation pairs, student t-test was conducted with an FDR-corrected p-value threshold of 0.05 to identify significant correlations. Figure 3-3 shows the average correlation and the corresponding t-values. The black circles determine the correlation pairs that survived the FDR-corrected t-test. It is seen that there are more significant correlation pairs (12) in the control group compared to patients group (10). Interestingly, the mean correlation between the auditory network (IC #2) with each of the visual networks (IC #15 and 20) and the motor network (IC # 18) is significant for the healthy group but not for the patients. To determine which correlation pairs are significantly different between the two groups, two sample t-tests were conducted with a FDR corrected p-value threshold of 0.05. Also a mean correlation difference between the two groups (control-patients) was computed for each correlation pair. These results are shown in Figure 3-4. Starred pairs indicate those features surviving the paired t-test.

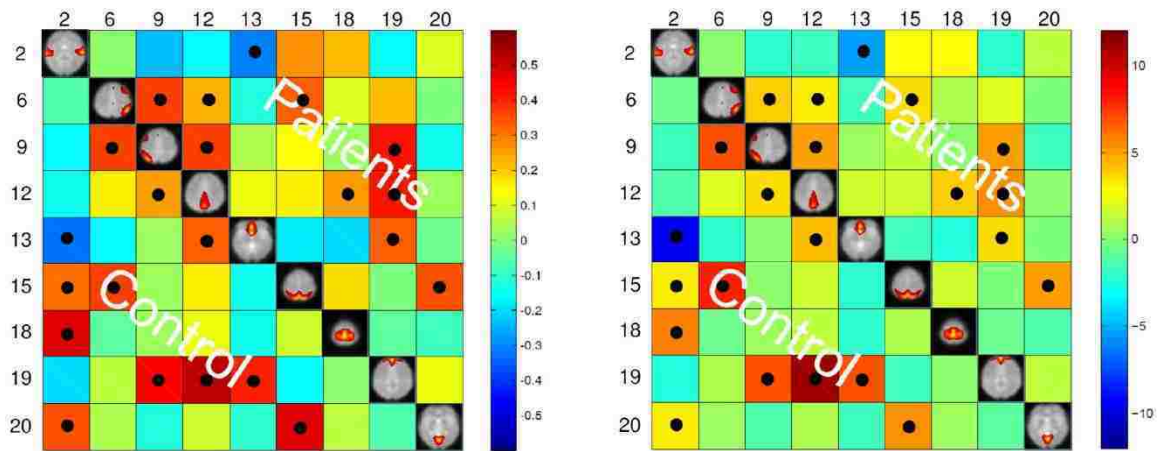


**Figure 3-3:** Left: Mean of correlation pairs for controls and patients. Right: T-value of each correlation pair resulted from Student t-test with p-value threshold of 0.05 corrected for FDR. Black circles indicate the pairs surviving the t-test.

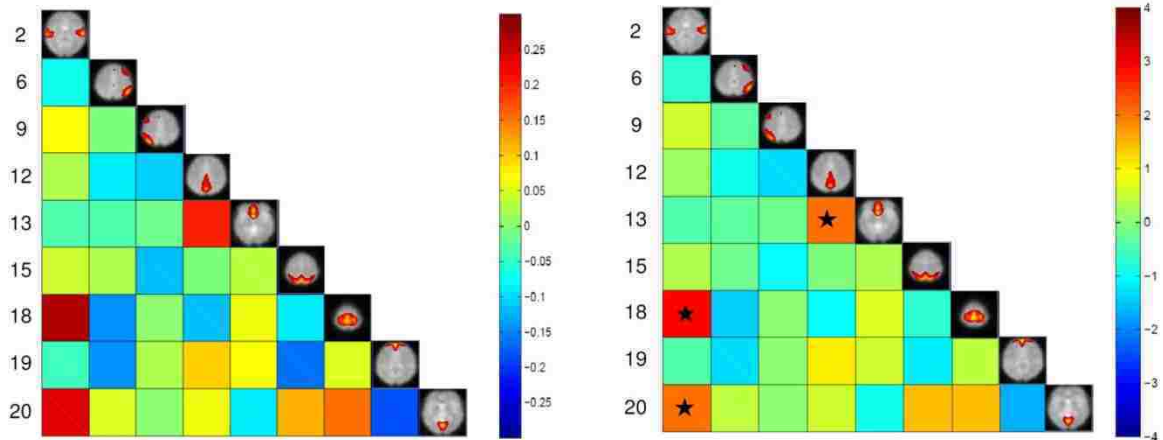


**Figure 3-4:** Left: Mean correlation difference between control subjects and patients(control-patient). Right: T-value resulting from two sample t-test with p-value threshold of 0.05 corrected for FDR. Stars show pairs that survived the paired t-test.

The classification results on the testing dataset for described classification methods (section 3.6.1) are summarized in Table 3-2. For each method, overall classification accuracy, sensitivity, specificity, positive predictive value (PPN) and negative predictive value (NPV) are provided. Moreover, we reported the Wilson’s binomial confidence interval (Wilson, 1927) for each classifier. For relevant methods, the choice of parameters selected during the training phase along with the topology of artificial neural networks are also included in Table 3-2. As discussed in section 3.6.3, to reduce the effect of medication on the classification results we repeated the analysis on the reduced set of features. Out of 36 features, 9 features that were more susceptible to medications were excluded from the feature set and the whole classification was repeated on the remaining 27 features. The excluded features are 8 motor related features (all FNC features involving IC18) along with a temporal-parietal feature (FNC between IC2 and IC15). The results are summarized in Table 3-3.



One of the main advantages of using decision trees is the graphical representation. One can represent decision alternatives and possible outcomes schematically. The visual approach is particularly helpful in comprehending sequential decisions and outcome dependencies. Decision trees for both the Fisher's and information gain criteria are illustrated in Figure 3-5 and Figure 3-6 respectively.

**Table 3-2:** Testing classification results using full set of features. Overall Acc.: overall accuracy, Sens: sensitivity, Spec: Specificity, PPV: positive predictive value, NPV: negative predictive value, CI: Wilson’s binomial confidence interval. Bold classifiers perform above the chance (lower bound of confidence interval is greater than 50%).

	Method	Overall Acc.	Sens.	Spec.	PPV	NPV	CI	Parameters
<b>Linear Methods</b>	<b>Linear Discriminant (LDC)</b>	<b>71%</b>	<b>42%</b>	<b>100%</b>	<b>100%</b>	<b>63%</b>	[51% 85%]	
	Fisher Linear (FLC)	67%	42%	92%	83%	61%	[47% 82%]	
	Logistic linear classifier (LLC)	63%	33%	92%	80%	58%	[42% 78%]	
	<b>Linear Perceptron</b>	<b>79%</b>	<b>75%</b>	<b>83%</b>	<b>82%</b>	<b>77%</b>	[59% 91%]	
	<b>SVM (Linear)</b>	<b>83%</b>	<b>75%</b>	<b>92%</b>	<b>90%</b>	<b>79%</b>	[66% 94%]	C=1.5
<b>Non-Linear Methods</b>	<b>KNN (Euclidean)</b>	<b>96%</b>	<b>100%</b>	<b>92%</b>	<b>92%</b>	<b>100%</b>	[78% 100%]	K=1
	<b>Naive Bayes classifier</b>	<b>79%</b>	<b>75%</b>	<b>83%</b>	<b>82%</b>	<b>77%</b>	[59% 91%]	
	quadratic classifier (QDC)	63%	33%	92%	80%	58%	[42% 78%]	
	<b>Decision Tree (Info. Gain)</b>	<b>88%</b>	<b>92%</b>	<b>83%</b>	<b>85%</b>	<b>91%</b>	[68% 96%]	No Pruning
	<b>Decision Tree (Fisher Criterion)</b>	<b>96%</b>	<b>100%</b>	<b>92%</b>	<b>92%</b>	<b>100%</b>	[78% 100%]	No Pruning
	<b>Neural Net. by back-propagation</b>	<b>92%</b>	<b>100%</b>	<b>83%</b>	<b>86%</b>	<b>100%</b>	[73% 99%]	Layers: 3 Hidden Nodes: 6
	<b>RBF Neural Net.</b>	<b>96%</b>	<b>100%</b>	<b>92%</b>	<b>92%</b>	<b>100%</b>	[78% 100%]	Layers: 3 Hidden Nodes: 12
	<b>SVM (RBF)</b>	<b>96%</b>	<b>100%</b>	<b>92%</b>	<b>92%</b>	<b>100%</b>	[78% 100%]	C= 1.25 $\sigma=1$
<b>SVM (Polynomial)</b>	<b>96%</b>	<b>92%</b>	<b>100%</b>	<b>100%</b>	<b>93%</b>	[78% 100%]	C=.12 P=3	

**Table 3-3:** Testing classification results using reduced set of features (27 features). Overall Acc.: overall accuracy, Sens: sensitivity, Spec: Specificity, PPV: positive predictive value, NPV: negative predictive value, CI: Wilson’s binomial confidence interval. Bold classifiers perform above the chance (lower bound of confidence interval is greater than 50%).

	Method	Overall Acc.	Sens.	Spec.	PPV	NPV	CI	Parameters
<b>Linear Methods</b>	<b>Linear Discriminant (LDC)</b>	79%	58%	100%	100%	71%	[59% 91%]	
	<b>Fisher Linear (FLC)</b>	79%	58%	100%	100%	71%	[59% 91%]	
	<b>Logistic linear classifier (LLC)</b>	71%	42%	100%	100%	63%	[51% 85%]	
	<b>Linear Perceptron</b>	75%	58%	92%	87%	69%	[55% 88%]	
	<b>SVM (Linear)</b>	83%	67%	100%	100%	75%	[64% 94%]	C=2
<b>Non-Linear Methods</b>	<b>KNN (Euclidean)</b>	96%	92%	100%	100%	92%	[78% 100%]	K=1
	<b>Naive Bayes classifier</b>	67%	58%	75%	70%	64%	[47% 82%]	
	<b>quadratic classifier (QDC)</b>	58%	75%	42%	56%	62%	[38% 75%]	
	<b>Decision Tree (Info. Gain)</b>	83%	83%	83%	83%	83%	[64% 94%]	No Pruning
	<b>Decision Tree (Fisher Criterion)</b>	79%	83%	75%	77%	82%	[59% 91%]	No Pruning
	<b>Neural Net. by back-propagation</b>	88%	83%	92%	91%	85%	[68% 96%]	Layers: 3 Hidden Nodes: 4
	<b>RBF Neural Net.</b>	75%	50%	100%	100%	67%	[55% 88%]	Layers: 3 Hidden Nodes: 18
	<b>SVM (RBF)</b>	88%	100%	75%	80%	100%	[68% 96%]	C= 1.5 $\sigma= .75$
	<b>SVM (Polynomial)</b>	83%	83%	83%	83%	83%	[64% 94%]	C=.12 P=3

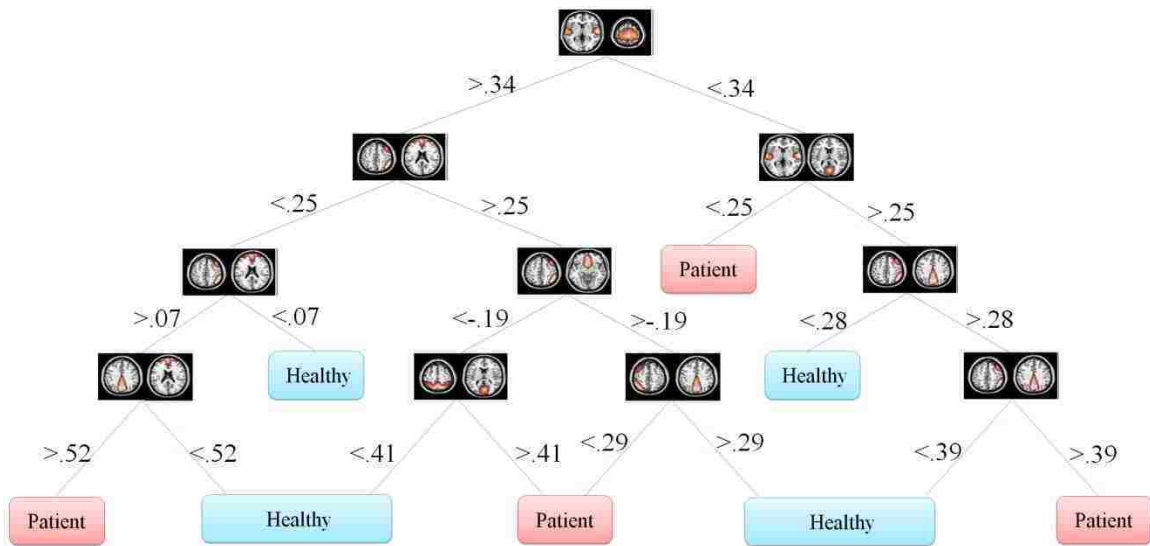


**Figure 3-5:** Fisher's decision tree using full set of features. This tree includes 8 features in 10 nodes. The number on each branch is FNC between the two networks preceding the branch.

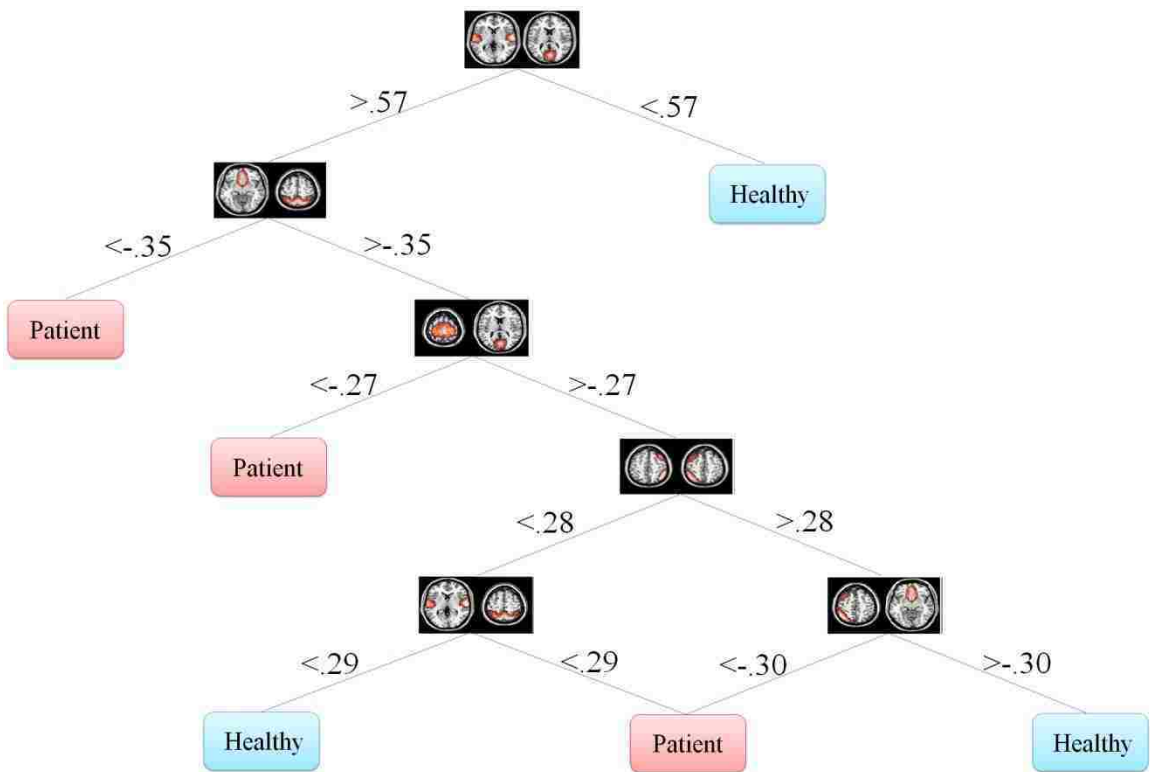


**Figure 3-6:** Information gain decision tree using full set of features. This tree includes 6 features in 6 nodes. The number on each branch is FNC between the two networks preceding the branch.

### 3.8 Discussion

We investigated whether resting-state functional connectivity features are able to discriminate between schizophrenia patients and healthy control groups. Using group ICA, the training dataset was decomposed into independent spatial components and their corresponding time courses. Then, FNC was computed between each pair of functional networks on the back reconstructed data using the maximum lagged correlation method. Several linear and non-linear classifiers were trained using the training data and were evaluated using the testing data. One of the common pitfalls in classification of mental diseases is using cross-validation to measure the generalized error (Demirci et al., 2008b; Wood et al., 2007). Another pitfall is selection of parameter/model in a way that maximize the performance in the final classifier in the testing dataset (Demirci et al., 2008b). To avoid this, we used separate training and testing datasets. Separate ICAs were performed on training and testing datasets. Cross validation was used in the training phase just for parameter/model selection. ICA successfully extracted similar non-artifactual networks from both training and testing datasets. This not surprising since it has been shown that there are several consistent functional networks across subjects in the resting state (Allen et al., 2011; Damoiseaux et al., 2006; Smith et al., 2009b).

The high accuracy of different classifiers in this study consolidates the disconnection hypothesis in schizophrenia patients (Bokde et al., 2006; Friston and Frith, 1995; Frith et al., 1995; Josin and Liddle, 2001; Mikula and Niebur, 2006; Salvador et al., 2010). Using functional connectivity methods, researchers have shown disrupted connectivity patterns in schizophrenia patients during rest and task in several brain regions (Boksman et al., 2005; Honey et al., 2005; Jafri et al., 2008; Liang et al., 2006;

Meyer-Lindenberg et al., 2001). In our experiment, connectivity between two DMN nodes (IC # 12& 13) was found to be significantly lower in schizophrenia patients compared to healthy controls (Figure 3-4). This reduced within DMN connectivity is interesting and in line with recent findings (Camchong et al., 2011; Mingoia et al., 2012; Orliac et al., 2013). One explanation can be gray matter thinning and greater psychopathology in patients (Goghari et al., 2007; Jang et al., 2011). Some recent DTI studies have shown anatomical disconnection in several brain regions in temporal and frontal lobe in schizophrenia patients (Buchsbaum et al., 2006). Moreover some studies have associated anatomical damage and FC disconnection in patients by analyzing DTI and functional data together (Zhou et al., 2008). This anatomical-functional association may be the reason for successful automatic diagnosis studies using DTI (Ardekani et al.,; Caprihan et al., 2008) and fMRI studies (Arribas et al., 2010; Calhoun et al., 2008b; Demirci et al., 2008a; Georgopoulos et al., 2007; Michael et al., 2008; Shen et al., 2010). While anatomical studies using either DTI or structural MRI are popular in classification of schizophrenia patients, functional studies are limited mostly to task-based studies. Resting-state studies in case of classification of schizophrenia are rare and have been just recently started (Shen et al., 2010; Venkataraman et al., 2012). Most of the connectivity fMRI studies (resting-state or task-based) have used FC features which means that the features are temporal statistical dependencies among brain regions. Using FC methods have some limitation such as the choice of seed-voxel in each region (that may be different for patients and controls) and very high number of extracted features. Shen et al., extracted average time-courses from 116 brain regions which means 6670 features for each subject. High number of features requires additional step such as feature selection

and reduction to avoid curse of dimensionality. Moreover, most of the features in that fashion are not discriminative. Using functional network connectivity on the other hand, doesn't require seed-voxel selection. Moreover, the number of extracted features is much less than FC methods (36 features in our experiment based on 9 functional networks). Based on our experiments, it can be inferred that FNC methodology is a concise abstraction of the connectivity pattern in the brain that can successfully capture the differences between schizophrenia patients from healthy controls.

We have reported detailed classification results (sensitivity, specificity, positive predictive value and negative predictive value) as well as Wilson's binomial confidence interval for each classification method. The classification results in Table 3-2 show that non-linear methods outperform linear methods, which was expected. Among the linear methods, LDC, Perceptron and linear SVM performed above the chance (lower bound of Wilson's binomial confidence interval is greater than 50%). All linear methods show high specificity than sensitivity. Except for quadratic classifier, all non-linear methods, performed above the chance. In overall, discriminative approaches outperformed generative methods. As a general rule in this study, the less assumptions about the data, the better the performance. Simple classifiers such as KNN and decision tree performed very well on this specific machine learning problem. Also, non-linear SVM showed significant performance with only one misclassified sample. Despite of oversimplified assumptions and little training data available in this study, the performance of naïve Bayes is marginally above the chance (79.17% overall performance). A poor classification was achieved using the quadratic classifier. It can be hypothesized that whether the assumptions of this classifier that two classes are normally distributed with

different mean and covariance matrices are not valid or small amount of data is not sufficient to accurately estimate the mean and covariance matrix of each classifier. It should be noted that conclusions regarding the performance of different classifiers are limited to this specific problem using one dataset. Performance of each machine learning algorithm depends on the dataset and comparison among different classifiers has been heavily investigated in the machine learning literature. Since our main goal is not comparing classifiers, we didn't conduct statistical tests to compare their performances and just reported Wilson's binomial score interval for each classifier

Table 3-3 shows the result of classification on reduced set of features. Surprisingly, the overall error was reduced for all the linear methods except for linear perceptron. The main reason for this phenomenon may be the curse of dimensionality (Pearlson, 2009) since we have only 32 samples for training and 36 features. Using the reduced feature set (27 features), most of the linear methods could estimate more accurate hyperplane. Linear SVM performs robustly and equally on both full and reduced set of features. Most non-linear classifiers still show above the chance performance with lower overall performance compared to the full feature set. KNN still classifies with high accuracy. Again, QDC performed very poorly. In overall, reduction of features didn't greatly affect the results and very high performances were still achievable. This suggests that medication didn't bias the classification.

Decision trees don't transform the data from the original feature space. Moreover, they classify the data based on thresholds they put on each of the features. This makes it possible for the investigator to observe the decision tree and analyze it. One can see how features are distributed in different levels of the decision tree and what thresholds on



which features discriminate the classes. This property is especially of interest in the medical diagnosis field since decision tree provides classification structure which includes thresholds on the symptoms. This discriminative information of each feature is very valuable in medical problems.

In our problem the symptoms are FNC features. One can observe that how each feature discriminate the two groups. This information may reflect FNC abnormalities in schizophrenia patients. First of all decision tree introduces the important features which are 8 and 6 in Figure 3-5 and Figure 3-6 respectively. Top node features are among the most important features which are among the feature identified by the two-sample t-test. Also, the decision tree can identify the type abnormality which is discriminative between the two groups. For example, it is seen from Figure 3-5 that subjects with temporal-motor FNC lower than 0.34 and temporal-visual higher than 0.25 are patients. Or from Figure 3-6 it is evident that all subjects with temporal-visual FNC lower than 0.57 are healthy controls. In other words, all patients have higher temporal-visual FNC (as do some of the healthy controls).

Prior studies mentioned in the introduction section reported accuracies ranging from 79% to 98% as described in 3.3 and 3.4. Several limitations and considerations make it very hard to compare different approaches of automatic classification of mental disorders. For example, study size, MRI scanner parameters, nature of extracted features, type of classifier, medication and disease severity in the patient group varies among the different studies. In the absence of standard training and testing datasets, comparison of different approaches based only on the classification rate is ambiguous.

One of the issues in the current study was that the patients were slightly older than healthy controls. We looked at the misclassified subjects in each of the classification experiments and couldn't find any systematic age pattern. Note also, it has been shown that schizophrenia patients have stronger FNC (Jafri et al., 2008) whereas subjects that are older have reduced FNC (Allen et al, 2010). So, this potential confound would likely have a cancelling effect making the diagnosis even harder. Regardless, based on the above observation we do not believe age is a factor in our classification results. To avoid any bias, we also repeated the classification when age was regressed out from the FNC features and exactly same performance was achieved.

In this study, we separated the data into training and testing dataset. One may wonder how our method works in a clinical situation when we have only one new subject. We assume that we have trained our model using enough training data. In this situation here are two options: 1) we can use the group ICA components of the training data as regressors and calculate the subject specific time-courses. 2) For a more accurate estimation another ICA can be done on an extended dataset containing training data and the new subject data. Note that we won't use the information of this new ICA analysis for training the classifiers/models but just to extract IC networks/time-series for the new test subject. This approach is more accurate but slower especially in the case of big training data. Since the main goal of this study is to investigate the feasibility of using FNC features, we didn't investigate methods.

It was shown that the resting state FNC features can be successfully exploited in order to automatically discriminate schizophrenia patients. To the best of our knowledge this the first study using resting-state FNC features to classify schizophrenia patients.

Acquiring scans from schizophrenia patients is more feasible in the resting state due to the short acquisition time and avoidance of cognitive task-related impairment confounds. Moreover, the data is less prone to multi-site variability (Pearlson and Calhoun, 2009). It was demonstrated that just 5min resting state data can be used to classify patients reliably and accurately using FNC features and simple classifiers such as KNN. Moreover, performance of several linear and non-linear methods were evaluated and compared.

## **Chapter 4: Impact of Autocorrelation of Functional connectivity**

## 4.1 Introduction and Motivation

As discussed in section 1.11, less attention has been given to the statistical assumptions underlying functional connectivity. As discussed in section 1.5 and 1.6, the usual way for assessing functional connectivity or functional network connectivity is by calculating the Pearson correlation coefficient between the time-series of two brain regions or networks. From statistical point of view, those time-series should meet certain conditions such as being stationary and white in order to result in valid correlation coefficient. However, it is well-known that fMRI time-series are neither stationary nor white. The non-stationarity is attributed to several factors such as scanner drift. The intrinsic autocorrelation in fMRI time-series is assumed to originate from physical and physiological noise (Aguirre et al., 1997; Bullmore et al., 2001; Friston et al., 2000; Lenoski et al., 2008; Lund et al., 2006; Purdon and Weisskoff, 1998; Rajapakse et al., 1998; Zarahn et al., 1997).

In recent years, there has been a debate in the neuroimaging community regarding the possible impact of intrinsic autocorrelation in fMRI time-courses on functional connectivity analysis outcome. Some researchers have even questioned the validity of previous connectivity studies by arguing that not correcting for autocorrelation in fMRI time-series may result in spurious high correlation values (Christova et al., 2011; Georgopoulos and Mahan, 2013). These subject-level studies have confirmed that fMRI time-series are autocorrelated through the use of the Durbin-Watson statistic and have suggested to reduce the autocorrelation by using an autoregressive integrated moving average (ARIMA) model which is called prewhitening (Granger and Morris, 1976; Haugh, 1976).

It should be noted that most of the recent discussions (Christova et al., 2011; Georgopoulos and Mahan, 2013) are based on previous works in economics and econometrics most notably those initiated by Granger. In his seminal paper, "Spurious regression in economics", published in 1974, he strongly warned economists regarding the side-effects of ignoring autocorrelated residuals in a regression model (Granger and Newbold, 1974). While these conclusions are fully valid when dealing with just two autocorrelated time-series, to the best of our knowledge, no one has investigated the impact of autocorrelation on functional connectivity based on a careful consideration of the specific differences that reign between the two fields.

In neuroimaging, inference is largely related to hypothesis testing and not necessarily focused on the point estimation of the actual correlation value. Most connectivity analyses are performed at the group level. Answers to questions like "Is the connectivity between two brain regions/networks significant?" or "Is there any significant difference in connectivity between two groups/tasks?" are typically of greater interest than estimating the correlation coefficients themselves. While most of economics discussion on this issue consider point estimation, it is not clear to what extent autocorrelation affects group level statistics in functional connectivity studies. Another surprising fact is the lack of explicit calculation of the correlation coefficient of two autocorrelated time-series in the literature, at least to the best of our knowledge.

The goal of this study is to investigate the impact of autocorrelation on functional connectivity, defined in this study as the Pearson correlation coefficient between time-series of voxels, regions or networks. To better understand the impact of autocorrelation on Pearson correlation coefficient, first, we theoretically derive an approximation of the

bias and variance of correlation coefficient estimator in the presence of autocorrelation in a very simple case with the intent to better understand the process (this is distinct from fMRI time-series simulation, which is outside of the scope of this manuscript). These theoretical results don't necessarily generalize to more complicated models due to the simplifying assumptions of this study. This is followed by simulations in order to validate the theoretical results. Finally, the impact of autocorrelation on real resting-state fMRI time-series is assessed. We also discuss proper preprocessing for connectivity analysis based on these observations. We focus on the resting-state FC given the growing interest in this condition and to avoid the confound that autocorrelation in task-based fMRI heavily depends on the task design.

## 4.2 Theoretical Background

### 4.2.1 Pearson Correlation Coefficient

We start by taking a close look at the Pearson correlation coefficient and some of its properties. Let  $w$  and  $z$  denote two random processes (time series). The Pearson correlation coefficient is defined as the covariance between two random processes divided by the product of their standard deviations:

$$\rho_{w,z} = \frac{cov(w,z)}{\sqrt{var(w)var(z)}} \quad (4-1)$$

$\rho_{w,z}$  measures the normalized linear dependency between  $w$  and  $z$ . In practice, the correlation coefficient is estimated from a limited sample from random variables  $w$  and  $z$ :

$$r_{w,z} = \frac{\sum_{i=1}^N (w_i - \bar{w})(z_i - \bar{z})}{\sqrt{\sum_{i=1}^N (w_i - \bar{w})^2} \sqrt{\sum_{i=1}^N (z_i - \bar{z})^2}} \quad (4-2)$$

where  $N$  is the number of samples and  $\bar{w}$  and  $\bar{z}$  are the empirical mean values of  $w$  and  $z$ . Fisher (Fisher, 1914) derived the distribution of the Pearson correlation coefficient,  $p(r_{w,z})$  assuming a bivariate normal distribution for  $w$  and  $z$ :

$$p(r_{w,z} | \rho_{w,z}) = \frac{1}{\pi} (N-2) (1 - r_{w,z}^2)^{\frac{N-4}{2}} (1 - \rho_{w,z}^2)^{\frac{N-1}{2}} \times \int_0^\infty \frac{d\beta}{(\cosh\beta - \rho_{w,z} r_{w,z})^{N-1}} \quad (4-3)$$

The integral in (4-3) can be written in terms of a hypergeometric and gamma functions:

$$p(r_{w,z} | \rho_{w,z}) = \frac{1}{\pi} (N-2) (1 - r_{w,z}^2)^{\frac{N-4}{2}} (1 - \rho_{w,z}^2)^{(N-1)/2} \times \frac{\sqrt{\pi} \Gamma(N-1)}{\sqrt{2} \Gamma(N-0.5)} (1 - \rho_{w,z} r_{w,z})^{-\frac{N-1}{2}} {}_2F_1\left(\frac{1}{2}, \frac{1}{2}, \frac{2N-1}{2}; \frac{\rho_{w,z} r_{w,z} + 1}{2}\right) \quad (4-4)$$

where  ${}_2F_1(a, b, c; z)$  is Gaussian hypergeometric function and  $\Gamma()$  is the gamma function. The first two moments of  $r_{w,z}$  are:

$$E[r_{w,z}] \cong \rho_{w,z} - \frac{\rho_{w,z}(1 - \rho_{w,z}^2)}{2N} \quad (4-5)$$

$$var(r_{w,z}) \cong \frac{(1 - \rho_{w,z}^2)^2}{N} \left(1 + \frac{11\rho_{w,z}^2}{2N}\right) \quad (4-6)$$

It is evident from (4-5) that  $r_{w,z}$  is a biased estimator of  $\rho_{w,z}$ . If  $w$  and  $z$  are uncorrelated ( $\rho_{w,z} = 0$ ), then the distribution  $r_{w,z}$  reduces to:



$$p(r_{w,z}) = \frac{(1 - r_{w,z}^2)^{(N-4)/2}}{B\left(\frac{1}{2}, \frac{N-2}{2}\right)} \quad (4-7)$$

where  $B$  is the beta distribution. The mean and variance of  $r_{w,z}$  in this special case are 0 and  $1/N$  respectively. The correlation coefficient  $r_{w,z}$  is a consistent estimator for  $\rho_{w,z}$ . Its variance is inversely proportional to the sample size,  $N$ , and its asymptotic bias is zero as can be read from (4-6).

### 4.3 Pearson Correlation Coefficient of Two Autocorrelated Time-Series

The most well-known method to model autocorrelation in a time-series is the Box-Jenkins methodology (Box and Jenkins, 1970). In this method, the time-series are observed as outputs of autoregressive integrated moving average (ARIMA) processes. Since calculating the correlation coefficient between two time-series can quickly become highly involved in high ARIMA model orders, we try to assess the impact of autocorrelation in a simple case.

Let  $w$  and  $z$  denote two white bivariate normally distributed time-series. We assume that the Pearson correlation coefficient between  $w$  and  $z$ ,  $\rho_{w,z}$ , is of interest but we only observe  $x$  and  $y$  that are autocorrelated versions of  $w$  and  $z$  respectively. In other words,  $w$  and  $z$  are latent random variables only observable through autocorrelated time-series  $x$  and  $y$ . We can assume that the time-series are in stationary state. Also, we assume that time-series are de-meaned and de-trended without loss of generality, since the time-series can always be de-meaned and de-trended empirically. Moreover, this is almost always part of the preprocessing of functional connectivity analysis. We denote the sample correlation coefficient between  $w$  and  $z$  and between  $x$  and  $y$  with  $r_{w,z}$  and  $r_{x,y}$  respectively. Sample variances of  $w$ ,  $z$ ,  $x$  and  $y$  are denoted by  $s_w^2$ ,  $s_z^2$ ,  $s_x^2$  and  $s_y^2$ ,

respectively. The variables  $s_{w,z}$  and  $s_{x,y}$  denote sample covariance between  $w$  &  $z$  and  $x$  &  $y$ , respectively. We consider simple case of autoregressive process of model order one.

#### 4.3.1 Modeling the Time-Series with Autoregressive Process of Model Order One:

##### AR(1)

An AR(1) process can be written in its recursive form as:

$$x_t = \alpha x_{t-1} + w_t \quad (4-8)$$

$$y_t = \beta y_{t-1} + z_t \quad (4-9)$$

where the subscript  $t$  denotes the time index in the time-series and  $\alpha$  and  $\beta$  are AR(1) coefficients of absolute value less than 1. This condition is necessary for  $x$  and  $y$  to be stationary. First, we calculate the variance of  $x$  and  $y$ . Since  $x$  and  $y$  are demeaned, the first moments of both series are zero. Also, without loss of generality—and for sake of simplicity—we may assume that initial point in both series is zero. The expected value of the sample variance can be derived and expressed as follows:

$$E[s_x^2] = E\left[\sum_{i=1}^N \frac{x_i^2}{N-1}\right] = \frac{1}{N-1} \left[ \frac{N}{1-\alpha^2} - \frac{1-\alpha^{2N}}{(1-\alpha^2)^2} \right] E[s_w^2] \quad (4-10)$$

$$E[s_y^2] = E\left[\sum_{i=1}^N \frac{y_i^2}{N-1}\right] = \frac{1}{N-1} \left[ \frac{N}{1-\beta^2} - \frac{1-\beta^{2N}}{(1-\beta^2)^2} \right] E[s_z^2] \quad (4-11)$$

The expected value of the sample covariance between  $x$  and  $y$  can be calculated in the same fashion:

$$E[s_{x,y}] = E\left[\sum_{i=1}^N \frac{x_i y_i}{N-1}\right] = \frac{1}{N-1} \left[ \frac{N}{1-\alpha\beta} - \frac{1-(\alpha\beta)^{2N}}{(1-\alpha\beta)^2} \right] E[s_{w,z}] \quad (4-12)$$

In order to find the expected value of  $r_{x,y}$ , we need to calculate:

$$E[r_{x,y}] = E\left[\frac{S_{x,y}}{\sqrt{S_x^2 S_y^2}}\right] \quad (4-13)$$

which is theoretically complicated. In order to be able to simplify (4-13), we propose first-order multivariate Taylor series expansion approximation of the mean which is commonly used in many scientific and engineering applications (Ang and Tang, 1975; Hahn and Shapiro, 1967):

$$E[r_{x,y}] \cong \frac{E[S_{x,y}]}{\sqrt{E[S_x^2]E[S_y^2]}} \quad (4-14)$$

Eq. (4-14) enables us to simplify Eq. (4-13) by replacing corresponding terms in Eq. (4-13) with (4-12), (4-13) and (4-14). So, the approximate expected value of sample correlation between  $x$  and  $y$  can be calculated as follows:

$$\begin{aligned} E[r_{x,y}] & \cong \frac{\frac{1}{N-1} \left[ \frac{N}{1-\alpha\beta} - \frac{1-(\alpha\beta)^{2N}}{(1-\alpha\beta)^2} \right] E[S_{w,z}]}{\sqrt{\left( \frac{1}{N-1} \left[ \frac{N}{1-\alpha^2} - \frac{1-\alpha^{2N}}{(1-\alpha^2)^2} \right] E[S_w^2] \right) \left( \frac{1}{N-1} \left[ \frac{N}{1-\beta^2} - \frac{1-\beta^{2N}}{(1-\beta^2)^2} \right] E[S_z^2] \right)}} \end{aligned} \quad (4-15)$$

If we use the proposed approximation in Eq. (4-14) in reverse direction the above equation can be simplified as:

$$E[r_{x,y}] \cong \frac{\left[ \frac{N}{1-\alpha\beta} - \frac{1-(\alpha\beta)^{2N}}{(1-\alpha\beta)^2} \right]}{\sqrt{\left[ \frac{N}{1-\alpha^2} - \frac{1-\alpha^{2N}}{(1-\alpha^2)^2} \right] \left[ \frac{N}{1-\beta^2} - \frac{1-\beta^{2N}}{(1-\beta^2)^2} \right]}} E[r_{w,z}] \quad (4-16)$$

The first result is that the expected value of correlation coefficient between  $x$  and  $y$  is approximately a linear function of the expected value of correlation coefficient between  $w$  and  $z$ . Asymptotically (as  $N \rightarrow \infty$ ), (4-16) reduces to:

$$E[r_{x,y}] \cong \frac{\sqrt{(1-\alpha^2)(1-\beta^2)}}{(1-\alpha\beta)} E[r_{w,z}] \quad (4-17)$$

**(4-17) tells us that the asymptotic expected value of approximate correlation coefficient between  $x$  and  $y$  is always smaller than or equal to the expected value of the correlation coefficient between  $w$  and  $z$  since the numerator is always equal or smaller than the denominator.** Expected values of  $r_{x,y}$  and  $r_{w,z}$  are approximately equal only if  $\alpha = \beta$ . As the distance between  $\alpha$  and  $\beta$  increases, expected value of  $r_{x,y}$  shrinks towards zero.

The variance of the sample correlation coefficient estimator when the time-series follow an AR(1) model and with true correlation,  $\rho_{w,z}$  equal to zero was approximated about 80 years ago (Bartlett, 1935):

$$var(r_{x,y}) \cong \frac{1}{N} \frac{1+\alpha\beta}{1-\alpha\beta} \quad (4-18)$$

In the above equation  $1/N$  is the variance of the estimator when the true correlation between  $w$  and  $z$  is zero. We propose to generalize (4-18) to the case of non-zero  $\rho_{w,z}$  by replacing  $1/N$  in (4-18) with the first term in (4-6):

$$var(r_{x,y}) \cong \frac{(1-\rho_{w,z}^2)^2}{N} \frac{1+\alpha\beta}{1-\alpha\beta} \quad (4-19)$$

The variance of the estimator,  $r_{x,y}$ , approximately decreases as the absolute value of the true correlation,  $\rho_{w,z}$  increases. The most important observation is that this variance increases as the product of autoregressive parameters,  $\alpha\beta$ , increases. In other words,

**autocorrelation reduces the effective degrees of freedom for variance of the sample Pearson correlation coefficient** which is a well-known phenomenon (Davey et al., 2013; Friston et al., 1994; Kruggel et al., 2002).

### 4.3.2 Autoregressive Process in the Frequency Domain

It is useful to look at the autoregressive process in the frequency domain. The autoregressive process can be modeled as a linear time-invariant (LTI) system with input of  $w_t$ , impulse response of  $h_t$  and output of  $x_t$ . Note that all signals are discrete-time. The relationship between  $w_t$  and  $x_t$  can also be expressed in frequency domain as illustrated in Figure 4-1:

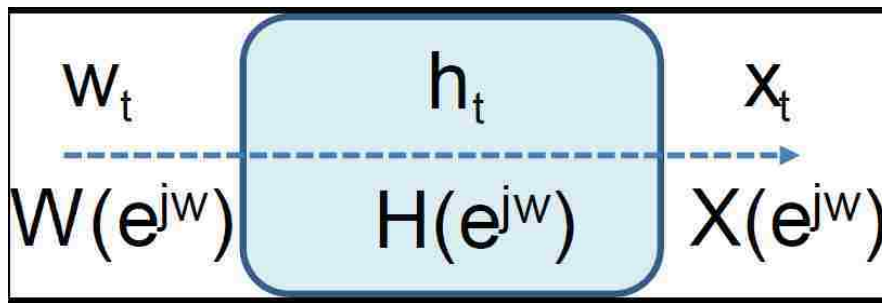


**Figure 4-1:** Autoregressive process modeled as a linear time-invariant system with the input of a white time-series ( $w_t$ ) and output of a autocorrelated time-series ( $x_t$ ).

We can derive the frequency response of the above system,  $H(e^{j\omega})$  for the AR(1) model by taking the Fourier transform of Eq. (4-8):

$$\begin{aligned}
 X(e^{j\omega}) &= \alpha e^{-j\omega} X(e^{j\omega}) + W(e^{j\omega}) \\
 \Rightarrow H(e^{j\omega}) &= \frac{X(e^{j\omega})}{W(e^{j\omega})} = \frac{1}{1 - \alpha e^{-j\omega}}
 \end{aligned}
 \tag{4-20}$$

This is a single pole system with  $|\alpha| < 1$  to ensure causality and stability. The magnitude of frequency response function can be easily derived:

$$|H(e^{jw})| = \frac{1}{\sqrt{1 + \alpha^2 - 2\alpha \cos(w)}} \quad (4-21)$$

For positive and negative values for  $\alpha$ ,  $H(e^{jw})$  is a lowpass and highpass filter respectively. The magnitude of the frequency response function is plotted with different  $\alpha$  values in Figure 4-2:

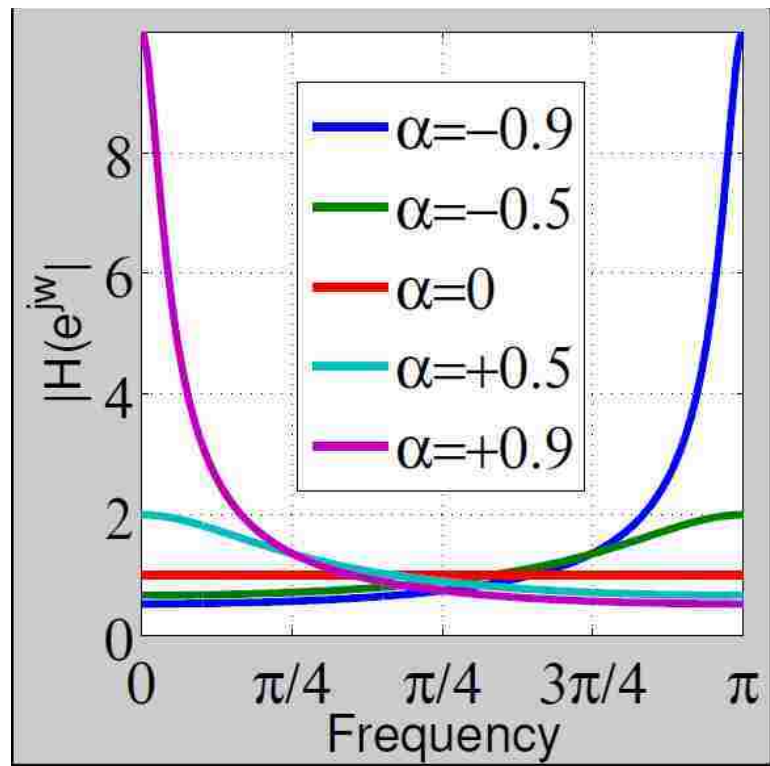


**Figure 4-2:** AR(1) as a frequency filter: Magnitude of the frequency response function for AR(1) model for different  $\alpha$  values (Eq. (4-21)). Note that  $\pi$  corresponds to the highest frequency possible in the signal.

Positive and negative values of  $\alpha$  results in low and high pass filters respectively.

Note that in Figure 4-2,  $\pi$  is the highest frequency in the signal. It is evident that as  $|\alpha|$  increases the filter becomes sharper. We expect fMRI time-series to exhibit positive autocorrelation which corresponds to a low-pass filter. In other words, in a

AR(1) process with positive  $\alpha$ , high-frequencies are attenuated and low frequencies are amplified. The cut-off frequency for this filter depends on the value of  $\alpha$ . The purpose of autocorrelation correction is to cancel out the effect of this low-pass filter by applying a filter with inverse frequency response. Note in general case of AR(k) process, depending on the location of the poles, filter can be lowpass, highpass, bandpass or bandstop.

## **4.4 Methods**

### **4.4.1 Simulated Data**

The statistical software R, was used to generate simulated datasets under different scenarios. First, two spectrally white time-series ( $w$  and  $z$ ) were generated from a bivariate normal distribution with different lengths,  $N \in \{64, 256, 1024\}$  and correlation,  $\rho$  from -0.9 to +0.9 in 0.1 increments. Then,  $x$  and  $y$  were generated from  $w$  and  $z$  using Eq. (4-8) and Eq. (4-9) with different  $\alpha$  and  $\beta$  values. Each simulation scenario was repeated 10,000 times. The mean and standard deviation of  $r_{w,z}$  and  $r_{x,y}$  were calculated from the 10,000 collected samples. These values were compared to those derived from theoretical estimates as detailed in the previous section.

### **4.4.2 Real fMRI Data**

For this study we used the FBRIN Data set (See section 1.14.2 for more information).

### **4.4.3 Group Independent Component Analysis**

All of the preprocessed functional data from both control and patient groups were analyzed using spatial group independent component analysis (GICA) framework as implemented in the GIFT software (Calhoun and Adali, 2012; Calhoun et al., 2001a;

Erhardt et al., 2011). Spatial ICA decomposes the subject data into linear mixtures of spatially independent components that exhibit a unique time course profile. A subject-specific data reduction step was first used to reduce 162 time point data into 100 orthogonal directions of maximal variability using principal component analysis. Then subject reduced data were concatenated across time and a group data PCA step reduced this matrix further into 100 components along directions of maximal group variability. One hundred independent components were obtained from the group PCA reduced matrix using the *infomax* algorithm (Bell and Sejnowski, 1995). To ensure stability of estimation, we repeated the ICA algorithm 20 times and using ICASSO<sup>1</sup> aggregate spatial maps were estimated as the modes of component clusters. Subject specific spatial maps (SMs) and time courses (TCs) were obtained using the spatio-temporal regression back reconstruction approach (Calhoun et al., 2001a; Erhardt et al., 2011) implemented in GIFT software.

#### 4.4.4 Post ICA Processing

The subject specific TCs corresponding to the ICNs selected were detrended (with polynomial of order two), orthogonalized with respect to estimated subject motion parameters, and then despiked. The despiking procedure involved detecting spikes as determined by AFNI's 3dDespike algorithm and replacing spikes by values obtained from third order spline fit to neighboring clean portions of the data. The despiking process reduces the impact/bias of outliers on subsequent functional network connectivity (FNC) measures (Allen et al., 2012).

---

<sup>1</sup> <http://www.cis.hut.fi/projects/ica/icasso>



It is important to note that raw fMRI time-series are not stationary with respect to the mean due to many factors such as the scanner drift. This undesired property violates an important assumption in many statistical procedures. The common practice in analyzing fMRI time-series is to detrend them (e.g. by polynomial of order 2). This preprocessing step makes the stationary assumption much more realistic.

#### 4.4.5 Functional Network Connectivity

FNC was computed as described in section 2.2.4. We use the term “uncorrected FC/FNC” to describe correlations between the original time series, whereas “correct FC/FNC” describes correlations between the autocorrelation corrected time-series hereafter.

#### 4.4.6 Autocorrelation Correction

AR models with orders ranging from 1 to 15 were fit to each ICA time-series for each subject. The best model order was selected based on the Akaike information criterion (AIC) (Akaike, 1974). The residuals of the best model were used as the corrected, white time-series. The Durbin-Watson (DW) statistic is a common statistic to measure autocorrelation in a time-series (Durbin and Watson, 1950, 1951). A DW statistic of 2 signifies no autocorrelation and DW values less or greater than 2 signify positive and negative autocorrelation structure, respectively. The DW statistics for a time-series ( $w_t$ ) with  $N$  time points can be calculated as follows:

$$d = \frac{\sum_{t=2}^N (w_t - w_{t-1})^2}{\sum_{t=1}^N w_t^2} \quad (4-22)$$

## 4.5 Results

### 4.5.1 Simulated Data

The theoretical results in the previous sections established the properties of the sample correlation coefficient between two autocorrelated time-series ( $r_{x,y}$ ). To verify the validity of the theoretical results, time-series  $w$ ,  $z$ ,  $x$  and  $y$  were simulated with different  $\alpha$ ,  $\beta$ ,  $N$  and  $\rho_{w,z}$  values (see Section 4.3.1 for more details). The empirical bias of  $r_{w,z}$  and  $r_{x,y}$  was computed by subtracting  $\rho_{w,z}$  from mean of  $r_{w,z}$  and  $r_{x,y}$  averaged over 10,000 runs respectively. The empirical standard deviation of observed  $r_{w,z}$  and  $r_{x,y}$  averaged over 10,000 runs is also reported. In Figure 4-3 summary of the simulation and theoretical results for  $\rho_{w,z} = 0.5$  is depicted. The results for other correlation values are omitted from the main text since results followed Eq. (4-16) and Eq. (4-19), similar to the case of  $\rho_{w,z} = +0.5$ , though results for  $\rho_{w,z} = +0.2$  and  $\rho_{w,z} = +0.8$  are provided in the supplementary material. The bias for negative values of  $\rho_{w,z}$  was of the same size as for the positive values but in the opposite direction (bias was positive); variance for negative and positive  $\rho_{w,z}$  were the same. It is evident from Figure 4-3 that our theoretical approximations follow the empirical results closely. In only extreme autocorrelation coefficient values (e.g.  $\alpha = \beta = 0.9$ ) our theoretical approximation overestimate the empirical variance.

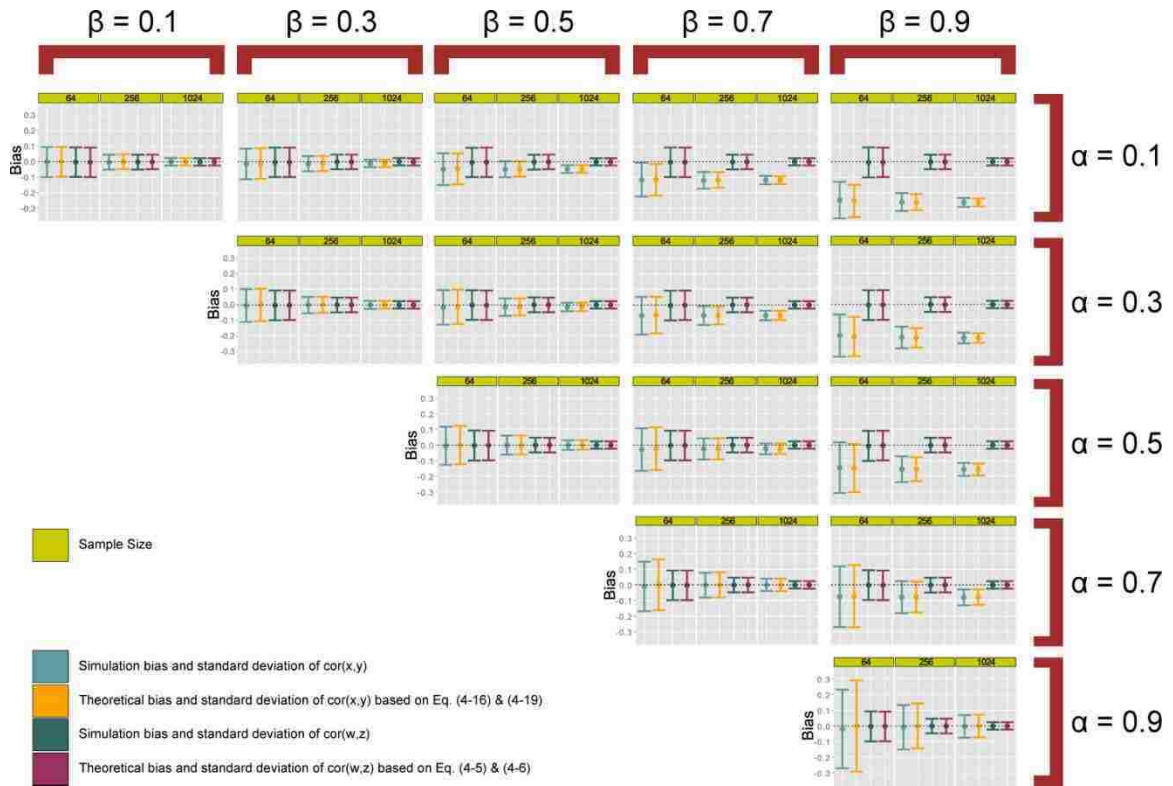


**Figure 4-3:** Empirical bias and standard deviation of estimation of true  $\rho_{w,z} = +0.5$  based on  $r_{x,y}$  and  $r_{w,z}$  for different combination of AR(1) coefficients ( $\alpha$  and  $\beta$  in Eq. (4-8) and (4-9) for time-series  $x$  and  $y$  and different sample sizes (length of time-series  $x$  and  $y$ ) of (64, 256, 1024) obtained from 10,000 simulations. The empirical results are compared with theoretical bias and standard deviation of  $r_{w,z}$  and  $r_{x,y}$  derived in Eq. (4-5) & (4-6) and Eq. (4-16) & (4-19) respectively. The whiskers show standard error of the estimation of the mean (square root of variance of the estimator). It is evident that theoretical and empirical results agree with each other. For equal coefficients, estimation of  $\rho_{w,z}$  based on  $r_{x,y}$  is unbiased. For different AR(1) coefficients, estimation is biased. The variance of the estimator increases as the product of AR(1) coefficients if  $x_t$  and  $y_t$  increases.

To better portray the effect of autocorrelation on correlation coefficients in the simulated data, Figure 4-4 displays histograms of  $r_{w,z}$  and  $r_{x,y}$  as well as scatter plot of  $r_{x,y}$  against  $r_{w,z}$  for three simulation scenarios, all with a sample size of 256.

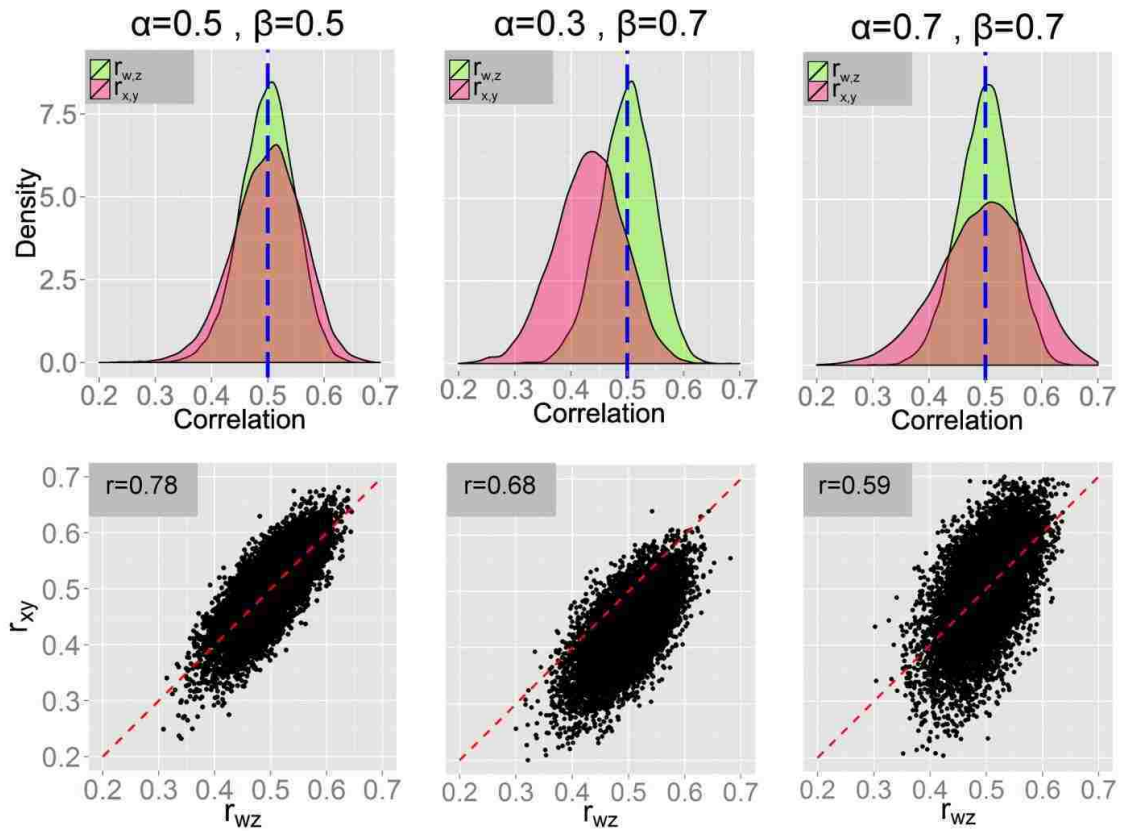


**Figure 4-4:** Top row: Histogram of corrected and uncorrected empirical Pearson cross correlation coefficients ( $r_{w,z}$  and  $r_{x,y}$ ) obtained from 10,000 simulations based on (4-8) and (4-9) with sample size of 256 and true correlation of +0.5 for 3 different combination of  $\alpha$  and  $\beta$  ((4-8) & (4-9)). Bottom Row: Scatter plot of uncorrected correlation coefficients,  $r_{x,y}$ , against corrected correlation coefficients  $r_{w,z}$ . Correlation coefficient between  $r_{w,z}$  and  $r_{x,y}$  is provided in the bottom row scatter plots ( $r$ ).

#### 4.5.2 Real fMRI Data

After standard preprocessing, the functional imaging data from all subjects was decomposed into a set of 100 statistically independent spatial regions with common time course profile using group independent component analysis using GIFT toolbox (<http://mialab.mrn.org/software/gift>). Subject-specific spatial maps and time courses were obtained using spatio-temporal regression (Erhardt et al., 2011). Of these 100 components, 47 components were identified as resting-state networks using the

procedures described in our earlier work (Allen et al., 2012; Allen et al., 2011). For each subject, we computed the functional network connectivity, referred to as FNC, by computing pairwise Pearson correlation using the whole processed ICA time-courses resulting in 1081 connectivity values. ICA spatial maps were broadly categorized based on anatomical proximity and prior knowledge of their function into the following sub-categories: subcortical (SC), auditory (AUD), visual (VIS), somatomotor (SM), a heterogeneous set of regions involved in various attentional and cognitive control processes (CC), default-mode (DMN), and cerebellar (CB) networks. These resting-state networks are illustrated in Figure 4-5:

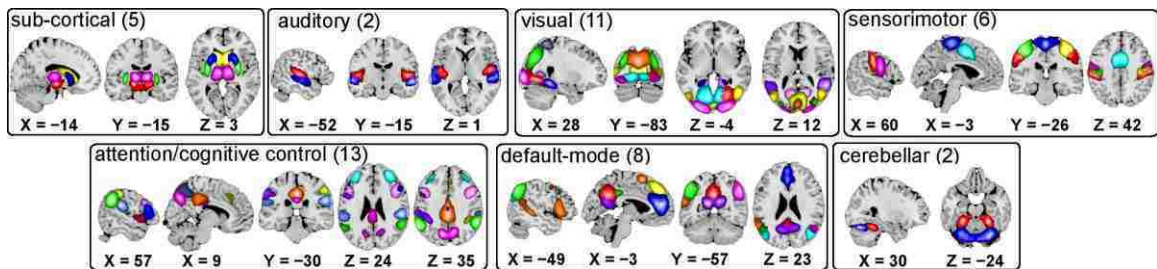


**Figure 4-5:** Spatial maps of selected 47 independent components grouped based on functionality into 7 categories: subcortical (5 components), auditory (2 components), visual (11 components), sensorimotor (6 components), attention/cognitive control (13 components), default-mode network (8 components) and cerebellar (2 components).

To assess the impact of autocorrelation on FC, ICA-time courses were corrected using autoregressive model. Best AR model order was selected based on AIC. The Durbin-Watson (DW) statistic was used to measure autocorrelation in the time-series before and after autocorrelation correction. Histograms of the DW statistics of ICA time-series for both healthy and patient groups before and after autocorrelation correction are plotted in Figure 4-6.

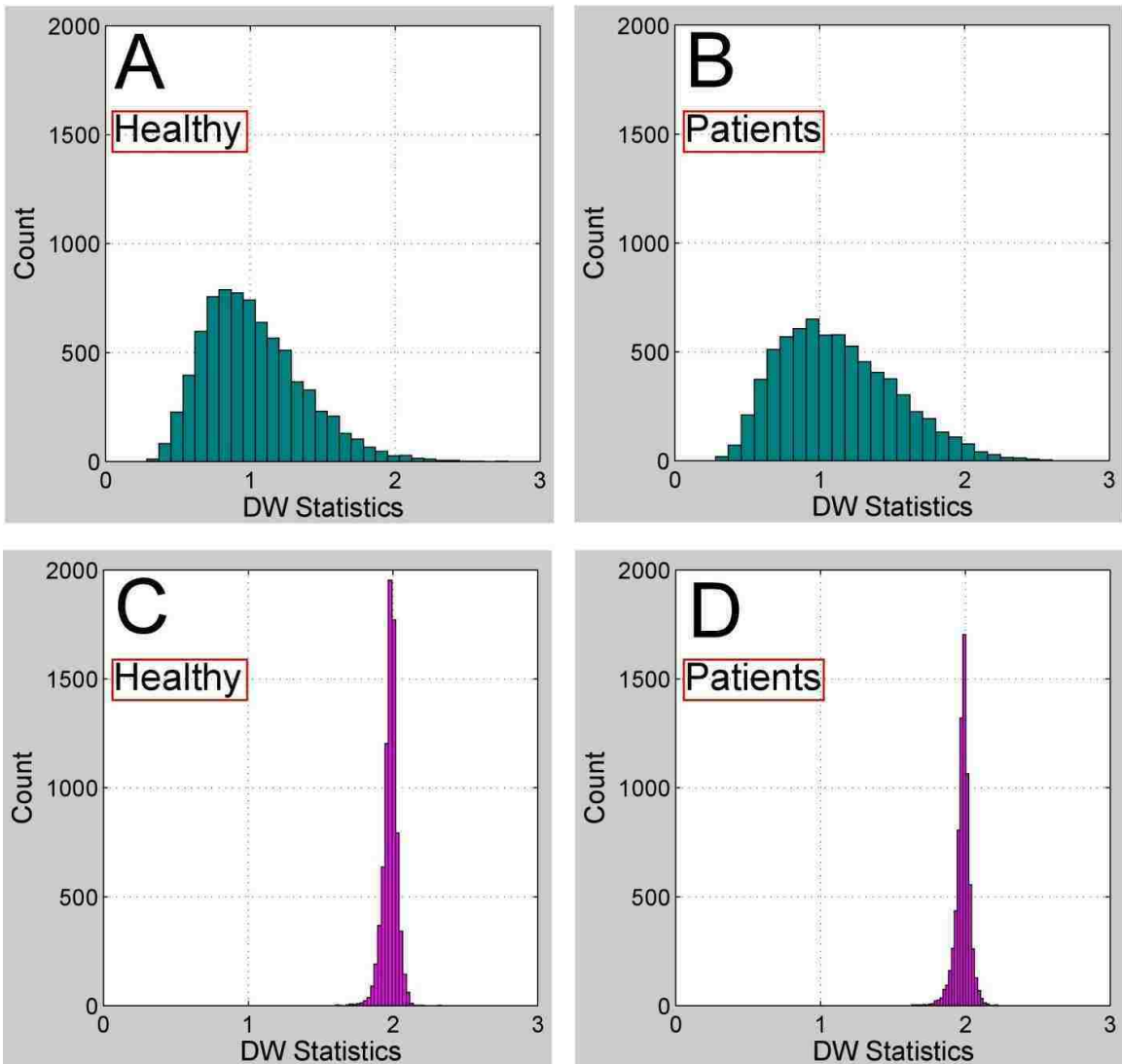


Figure 4-6: Durbin-Watson statistics histogram for A: Uncorrected IC time-series for healthy controls B: Uncorrected IC time-series for schizophrenia patients C: Corrected IC time-series for healthy controls D: Corrected IC time-series for schizophrenia patients. Autocorrelation correction could successfully concentrate DW statistics around 2 which is a sign for absence of autocorrelation.

We also performed a one-sample t-test on Fisher-Z transformed FNC values. The mean and standard deviation of FNC values along with corresponding p-values before and after autocorrelation correction for both healthy controls and schizophrenia patients are reported in Figure 4-7A,B and Figure 4-8A,B respectively. It is evident that both mean and standard deviation are inflated before autocorrelation correction. The bias in

the mean and standard deviation of FNC values cancel each other significantly in the t-tests as illustrated in Figure 4-7C and Figure 4-8C making the hypothesis testing results very similar before and after correction.

One of the common purposes of connectivity analysis is to compare groups (e.g. healthy controls and patients). To investigate the effect of autocorrelation on such problems, FNC was compared between healthy controls and schizophrenia patients using two-sample t-test before and after autocorrelation correction. The resulting p-values along with the difference in FNC before and after autocorrelation correction are illustrated in Figure 4-9.

To better observe the relationship between FNC values before and after autocorrelation correction, histogram of FNC values (all pairs for all subjects pooled) before and after autocorrelation correction are plotted in Figure 4-10(A). Scatter plots of uncorrected FNC values (pooled) against corrected FNC values are illustrated in Figure 4-10(B). We also plotted  $-\log_{10}(p\_value) \times \text{sign}(T\_Statistics)$  (Figure 4-7C, Figure 4-8C) before and after correction for both groups in Figure 4-10(C) which shows a strong linear relationship.

We also repeated the autocorrelation correction with just an AR(1) model to determine the range of AR(1) coefficients for real fMRI data and compare it to the theoretical and simulation results. The model worked reasonably well based on DW statistics. The histogram of AR(1) coefficients for healthy controls and schizophrenia patients are illustrated in Figure 4-11.

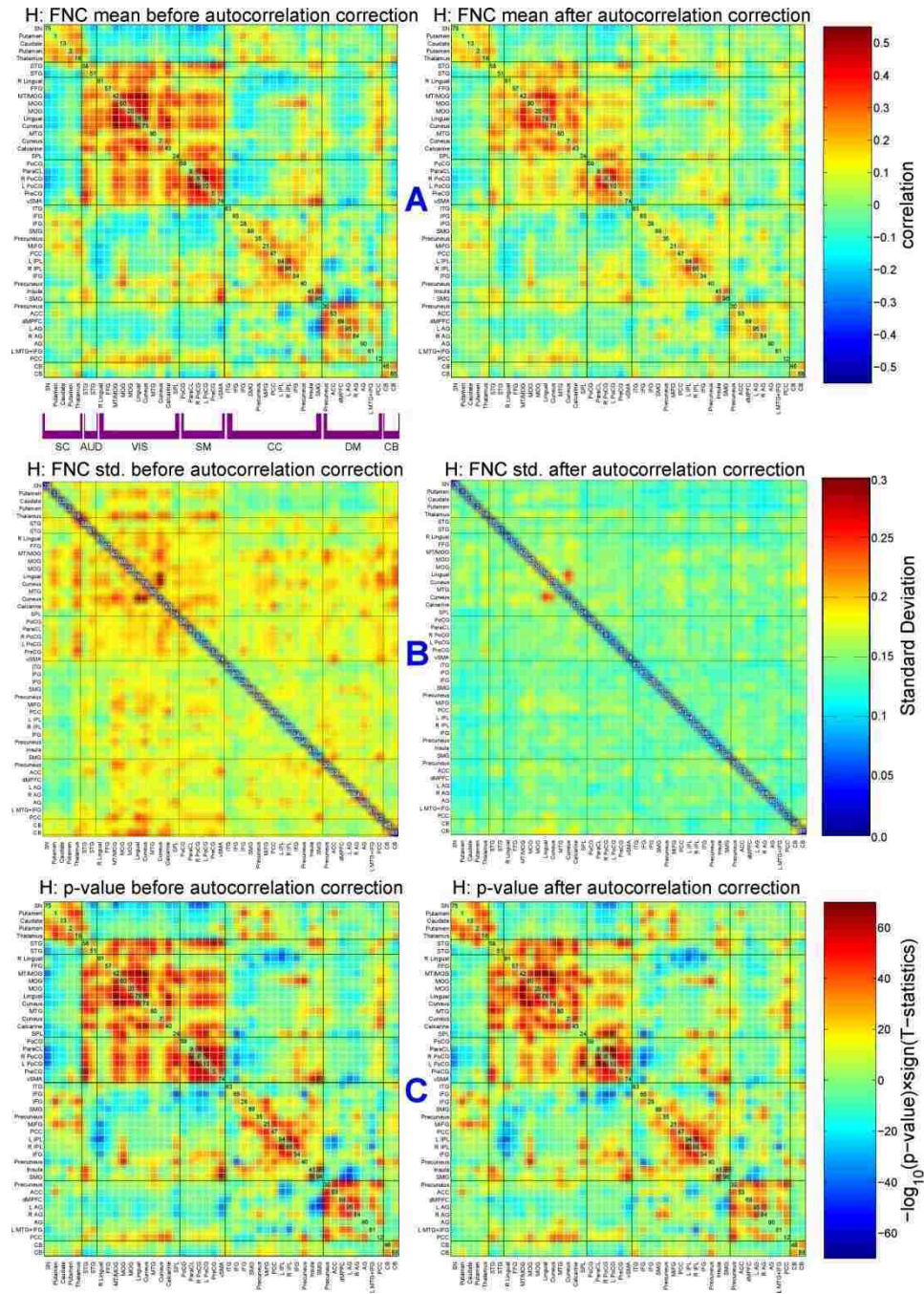


**Figure 4-7:** A,B: Mean and standard deviation of FNC grouped by functionality of brain networks (Figure 2) for healthy controls before and after autocorrelation correction. C:  $-\log_{10}(p\text{-value}) \times \text{sign}(T\text{-statistics})$  after subject-wise 1-sample t-test on each FNC pair before and after autocorrelation correction. Although the FNC values alter noticeably before and after autocorrelation correction, p-values remain very similar.



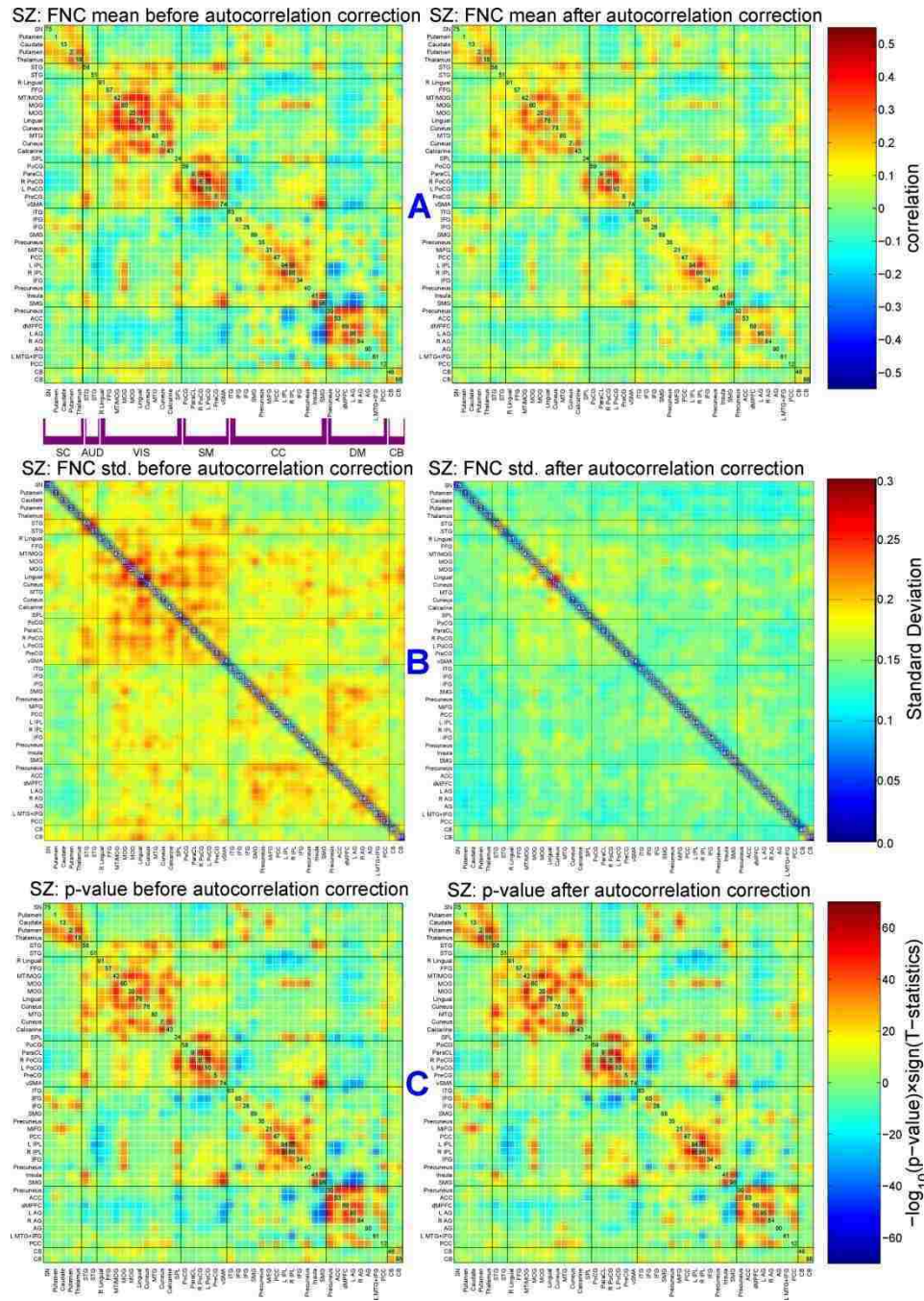


**Figure 4-8:** A,B: Mean and standard deviation of FNC grouped by functionality of brain networks (Figure 2) for schizophrenia patients before and after autocorrelation correction. C:  $-\log(p\text{-value}) \times \text{sign}(T\text{-statistics})$  after subject-wise 1-sample t-test on each FNC pair before and after autocorrelation correction. Although the FNC values alter noticeably before and after autocorrelation correction, p-values remain very similar.

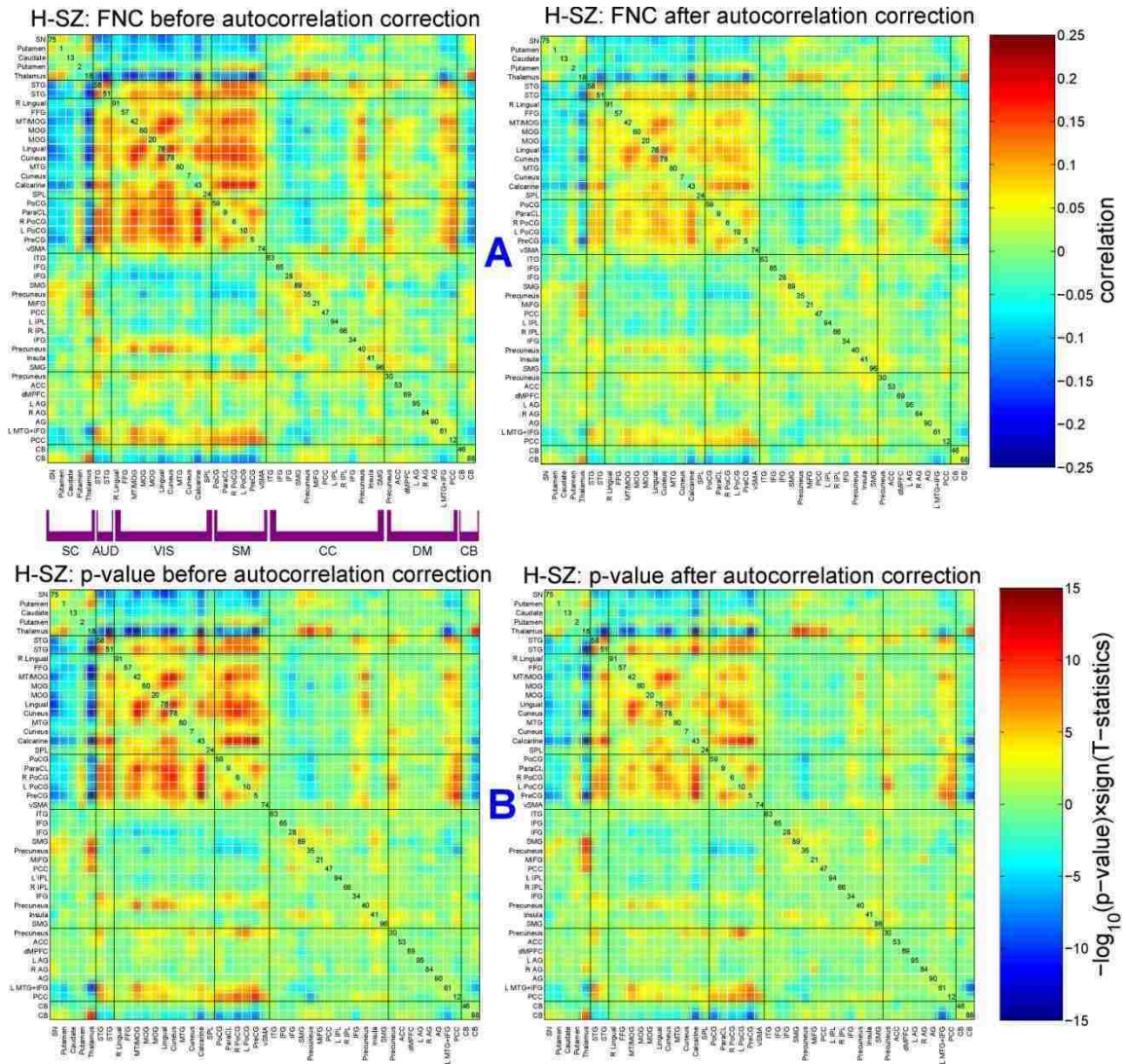


**Figure 4-9:** A: Difference in mean of FNC between healthy controls and schizophrenia patients (healthy-patients) grouped by functionality of brain networks (Figure 1) before and after autocorrelation correction. B:  $-\log_{10}(\text{p-value}) \times \text{sign}(T\text{-statistics})$  after subject-wise 2-sample t-test between controls and patients before and after autocorrelation correction. Although the differences in FNC values between healthy controls and patients alter noticeably before and after autocorrelation correction, p-values of 2-sample t-test remain very similar.

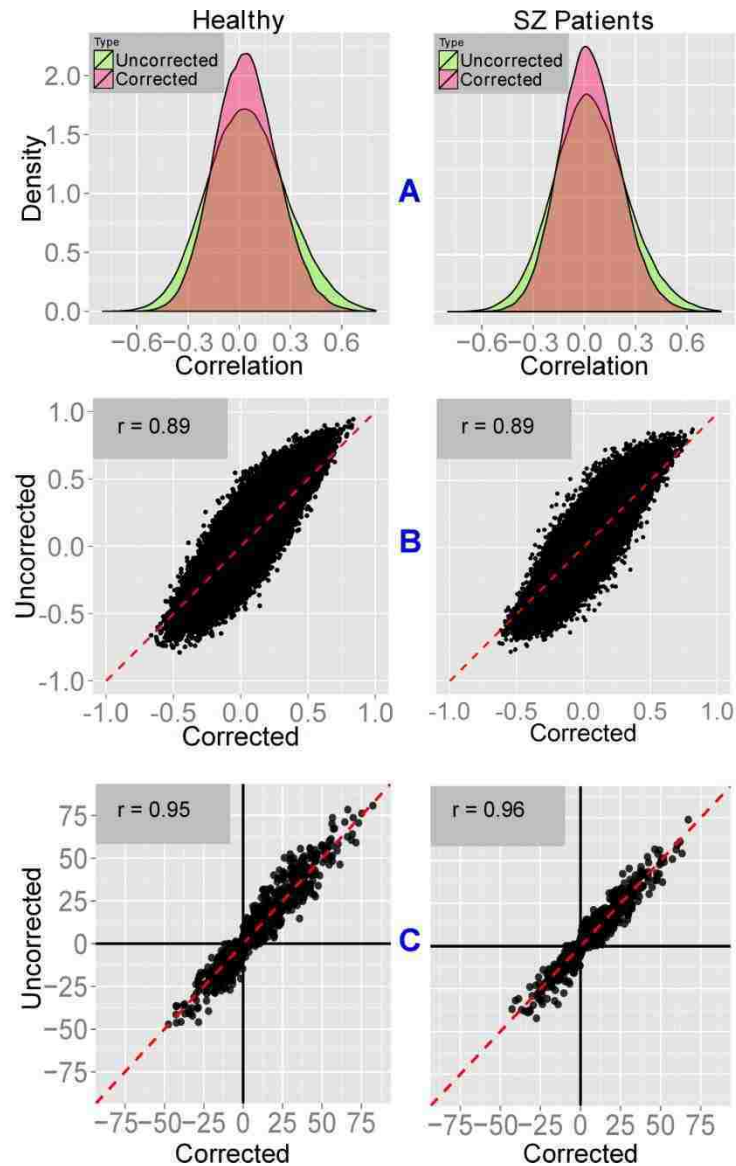


**Figure 4-10:** A: Histogram of corrected and uncorrected FNC values (pooled all subjects and pairs) for healthy controls and schizophrenia patients. B: Scatter plot of uncorrected FNC values against corrected FNC values for healthy controls and schizophrenia patients. Correlation coefficient between corrected and uncorrected FNC values is high for both groups ( $r = +0.89$ ). Compare these results with simulation results in Figure 4-4 (especially for  $\alpha = \beta = 0.5$ ). C: Scatter plot of  $-\log(p\_value) \times \text{sign}(T\_Statistics)$  before and after autocorrelation correction for healthy controls and schizophrenia patients (these are scatter plots of color-coded values in Figure 4-7C and Figure 4-8C).

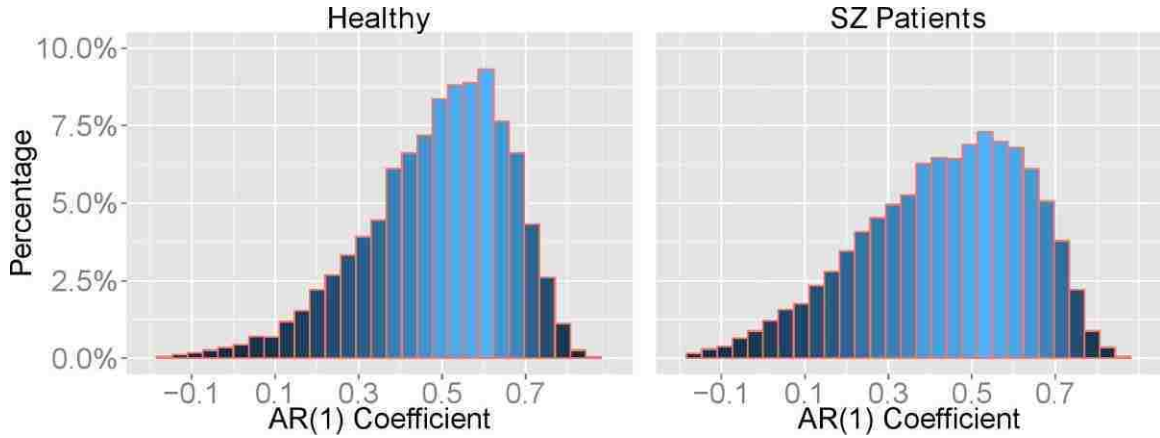


**Figure 4-11:** Histogram of AR coefficient for pooled IC time-series for all subject for healthy controls and schizophrenia patients if all time-series are corrected with AR(1).

## 4.6 Discussion

In this work, we comprehensively investigated the impact of autocorrelation on functional connectivity with theory, simulations and real fMRI data. We derived the approximate bias and variance of Pearson correlation coefficient for two autocorrelated time-series  $(x,y)$  with AR(1) structure as an estimator of the true correlation coefficient between white time-series component of the AR(1) models  $(w,z)$ . Based on Eq. (4-16), approximately the expected value between two autocorrelated time-series is equal or less than the expected value between the white latent time-series in the AR(1) model. If the AR(1) coefficients for both time-series are equal, the estimation is unbiased. The estimation becomes biased as the distance between AR coefficients of the two time-series increases. Based on Eq. (4-19), the variance of this estimator increases as the product of the AR(1) coefficient of the two time-series increases.

The autoregressive process has been investigated heavily in signal processing domain from frequency point of view. The AR(1) process has been modeled as a linear

time-invariant system with a white time-series input and autocorrelated time-series as the output (Figure 4-1). It was seen that feeding an AR(1) model (positive coefficient) with a white signal results in a lowpassed output signal (Figure 4-2). The process of autocorrelation correction (whitening) can be viewed as applying frequency response of the inverse system to the observed signal to even out the frequency spectrum.

Figure 4-3 shows how bias and variance of estimation of  $\rho_{w,z}$  changes based on theoretical and empirical results of  $r_{x,y}$  and  $r_{w,z}$  with respect to AR(1) coefficients. It is evident that empirical results agree with and validate the theoretical results at least in the context of this study. It is also clear that the bias in estimation of  $r_{w,z}$  based on  $r_{x,y}$  is a function of distance between AR(1) coefficients of  $x$  and  $y$  while the variance is a function of the product of AR(1) coefficients. To better investigate the effect of autocorrelation on Pearson correlation coefficient, histogram of  $r_{w,z}$  and  $r_{x,y}$  as well as scatter plot of  $r_{x,y}$  against  $r_{w,z}$  for 3 different AR(1) coefficient pairs were illustrated in Figure 4-4. The bias and variance effect of autocorrelation on estimating  $r_{w,z}$  based on  $r_{x,y}$  is obvious in these three simulations.

For real fMRI data, the FC values before and after autocorrelation correction show noticeable difference in both healthy controls and patients (Figure 4-7A, Figure 4-8A). We see the same pattern in standard deviation (Figure 4-7B, Figure 4-8B). The direction of change for both mean and standard deviation is the same. As a result, the p-values resulting from one-sample t-tests on each FC value across subjects are very similar before and after autocorrelation correction (Figure 4-7C, Figure 4-8C). In other words, bias in the mean is cancelled out significantly by bias in the standard deviation in the t-tests. The inflation in standard deviation of the correlation values is in line with theoretical results

(Eq. (4-19)) and simulation results (Figure 4-3). This is more clearly depicted in Figure 7C. This suggests that inference related to the significance of FC is not strongly affected by autocorrelation correction. This interesting result argues against the recent debates about spuriousness of functional connectivity based on uncorrected correlation coefficient (Christova et al., 2011; Georgopoulos and Mahan, 2013). While the argument regarding the correlation values themselves remain valid, it appears that hypothesis testing remains relatively unbiased in the presence of autocorrelation. This observation is also present in differences in FC between healthy controls and schizophrenia patients (Figure 4-9). As illustrated in Figure 4-10, corrected and uncorrected functional network connectivity values are highly correlated with each other and exhibit a linear relationship. The scatter plots of p-values before and after autocorrelation correction show even stronger linear relationship as illustrated in Figure 4-10C. The uncorrected FNC values show larger variance compared to the corrected values, as expected from Eq. (4-19).

In order to compare the real fMRI data with the simulation results, we also corrected for autocorrelation using AR(1) model. Based on DW statistics, AR(1) model was able to remove the autocorrelation reasonably well. The histogram of AR(1) model coefficients as illustrated in Figure 4-11 shows that the fMRI time-series in this study have AR(1) coefficients less than +0.8 and mostly in the range of [+0.1 +0.7]. Thus we don't expect to see the extreme cases in real fMRI that we observed in the simulation results (Figure 4-3).

It should be noted that in cases where the correlation coefficient itself is of interest, autocorrelation correction is more critical. However, it is always recommended to check for autocorrelation structure in fMRI time-series. Although the statistical analysis in this

study was conducted using R software, we provide MATLAB code for autocorrelation correction as it is the main technical computing software used by neuroimaging community<sup>1</sup>. There are several important issues regarding autocorrelation correction that we discuss below.

#### **4.6.1 Autocorrelation Correction and Frequency Filtering**

Temporal filtering is one the common preprocessing steps in functional connectivity studies. The reason for temporal filtering is that it is believed that signals of interest in connectivity studies reside in a narrow frequency band mainly from 0.01 Hz to 0.08~0.15 Hz (Auer, 2008; Biswal et al., 1995a; Cordes et al., 2001b; Salvador et al., 2005; Zhong et al., 2009) while scanner drift and physiological noise are in lower and higher frequency, range respectively (Bianciardi et al., 2009; Lowe et al., 1998; Thomas et al., 2002). Although some functional connectivity studies have shown that temporal filtering does not significantly impact the results in group studies (Arbabshirani et al., 2013a), it is a common practice. It should be noted that modifying frequency spectrum of a signal with filtering changes the autocorrelation profile of the signal. Specifically, frequency filtering of a white signal induces autocorrelation. Thus, if fMRI time-series are corrected for their intrinsic autocorrelation with methods like ARIMA, frequency filtering can introduce a more complicated autocorrelation problem (Davey et al., 2013). This is demonstrated in Figure 4-12.

---

<sup>1</sup> <http://mialab.mrn.org/software/autocorrection/index.html>

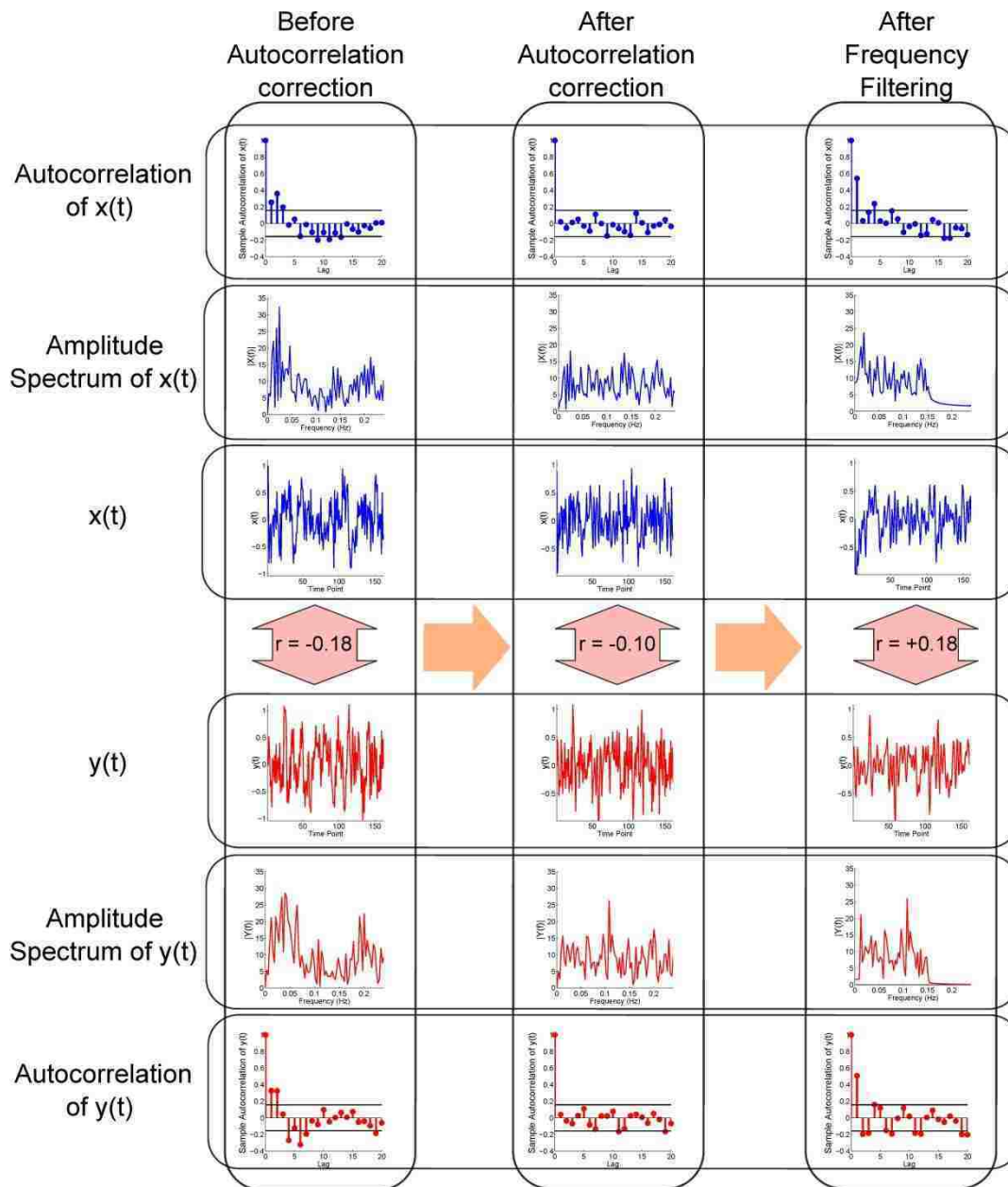


**Figure 4-12:** Autocorrelation function with 95% confidence interval lines and amplitude of frequency spectra for two fMRI time-series,  $x(t)$ ,  $y(t)$  before autocorrelation correction (left column), after autocorrelation correction with AR(4) model (middle column) and after frequency filtering with a order 6 Butterworth passband filter with cutoff frequencies of 0.01 Hz and 0.10 Hz (right column). While autocorrelation correction improves the autocorrelation function (all values are inside 95% confidence interval), frequency filtering introduce back the autocorrelation in a more severe and complicated manner.



In this example, two real fMRI time-series are shown along with their amplitude frequency spectra and autocorrelation functions. Some values of the autocorrelation function are outside the 95% confidence interval indicating significant autocorrelation. Also, the frequency spectra are not flat. After applying AR(4) model to correct both time-series, the frequency spectra are closer to flat and autocorrelation functions is bounded inside the 95% confidence interval. Applying a bandpass frequency filter (0.01-0.10 Hz), reintroduces autocorrelation to an even more severe degree than compared to the intrinsic fMRI autocorrelation. This problem has been studied carefully and a correction on the correlation values between filtered time-series has been proposed based on degrees of freedom correction which is related to filter parameters (Davey et al., 2013). The assumption in this method is that two time-series are white before filtering. A reasonable preprocessing for connectivity studies is to correct for autocorrelation, perform frequency filtering, and then correct the correlation values based on the filter parameters.

#### **4.6.2 Model Order for Autocorrelation Correction**

One of the main issues in autocorrelation correction is the model order selection problem. As briefly discussed in the introduction, autocorrelation in fMRI time-series originates from physical and physiological noise. One of the main sources of autocorrelation is the hemodynamic response function (Friston et al., 1995; Rajapakse et al., 1998). FMRI time-series can be seen as samples from the hemodynamic response function (HRF) with sampling rate of  $1/TR$  where  $TR$  is the repetition time of the scanner. Since the HRF is a smooth curve, samples exhibit autocorrelation. A faster  $TR$  results in a higher sample rate but come with higher autocorrelation, thus model order should be directly related to  $TR$ . Assume that there is a single event fMRI time-series. In

this case the resulting time-series is the sampled HRF. We sampled the HRF with different  $TR$ s and corrected for autocorrelation by finding the best AR model order based on AIC. Figure 4-13A show a canonical HRF function. Figure 4-13B plots  $TR$  against the estimated model order. The best AR model order grows exponentially as  $TR$  decreases. This example is for a single event while typical task-based fMRI consists of series of events or blocks which can result in different autocorrelation structure. However, Figure 4-13B gives a rough idea of the model order required to correct for autocorrelation, and shows that autocorrelation correction becomes more crucial as the experimental  $TR$  decreases.

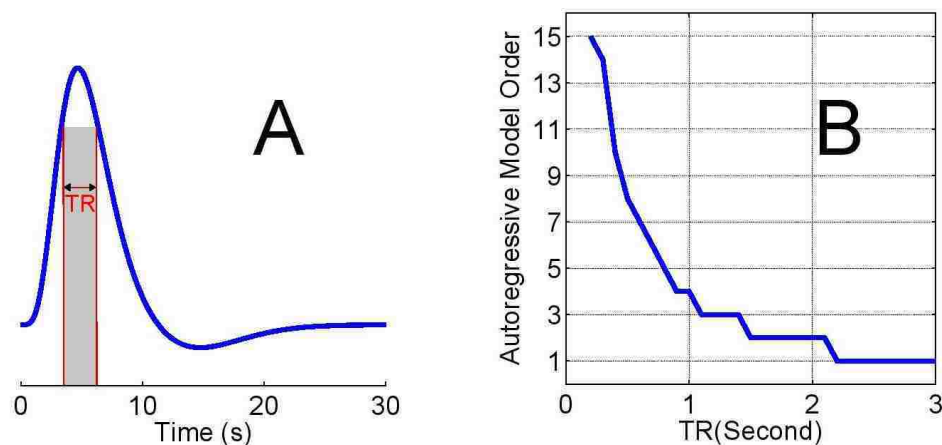


**Figure 4-13:** A: Canonical HRF function B: Best model order based on AIC for correcting autocorrelation of samples taken with different  $TR$  (repetition time) from the HRF function. Best model order increases exponentially as  $TR$  decreases.

### 4.6.3 Impact of Autocorrelation on FC: Hyperconnectivity, Hypoconnectivity or No Impact?

In regression analysis it has been shown that estimation of model parameters ( $\beta$ ) in the presence of serial correlation in the residuals is still unbiased but not efficient

(Granger and Morris, 1976; Monti, 2011). It is important not to extend this result to the impact of autocorrelation on functional connectivity. Autocorrelation can bias the estimation of Pearson correlation coefficient based on our theoretical, simulated and real fMRI results. Eq. (4-16) as demonstrated by our empirical results in Figure 4-3, shows that if AR(1) coefficient of the two time-series differ, then the Pearson correlation coefficient is underestimated. If the coefficients are the same, then the estimation is unbiased. These results are plausible since we consider AR(1) as a filter (Figure 4-1 and Figure 4-2), then applying the same filter to two white time-series should not change their correlation coefficient but applying different filters can reduce it. However, our real fMRI results in Figure 4-7 and Figure 4-8 are consistent with other studies (Christova et al., 2011; Davey et al., 2013), suggest hyperconnectivity for uncorrected time-series, seemingly contradicting our theoretical and simulation results.

The approximate theoretical results are just for AR(1) process while the real fMRI data was corrected with AR of order 1 to 15 based on AIC criterion. Also, it is assumed that the two time-series are uniformly correlated with respect to frequency. In other words, correlation is equally present in all frequency bands between  $w$  and  $z$ . This assumption is not generally true for real fMRI time-series. fMRI time-series consists of a low frequency component that is the major source of correlation which is corrupted with noise that is assumed to be more in higher frequencies (Cordes et al., 2001b). Thus, applying a low pass filter can remove the noise (or part of the noise) and enhance the correlation between the two time-series. To better illustrate this, we simulated a simple case where two correlated low frequency time-series (Figure 11A) were generated and

then high frequency noise was added (Figure 11B). Finally the noisy signals were passed through an AR(1) process (Figure 11C).

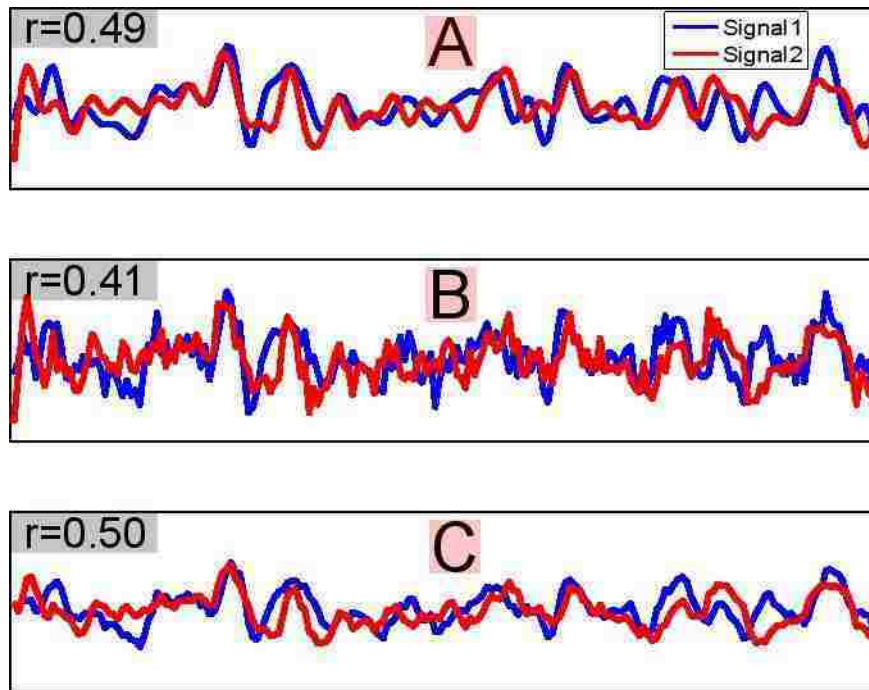


**Figure 4-14:** A: Two correlated low frequency time-series (200 time-points) B: After adding high frequency noise to the original time-series in part A ( $SNR = 20db$ ) C: Time-series in part B passed through AR(1) process with coefficients of +0.6. Autocorrelation acts as a low pass filter and enhances the correlation between two noisy signals in part B close to the original level in part A.

It is evident that autocorrelation (Figure 4-14C) behaves as a low pass filter as expected (refer to supplementary material for more detailed discussion) and removes part of the high frequency noise and therefore enhanced the correlation compared to the noisy situation (Figure 4-14B). Note that this increased correlation is very close to the original correlation between the two time-series before adding noise (Figure 4-14A). So, autocorrelation process is capable of removing noise (depending on the model order, coefficients and frequency spectra of the signals) and increasing correlation. We believe that this is the primary reason for hyperconnectivity in uncorrected functional

connectivity studies. Despite the hyperconnectivity, the result of hypothesis tests such as the t-test remain similar for corrected and uncorrected FC values since overestimation of the mean is significantly compensated with the bias in standard error of the mean (Figure 4-7, Figure 4-8 and Figure 4-10). This simple example shows that autocorrelation correction may result in unwanted amplification of high frequency bands that is assumed to be dominated by noise in fMRI time-series.

#### **4.6.4 Limitations and Future Studies**

The current study compares FC before and after autocorrelation study with a specific choice of analysis pathway. There are several other choices for each analysis step that have not been considered in this study. For example, we removed autocorrelation by using autoregressive model while there are several more advanced methods to model autocorrelation. For functional connectivity we used group ICA followed by Pearson correlation coefficient among ICA time-courses (FNC). Seed-based analysis is another common method for connectivity studies. Correlation is not the only way of measuring statistical dependency and other methods such as mutual information are common too. We compared FNC before and after autocorrelation correction via t-tests on each FNC value. Although mean and standard error are the main component of many statistical tests such as t-test, we should emphasize that there are several other statistical analysis methods (like multivariate methods) to compare functional connectivity values within a group and between groups. Also, p-values are not the only measures of statistical significance. These choices were guided by our previous functional connectivity studies (Arbabshirani and Calhoun, 2011; Arbabshirani et al., 2013a; Arbabshirani et al., 2013b; Jafri et al., 2008; Meda et al., 2012) and others (Greicius et al., 2003; Wang et al., 2007).

One important subject for future studies is to assess the impact of autocorrelation in task-based studies. Such a study has its own complications since the design paradigm affects the autocorrelation structure in fMRI time-series.

With regard to theoretical results, an interesting topic of future studies may be to investigate the impact of autocorrelation on Pearson correlation in the general case of AR(N) where N is a positive integer. In the case of  $N > 1$ , autocorrelation affects the time-series as a more flexible frequency filter (compared to AR(1) as discussed in the supplementary material) depending on the AR coefficients which can impact the results differently. Moreover, theoretical results and simulation time-series characteristics could be matched more closely to the settings of real fMRI which is non-trivial due to complex signal and noise structure of fMRI time-series.

#### **4.7 Conclusion**

In this study, we assessed the effect of autocorrelation on functional connectivity. We started with approximate theoretical results in a simple AR(1) model and provided approximations for bias and variance of estimator of Pearson's correlation coefficient between two autocorrelated time-series. The approximated theoretical results were well validated using simulations. We found that bias of the estimation depends on the difference between AR(1) coefficients of the two time-series while the variance is a function of product of the coefficients. We further investigated the effect of autocorrelation on functional connectivity in real fMRI data in both healthy controls and schizophrenia patients. We found that autocorrelation can slightly alter the Pearson's correlation coefficients, however, the effect of this on the hypothesis tests of group differences based on t-statistics is very mild. It should be noted that the effect of

autocorrelation appears to directly depend on the  $TR$  parameter of the MRI acquisition and the problem becomes more serious for fast acquisitions. Our results do not support the hypothesis that ignoring intrinsic autocorrelation in fMRI time-series results in meaningless spurious connectivity results, unlike some recent studies. While it remains important to assess and correct autocorrelation with appropriate model order to ensure the most accurate results, within the discrete domain of functional connectivity neuroimaging studies it does not appear that autocorrelation has a universally strong and indiscriminate biasing effect.

**Chapter 5: Autoconnectivity, a New Perspective on Human Brain's  
Functionality**



## 5.1 Introduction and Motivation

As discussed in Chapter 4, Autocorrelation is a well-known characteristic of functional magnetic resonance imaging (fMRI) time-series attributed to colored physical and physiological noise (Aguirre et al., 1997; Bullmore et al., 2001; Friston et al., 2000; Lenoski et al., 2008; Lund et al., 2006; Purdon and Weisskoff, 1998; Rajapakse et al., 1998; Zarahn et al., 1997). Various sources such as scanner drift (Lund et al., 2006), undersampled cardiac and respiratory signals (Aguirre et al., 1997; Bullmore et al., 2001; Friston et al., 2000; Lenoski et al., 2008; Lund et al., 2006; Purdon and Weisskoff, 1998; Rajapakse et al., 1998; Zarahn et al., 1997), smooth hemodynamic response and preprocessing steps such as temporal smoothing have been identified as major sources of autocorrelation (Friston et al., 1995). Treated as unwanted colored noise, autocorrelation has been one of the main confounds in fMRI data analysis using general linear modeling framework (Friston et al., 2000; Gautama and Van Hulle, 2004; Lund et al., 2006; Woolrich et al., 2001) and recently in functional connectivity studies (Christova et al., 2011) since many statistical assumptions are getting violated in the presence of autocorrelation. In the past two decades, the main focus of the neuroimaging community in the context of autocorrelation in fMRI time-series has been on methods to remove or compensate for it. Methods such as prewhitening and precoloring have been widely adopted by researcher to eliminate or reduce the effect of autocorrelation on fMRI data analysis.

While the exact sources of autocorrelation and their contribution to observed temporal dependency in fMRI time-series has remained as an open question, it was shown more than a decade ago that autocorrelation is mostly significant in the cortical

regions of the brain (Worsley et al., 2002). Based on this observation it can be postulated that smooth hemodynamic plays an important role in fMRI time-series autocorrelation structure. This plausible assumption explains the source of autocorrelation but not necessarily the amount of autocorrelation in the fMRI time-series as the latter can depend on the neural activity which is the input to the HRF.

It is well known that the neuronal process can be decomposed into evoked transients and intrinsic activity (Friston et al., 1995). Similarly, autocorrelation can be decomposed into an evoked component which is phase-locked to the task and an intrinsic component (Friston et al., 1995).

The main purpose of this study is to investigate intrinsic autocorrelation in resting-state fMRI. We hypothesize that strength of intrinsic autocorrelation contains important information about brain's functionality. We provide three distinct clues that demonstrate the usefulness of autocorrelation in understanding healthy human brain functionality as well as a novel look at brain disorders such as schizophrenia. We consider simple autoregressive process of order one and map the coefficient to the brain of healthy controls and schizophrenic patients. Following a comparison of these maps, we classify patients from controls using just the autoregressive coefficients. At the end we investigate the relationship between autoregressive coefficient during rest and hemodynamic response function during task in healthy controls and propose a hypothesis that intrinsic autocorrelation during rest is negatively correlated with the magnitude of evoked neuronal response during an auditory oddball task (AOD). To the best of our knowledge no one has investigated the autocorrelation in fMRI time-series as a potential source of information about the functionality of human brain and for clinical use.

## **5.2 Methods**

For this study we used both the Hartford dataset (section 1.14.1) and the FBIRN dataset (section 1.14.2)

### **5.2.1 Time-Series Preprocessing**

Each fMRI time-series was detrended with polynomial of order two. In order to reduce effect of motion on the analysis, six motion parameters, six squared of motion parameters, six first differences of motion parameters and six squared of first difference of motion parameters (Friston et al., 1996) were regressed out of each time-series. All the time-series were z-scored.

### **5.2.2 Autoregressive Modeling**

Autoregressive model of order one (AR1) coefficient was estimated for each time-series using the maximum likelihood approach. See section 4.3.1 for more information on AR(1) modeling.

### **5.2.3 Classification**

AR1 coefficients for all the voxels were averaged together for each region in the automated anatomical labeling (AAL) atlas to form a 116 feature vector for each subject. Features were z-scored to bring them to the same scale. 10 fold cross validation was used to assess the strength of the classifier. In each run, 10 subjects were left out and a linear support vector machine (SVM) was trained on the rest of samples. The soft margin parameter for SVM was selected based on grid search over range of plausible values. The criterion for selecting the best parameter was overall accuracy which was achieved by leave-one-out cross validation inside the training set.

## **5.2.4 Hemodynamic Response Function Estimation**

All of the preprocessed functional data during AOD task from 28 healthy controls in the Hartford dataset were analyzed using spatial group independent component analysis (GICA) framework as implemented in the GIFT software (Calhoun and Adali, 2012; Calhoun et al., 2001a; Erhardt et al., 2011). First at the subject level, dimensionality was reduced to 80. Then reduced data from all subjects and all sessions were concatenated together and put through another reduction step. The number of components for the second level reduction was estimated to be 20 by minimum description length (MDL) criterion (Li et al., 2007). This is also the number of IC components. Note the MDL is a data driven approach, so it is not dependent on whether data are collected at rest or during a task. In order to estimate subject-specific SMs, back-reconstruction method was used (Calhoun et al. 2001b; Erhardt et al. 2010).

The ICA time-courses of the auditory network were deconvolved against the stimulus paradigm to recover the HRF of that network. Amplitude height (H), time-to-peak (T) and full-width at half-max (W) of the estimated HRFs were calculated.

## **5.3 Results**

### **5.3.1 Mapping Autocorrelation Coefficient to the Brain during the Resting-State**

For each of the datasets, fMRI resting-state time series were modeled using AR(1). The AR(1) coefficient shows the amount of correlation or linear dependency between consecutive time points in a time series. In other words, AR(1) coefficient tells us to what extent current time point value is impacted by its immediate predecessor.

Figure 5-1A shows mapping of voxel-wise AR(1) coefficient to the brain in healthy controls and schizophrenia patients in both datasets. The average AR(1) ranges from zero to about 0.5 in both groups.

In order to detect voxels with significant autocorrelation coefficient, 1-sample t-test was performed for each voxel across subjects at 0.05 level corrected for multiple comparisons using false discovery rate (FDR) method. The t-maps are illustrated in Figure 5-1B. Figure 5-1B shows that autocorrelation is most significant in calcarine cortex, cuneus, parts of the precuneous and anterior cingulate cortex (ACC). It is evident that autocorrelation is significantly higher in cortical regions compared to white matter and CSF. The autocorrelation is less significant in Hartford dataset which can be related to lower statistical power due to its smaller sample size compared to the FBIRN dataset.

The next question of interest is to see if there is any significant difference between healthy controls and patients in terms of strength of autocorrelation. We conducted two sample t-test between the two groups for each voxels. The T-maps (Figure 5-1C) shows that several regions in the visual system including cuneus and calcarine along with small regions in somatosensory and motor cortex have significantly lower autocorrelation in schizophrenia patients compared to healthy controls. Another interesting region following the same pattern is the thalamus. Similar to Figure 5-1B, the Hartford dataset exhibits fewer significant regions compared to FBIRN (which is expected in part because there are many fewer subjects) but also exhibits many similarities.

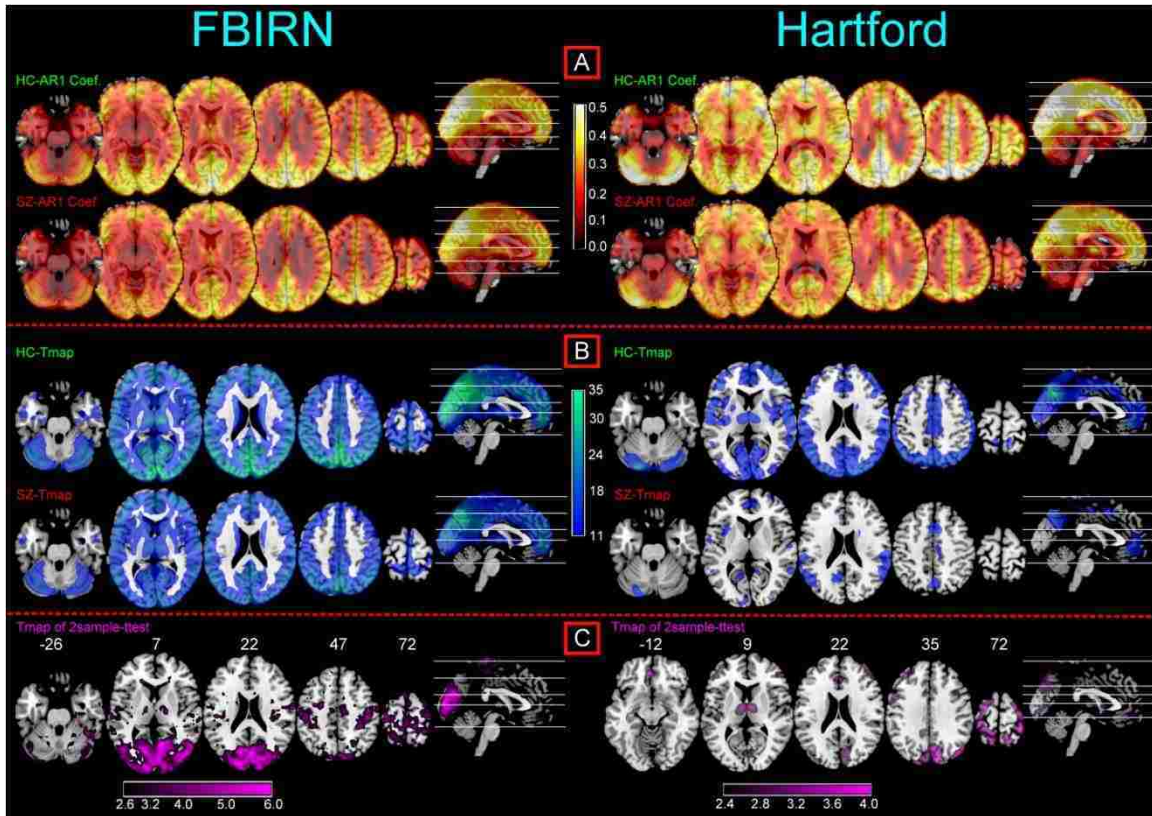


**Figure 5-1:** A: Resting-state AR(1) coefficient estimated for each voxel for both healthy control and schizophrenia patients. B: T-maps resulted from group-wise one-sample t-test on each voxel for both healthy control and schizophrenia C: T-maps resulted from two sample t-test between healthy controls and schizophrenia patients.

### 5.3.2 Mapping Autocorrelation Coefficient to the Brain during the AOD Task

Autocorrelation during performance of a task is composed of an evoked component as well as an intrinsic component. The evoked part is dependent on the task design which makes it hard to make inference about its strength as opposed to intrinsic autocorrelation during resting-state. However, it is interesting to compare autocorrelation during rest and task and see if autocorrelation changes meaningfully during performance of a simple task compared to the resting-state. The results are illustrated in Figure 5-2. Figure 5-2A shows the AR(1) mapping for both groups and Figure 5-2B shows results

from a of group-wise one sample t-test on each voxel's AR(1) coefficient. We did not find any significant difference between the two groups in contrast to the resting-state analysis (Figure 5-1C).

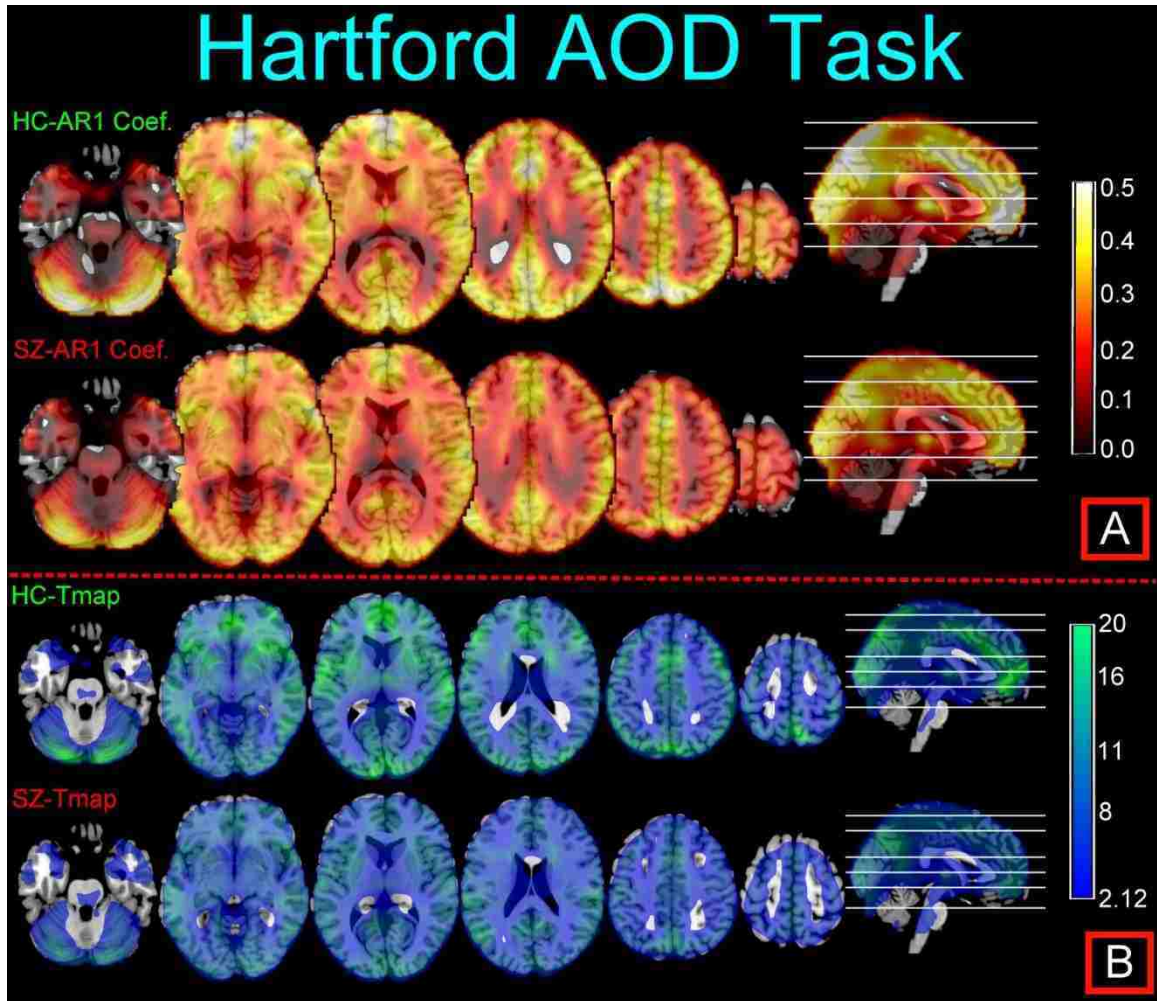


**Figure 5-2:** A: AOD task AR(1) coefficient estimated for each voxel for both healthy control and schizophrenia patients. B: T-maps resulted from group-wise one-sample t-test on each voxel for both healthy control and schizophrenia

### 5.3.3 Relationship Between AR(1) during Rest and Task

The AR(1) coefficients during rest and task for the Hartford dataset are illustrated in Figure 5-1 and Figure 5-2. In order to investigate the relationship between the

coefficients in the two states, AR1 coefficients were averaged for each region in automated anatomical labeling (AAL) atlas. Then the group-wise correlation between rest and task for each of the 116 regions in AAL atlas was calculated for both the healthy controls and schizophrenia patients.

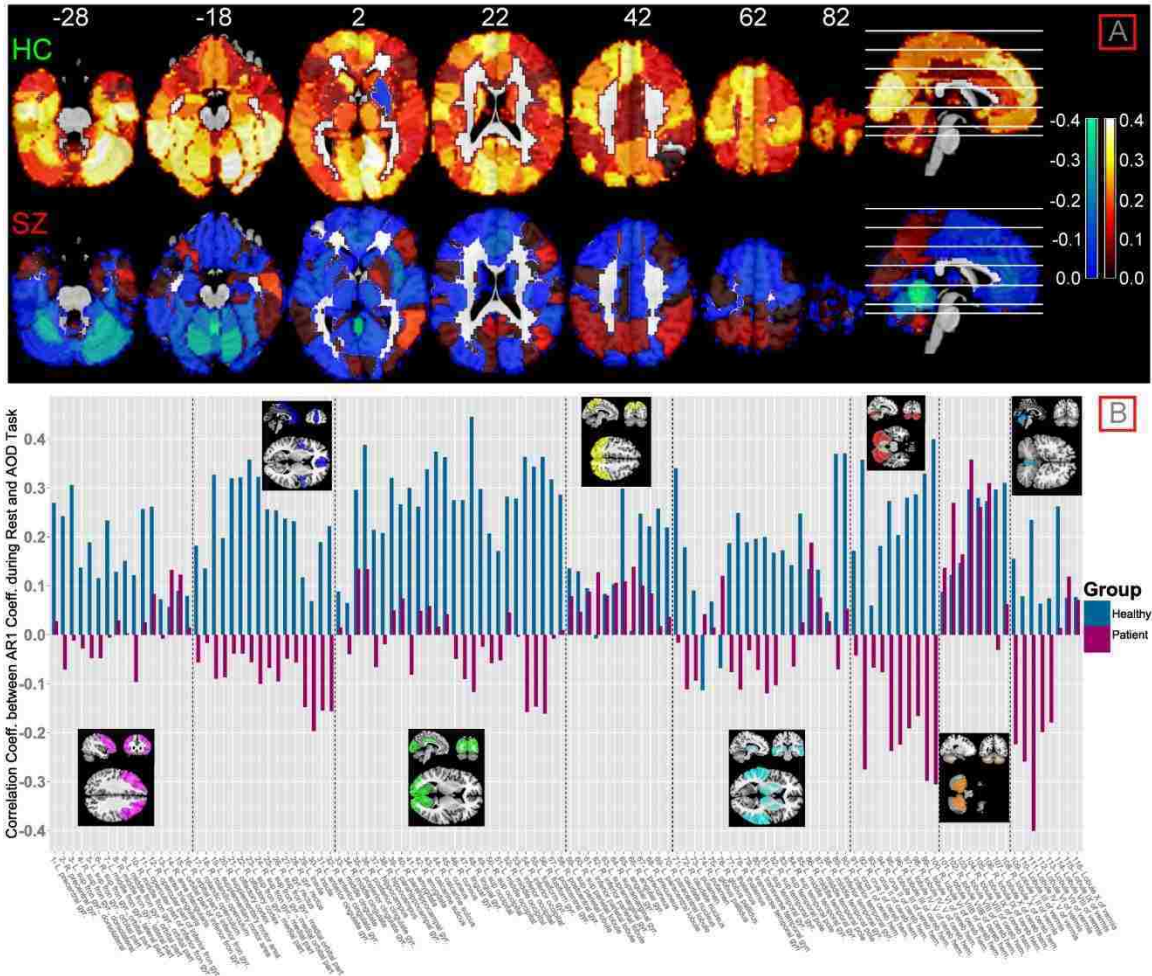


**Figure 5-3:** A: Group-wise correlation between average AR(1) coefficients during rest and AOD task for healthy controls (HC) and schizophrenia patients (SZ) B: Group-wise correlation between AR(1) coefficients during rest and task for each region in AAL atlas. The 116 regions are divided into eight groups based on the correlation pattern.



Figure 5-3A shows the correlation between average AR(1) for each AAL region during rest and task for both groups. Figure 5-3B illustrates the detailed information of Figure 5-3A for each of the 116 regions in the AAL atlas grouped into 8 categories.

#### **5.3.4 Classification of Schizophrenia Patients Based on Autoconnectivity Features**

To assess the discriminating power of AR1 coefficients, we investigated the possibility of classifying schizophrenic patients from healthy controls just based on AR1 coefficients. AR1 coefficients were averaged for each region in automated anatomical labeling (AAL) atlas to form vector of 116 features for each subject. Leave-one-out cross validation overall accuracy achieved with linear support vector machine (SVM) classifier was 78.21% (sensitivity: 75.08%, specificity: 79.47%). The relationship between AR(1) during rest and HRF during the AOD Task

We hypothesized that there is a relationship between the AR(1) coefficient during the resting-state with HRF during the performance of the task. To test this hypothesis, ICA was performed for the task data and the time-course for the auditory network was extracted. We chose this particular network since it is activated during the AOD task (Arbabshirani et al., 2013a). For each of the healthy subjects in the Hartford dataset, this time-course was deconvolved against the task paradigm to recover the HRF. From each HRF, 3 parameters were extracted: Amplitude height (H), time-to-peak (T) and full-width-half-max (W).

We also determined the activated voxels of the auditory network and extracted the same voxels from the resting-state data. AR(1) coefficients of those resting-state time-courses were calculated. We found a relationship between the amplitude of HRF during

the task and AR(1) during the rest as illustrated in Figure 5-4. A relationship between AR(1) and time-to-peak and full-width-half-max was not found.

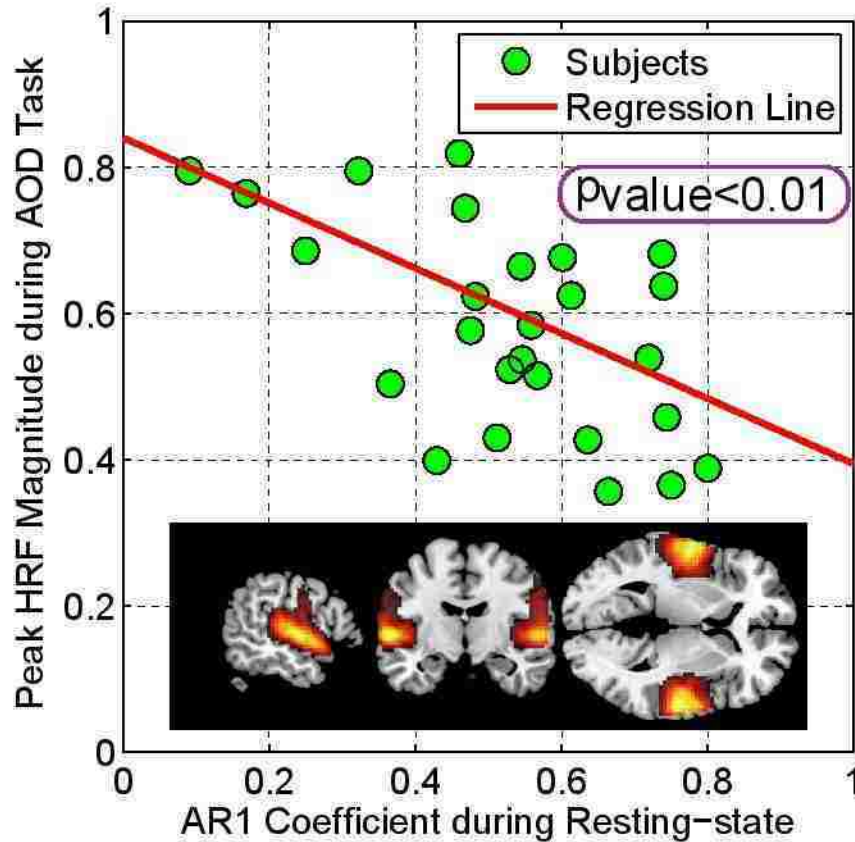


**Figure 5-4:** Scatterplot of peak HRF during AOD task vs. AR(1) during the resting-state for the auditory network.

## 5.4 Discussion

Autocorrelation as a measure of temporal dependency has been mostly attributed to noise in fMRI time-series. In this study we showed that autocorrelation is mostly significant in cortical regions. This was partially shown by Worsley (Worsley et al., 2002). We name this phenomenon as intrinsic autoconnectivity. While autocorrelation mostly originates from sampling a smooth HRF as discussed by Friston, the strength of autocorrelation in a typical fMRI time-series is also dependent on the underlying neural

activity. While we didn't investigate this hypothesis directly in this study, we provided distinct clues supporting this hypothesis.

We found lower autoconnectivity in schizophrenia patients compared to healthy controls in several brain structures such as calcarine, cuneus and thalamus (Figure 5-1). These areas have been reported repeatedly with abnormal activity in schizophrenia patients. Structural thalamus abnormalities in schizophrenia patients have been revealed in the past two decades (Andreasen et al., 1994; Buchsbaum et al., 1996; Konick and Friedman, 2001; Young et al., 2000). Schizophrenia patients have significantly lower number of neurons and volume in thalamic regions (Young et al., 2000). Also reduced thalamic activity and defect in sensory input filtering or gating have been proposed in the patient group (Andreasen et al., 1994; Buchsbaum et al., 1996; Tregellas et al., 2007). Moreover, thalamus malfunctioning has been highlighted in recent functional studies (Cetin et al., 2014; Rubia et al., 2001; Takahashi et al., 2004; Zhou et al., 2007).

During the AOD task, the highest AR(1) was found in the frontal part of the brain in areas such as orbitofrontal cortex and anterior part of the cingulate cortex as opposed to visual cortex during the resting-state. This interesting finding shows that autocorrelation as measured by AR(1) coefficients, is cognitive-state dependent and changes meaningfully during the performance of a task compared to the resting-state. This is another distinct clue confirming the neural basis of autocorrelation. To better compare autocorrelation during rest and task, correlation coefficient between the average AR(1) coefficients in the two states were computed for both groups and illustrated in Figure 5-3. While this correlation is mostly positive for the healthy controls, it is mostly negative for schizophrenia patients. In some regions such as cerebellum the difference is

very significant (Figure 5-3B). This considerable difference can be another biomarker for schizophrenia patients.

In order to investigate the discrimination power of resting-state AR(1), we classify patients from controls using just these features. The accuracy achieved using autocorrelation features is comparable with previous works based on structural features (Csernansky et al., 2004; Davatzikos et al., 2005), DTI features (Caan et al., 2006b; Caprihan et al., 2008), fMRI features (Arribas et al., 2010) and functional connectivity features. (Arbabshirani et al., 2013b) which is very promising.

Also we found a negative relationship between resting-state AR(1) and peak HRF during the AOD task in healthy controls. The peak of the HRF should be related to the strength of neural activity. This relationship provides evidence that the AR(1) may be related to neural activity and not just colored noise.

The evidences shown in this study suggest that neural activity may contribute to the autocorrelation of fMRI time-series. It was shown that autocorrelation is cognitive state dependent (resting-state vs. AOD task) and mental state dependent (healthy vs. controls). Autoconnectivity can be viewed as a complement to conventional functional connectivity (FC). FC documents interaction between brain regions while autoconnectivity documents temporal connection of voxel/region/network with itself. The results suggest that autoconnectivity is a new source of information about brain's functionality that has been ignored for a long time.

## **5.5 Classification of Schizophrenia Patients based on Combination of Resting-State FNC and Autoconnectivity Features**

In Chapter 3, we propose a framework for classification of schizophrenia patients based on resting-state FNC features. In this chapter, it was shown that autoconnectivity features can classify the patients with high accuracy as well (section 5.3.4). The natural extension is to combine the two types of features and see if the classification is improved compared to each type of the features. The FBIRN data set was decomposed with group ICA as explained in section 4.4.3 into 47 networks (Figure 4-5). For each subject, we computed the functional network connectivity, referred to as FNC, by computing pairwise Pearson correlation using the processed ICA time-courses. We selected 47 ICNs, resulting in 1081 FNC features for each subjects. Also the AR(1) coefficient of each ICA time-course was extracted as explained in section 5.2.2. This produced 47 autoconnectivity features for each subject.

### **5.5.1 Feature Selection**

In total we extracted 1128 features for each subject (1081+47). The high number of features compared to the subjects in our dataset can cause curse of dimensionality. To avoid this problem we used minimum redundancy maximum relevancy (MRMR) feature selection method. This method tries to maximize the mutual information between the selected features and class labels while minimize the mutual information among the selected features. We reduced the features to 50 by using MRMR (40 FNC feature, 10 autoconnectivity features).

### 5.5.2 Classification

Linear support vector machine was used for classification. We used 10 fold cross validation to calculate the generalized error of the classifier. In each run 10 subjects were set aside for testing and the rest were used for training. A leave-one out method was used inside the training set to find the optimal value for SVM hyperparameters along with optimal number of features to be selected by MRMR feature selection approach. Table 5-1 summarizes the classification results based on each type of feature and the combination of both types.

**Table 5-1:** Classification Results

Accuracy Feature	Overall Accuracy	Sensitivity	Specificity
FNC	83.7%	81.4%	85.9%
Autoconnectivty	80.2%	78.1%	82.2%
FNC +Autoc	<b>88.21%</b>	<b>86.7%</b>	<b>89.5%</b>

Adding novel autoconnectivity features to FNC features thus improved the classification performance significantly. Our results show that using these features can result in a robust and accurate classifier with about 88% overall accuracy which is very promising.

## **Chapter 6: Conclusion and Future Works**

## 6.1 Summary

We discussed 4 main studies in this dissertation. All studies were related to functional connectivity as a method to assess functional integration of the brain. In chapter 2 functional network connectivity during rest and task were compared in healthy controls. We found that FNC is stronger during rest compared to AOD task. A global drop in FNC was observed during the performance of AOD task. We suggested that performing an active task like AOD requires larger and more active brain networks and not necessarily higher collaboration among networks.

In chapter 3, we proposed a framework for automatic classification of mental disorder such as schizophrenia based on resting-state FNC features. The results show that resting-state FNC features can accurately discriminate schizophrenia patients from healthy controls.

In chapter 4, impact of autocorrelation on FC and FNC was comprehensively investigated in theory, simulation and real fMRI data. We showed that despite the change in correlation coefficient with presence of autocorrelation in corresponding time-courses, the result of hypothesis testing remain very similar before and after correction of autocorrelation.

In chapter 5, we introduced the concept of autoconnectivity. While most of previous works suggest that autocorrelation in fMRI time-series is originated from noise, we provided distinct evidences that neural activity also plays a role in fMRI autocorrelation. We showed that autocorrelation is most significant in the gray matter area and is cognitive state dependent. Also it was shown that schizophrenia patients show different



autocorrelation pattern compared to healthy controls and it is possible to use autocorrelation features to classify them from healthy controls with high accuracy.

## **6.2 Future Works**

Each of the studies discussed in this dissertation can be extended in numerous ways. Here we provide suggestion for some the possible future works.

For comparison of FNC during rest and task, generalization of these results can be accomplished by evaluating additional task types, as well as exploring different subjects (e.g. patients with brain-based disorders may show different changes than healthy control subjects). It is interesting to see if our results generalize to other cognitive states or not. Also instead of univariate, assessment of each FNC value, multivariate methods such as graph theory can be used to compare FNC among cognitive states. Such methods have been suggested and used recently in the neuroimaging community (Bullmore and Sporns, 2009; Wang et al., 2010; Yu et al., 2012).

Combining resting-state FNC features with other types of features suggested by other researchers (section 3.3 and 3.4) can be one of the main future works. There are several biomarkers based on different neuroimaging modalities for mental disorders such as schizophrenia (see section 3.3 and 3.4). Ultimately, these biomarkers should be compared and combined with each to make strong and robust feature set for automatic classification frameworks. In recent years, limited studies have combined two or three modalities. Yang et al., combined fMRI and genetics data for automatic classification of schizophrenia patients from healthy controls (Yang et al., 2010). Sui et al. proposed a framework based on canonical correlation analysis and joint ICA to combine fMRI and DTI data for classification of schizophrenia and bipolar (Sui et al., 2011). Sui et al.,

extended their work to combine fMRI, DTI and structural MRI to classify schizophrenia patients (Sui et al., 2013).

We investigated the impact of autocorrelation of functional connectivity in chapter 4. For future works, the problem can be investigated in general case of AR(N) process in theory and simulations. Also, in real fMRI data, other types statistical tests should be compared before and after autocorrelation correction. We suggested that maybe autocorrelation correction reduced the signal to noise ratio in fMRI time-series resulting in noisier estimation of correlation coefficient. This hypothesis should be studied in details for future works.

Finally in chapter 5, we introduced the concept of autoconnectivity. An important future work is to determine what portion of autocorrelation in fMRI time-series originates from noise and what portion has neural basis. A following interesting question is whether it is possible to separate these two from each other. While we provided highly autoconnected regions in the brain during rest and task, and we show that they are different. In future works the role of autoconnectivity in brain's functionality should be investigated more. Also the link between autoconnectivity and neural activity should be studied more rigorously.

## References:

- Abbott, C., Juarez, M., White, T., Gollub, R.L., Pearlson, G.D., Bustillo, J., Lauriello, J., Ho, B., Bockholt, H.J., Clark, V.P., Magnotta, V., Calhoun, V.D., 2011. Antipsychotic dose and diminished neural modulation: a multi-site fMRI study. *Progress in neuro-psychopharmacology & biological psychiatry* 35, 473-482.
- Aguirre, G.K., Zarahn, E., D'Esposito, M., 1997. Empirical analyses of BOLD fMRI statistics. II. Spatially smoothed data collected under null-hypothesis and experimental conditions. *Neuroimage* 5, 199-212.
- Akaike, H., 1974. New Look at Statistical-Model Identification. *Ieee Transactions on Automatic Control* Ac19, 716-723.
- Allen, E.A., Damaraju, E., Plis, S.M., Erhardt, E.B., Eichele, T., Calhoun, V.D., 2012. Tracking Whole-Brain Connectivity Dynamics in the Resting State. *Cereb Cortex*.
- Allen, E.A., Erhardt, E.B., Damaraju, E., Gruner, W., Segall, J.M., Silva, R.F., Havlicek, M., Rachakonda, S., Fries, J., Kalyanam, R., Michael, A.M., Caprihan, A., Turner, J.A., Eichele, T., Adelsheim, S., Bryan, A.D., Bustillo, J., Clark, V.P., Feldstein Ewing, S.W., Filbey, F., Ford, C.C., Hutchison, K., Jung, R.E., Kiehl, K.A., Koditwakk, P., Komesu, Y.M., Mayer, A.R., Pearlson, G.D., Phillips, J.P., Sadek, J.R., Stevens, M., Teuscher, U., Thoma, R.J., Calhoun, V.D., 2011. A baseline for the multivariate comparison of resting-state networks. *Front Syst Neurosci* 5, 2.
- Andreasen, N.C., Arndt, S., Swayze, V., 2nd, Cizadlo, T., Flaum, M., O'Leary, D., Ehrhardt, J.C., Yuh, W.T., 1994. Thalamic abnormalities in schizophrenia visualized through magnetic resonance image averaging. *Science* 266, 294-298.
- Ang, A.H.-S., Tang, W.H., 1975. *Probability concepts in engineering planning and design*. Wiley, New York.
- Arbabshirani, M.R., Calhoun, V.D., 2011. Functional network connectivity during rest and task: comparison of healthy controls and schizophrenic patients. *Conf Proc IEEE Eng Med Biol Soc* 2011, 4418-4421.
- Arbabshirani, M.R., Havlicek, M., Kiehl, K.A., Pearlson, G.D., Calhoun, V.D., 2013a. Functional network connectivity during rest and task conditions: a comparative study. *Hum Brain Mapp* 34, 2959-2971.
- Arbabshirani, M.R., Kiehl, K.A., Pearlson, G.D., Calhoun, V.D., 2013b. Classification of schizophrenia patients based on resting-state functional network connectivity. *Front Neurosci* 7, 133.
- Ardekani, B.A., Bappal, A., D'Angelo, D., Ashtari, M., Lencz, T., Szeszko, P.R., Butler, P.D., Javitt, D.C., Lim, K.O., Hrabe, J., Nierenberg, J., Branch, C.A., Hoptman, M.J., 2005. Brain morphometry using diffusion-weighted magnetic resonance imaging: application to schizophrenia. *Neuroreport* 16, 1455-1459.
- Ardekani, B.A., Tabesh, A., Sevy, S., Robinson, D.G., Bilder, R.M., Szeszko, P.R., 2011. Diffusion tensor imaging reliably differentiates patients with schizophrenia from healthy volunteers. *Hum Brain Mapp* 32, 1-9.
- Arfanakis, K., Cordes, D., Haughton, V.M., Moritz, C.H., Quigley, M.A., Meyerand, M.E., 2000. Combining independent component analysis and correlation analysis

- to probe interregional connectivity in fMRI task activation datasets. *Magn Reson Imaging* 18, 921-930.
- Arribas, J.I., Calhoun, V.D., Adali, T., 2010. Automatic Bayesian classification of healthy controls, bipolar disorder, and schizophrenia using intrinsic connectivity maps from FMRI data. *IEEE transactions on bio-medical engineering* 57, 2850-2860.
- Auer, D.P., 2008. Spontaneous low-frequency blood oxygenation level-dependent fluctuations and functional connectivity analysis of the 'resting' brain. *Magn Reson Imaging* 26, 1055-1064.
- Azevedo, F.A., Carvalho, L.R., Grinberg, L.T., Farfel, J.M., Ferretti, R.E., Leite, R.E., Jacob Filho, W., Lent, R., Herculano-Houzel, S., 2009. Equal numbers of neuronal and nonneuronal cells make the human brain an isometrically scaled-up primate brain. *J Comp Neurol* 513, 532-541.
- Bartels, A., Zeki, S., 2005. Brain dynamics during natural viewing conditions--a new guide for mapping connectivity in vivo. *Neuroimage* 24, 339-349.
- Bartlett, M.S., 1935. Some aspects of the time correlation problem in regard to tests of significance. *Journal of the Royal Statistical Society* 98, 536-543.
- Bell, A.J., Sejnowski, T.J., 1995. An Information Maximization Approach to Blind Separation and Blind Deconvolution. *Neural Computation* 7, 1129-1159.
- Benjamini, Y., Hochberg, Y., 1995. Controlling the False Discovery Rate - a Practical and Powerful Approach to Multiple Testing. *Journal of the Royal Statistical Society Series B-Methodological* 57, 289-300.
- Berger, H., 1929. Electroencephalogram in humans. *Archiv Fur Psychiatrie Und Nervenkrankheiten* 87, 527-570.
- Bhugra, D., 2005. The global prevalence of schizophrenia. *PLoS medicine* 2, e151; quiz e175.
- Bianciardi, M., Fukunaga, M., van Gelderen, P., Horovitz, S.G., de Zwart, J.A., Shmueli, K., Duyn, J.H., 2009. Sources of functional magnetic resonance imaging signal fluctuations in the human brain at rest: a 7 T study. *Magnetic resonance imaging* 27, 1019-1029.
- Bishop, C.M., 2006. *Pattern recognition and machine learning*. Springer, New York.
- Biswal, B., Yetkin, F.Z., Haughton, V.M., Hyde, J.S., 1995a. Functional connectivity in the motor cortex of resting human brain using echo-planar MRI. *Magnetic resonance in medicine : official journal of the Society of Magnetic Resonance in Medicine / Society of Magnetic Resonance in Medicine* 34, 537-541.
- Biswal, B., Yetkin, F.Z., Haughton, V.M., Hyde, J.S., 1995b. Functional connectivity in the motor cortex of resting human brain using echo-planar MRI. *Magn Reson Med* 34, 537-541.
- Biswal, B.B., Van Kylen, J., Hyde, J.S., 1997. Simultaneous assessment of flow and BOLD signals in resting-state functional connectivity maps. *NMR Biomed* 10, 165-170.
- Block, H.D., Knight, B.W., Rosenblatt, F., 1962. Analysis of a 4-Layer Series-Coupled Perceptron .2. *Reviews of Modern Physics* 34, 135-&.
- Bluhm, R.L., Miller, J., Lanius, R.A., Osuch, E.A., Boksman, K., Neufeld, R.W., Theberge, J., Schaefer, B., Williamson, P., 2007. Spontaneous low-frequency

- fluctuations in the BOLD signal in schizophrenic patients: anomalies in the default network. *Schizophrenia bulletin* 33, 1004-1012.
- Bokde, A.L., Lopez-Bayo, P., Meindl, T., Pechler, S., Born, C., Faltraco, F., Teipel, S.J., Moller, H.J., Hampel, H., 2006. Functional connectivity of the fusiform gyrus during a face-matching task in subjects with mild cognitive impairment. *Brain : a journal of neurology* 129, 1113-1124.
- Box, G.E.P., Jenkins, G.M., 1970. *Time series analysis; forecasting and control*. Holden-Day, San Francisco,.
- Bremner, D., Demaine, E., Erickson, J., Iacono, J., Langerman, S., Morin, P., Toussaint, G., 2005. Output-sensitive algorithms for computing nearest-neighbour decision boundaries. *Discrete & Computational Geometry* 33, 593-604.
- Broyd, S.J., Demanuele, C., Debener, S., Helps, S.K., James, C.J., Sonuga-Barke, E.J., 2009. Default-mode brain dysfunction in mental disorders: a systematic review. *Neurosci Biobehav Rev* 33, 279-296.
- Buchsbaum, M.S., Someya, T., Teng, C.Y., Abel, L., Chin, S., Najafi, A., Haier, R.J., Wu, J., Bunney, W.E., Jr., 1996. PET and MRI of the thalamus in never-medicated patients with schizophrenia. *The American journal of psychiatry* 153, 191-199.
- Buckner, R.L., Andrews-Hanna, J.R., Schacter, D.L., 2008. The brain's default network: anatomy, function, and relevance to disease. *Ann N Y Acad Sci* 1124, 1-38.
- Bullmore, E., Long, C., Suckling, J., Fadili, J., Calvert, G., Zelaya, F., Carpenter, T.A., Brammer, M., 2001. Colored noise and computational inference in neurophysiological (fMRI) time series analysis: resampling methods in time and wavelet domains. *Hum Brain Mapp* 12, 61-78.
- Bullmore, E., Sporns, O., 2009. Complex brain networks: graph theoretical analysis of structural and functional systems. *Nat Rev Neurosci* 10, 186-198.
- Burges, C.J.C., 1998. A tutorial on Support Vector Machines for pattern recognition. *Data Mining and Knowledge Discovery* 2, 121-167.
- Caan, M.W., Vermeer, K.A., van Vliet, L.J., Majoie, C.B., Peters, B.D., den Heeten, G.J., Vos, F.M., 2006a. Shaving diffusion tensor images in discriminant analysis: a study into schizophrenia. *Medical image analysis* 10, 841-849.
- Caan, M.W.A., Vermeer, K.A., van Vliet, L.J., Majoie, C.B.L.M., Peters, B.D., den Heeten, G.J., Vos, F.M., 2006b. Shaving diffusion tensor images in discriminant analysis: A study into schizophrenia. *Medical image analysis* 10, 841-849.
- Calhoun, V., Adali, T., Kraut, M., Pearlson, G., 2000. A weighted least-squares algorithm for estimation and visualization of relative latencies in event-related functional MRI. *Magn Reson Med* 44, 947-954.
- Calhoun, V.D., Adali, T., 2012. Multisubject independent component analysis of fMRI: a decade of intrinsic networks, default mode, and neurodiagnostic discovery. *IEEE reviews in biomedical engineering* 5, 60-73.
- Calhoun, V.D., Adali, T., Pearlson, G.D., Pekar, J.J., 2001a. A method for making group inferences from functional MRI data using independent component analysis. *Hum Brain Mapp* 14, 140-151.
- Calhoun, V.D., Adali, T., Pearlson, G.D., Pekar, J.J., 2001b. Spatial and temporal independent component analysis of functional MRI data containing a pair of task-related waveforms. *Hum Brain Mapp* 13, 43-53.

- Calhoun, V.D., Arbabshirani, M.R., 2013. Neuroimaging-based Automatic Classification of Schizophrenia. Bioprediction, biomarkers and bad behaviour : scientific, legal, and ethical challenges  
Oxford University Press.
- Calhoun, V.D., Eichele, T., Pearlson, G., 2009a. Functional brain networks in schizophrenia: a review. *Front Hum Neurosci* 3, 17.
- Calhoun, V.D., Kiehl, K.A., Liddle, P.F., Pearlson, G.D., 2004. Aberrant localization of synchronous hemodynamic activity in auditory cortex reliably characterizes schizophrenia. *Biological psychiatry* 55, 842-849.
- Calhoun, V.D., Kiehl, K.A., Pearlson, G.D., 2008a. Modulation of temporally coherent brain networks estimated using ICA at rest and during cognitive tasks. *Hum Brain Mapp* 29, 828-838.
- Calhoun, V.D., Liu, J., Adali, T., 2009b. A review of group ICA for fMRI data and ICA for joint inference of imaging, genetic, and ERP data. *Neuroimage* 45, S163-172.
- Calhoun, V.D., Maciejewski, P.K., Pearlson, G.D., Kiehl, K.A., 2008b. Temporal lobe and "default" hemodynamic brain modes discriminate between schizophrenia and bipolar disorder. *Hum Brain Mapp* 29, 1265-1275.
- Camchong, J., MacDonald, A.W., 3rd, Bell, C., Mueller, B.A., Lim, K.O., 2011. Altered functional and anatomical connectivity in schizophrenia. *Schizophrenia bulletin* 37, 640-650.
- Caprihan, A., Pearlson, G.D., Calhoun, V.D., 2008. Application of principal component analysis to distinguish patients with schizophrenia from healthy controls based on fractional anisotropy measurements. *Neuroimage* 42, 675-682.
- Cardoso, J.F., Soudoumiac, A., 1993. Blind Beamforming for Non-Gaussian Signals. *Iee Proceedings-F Radar and Signal Processing* 140, 362-370.
- Castro, E., Martinez-Ramon, M., Pearlson, G., Sui, J., Calhoun, V.D., 2011. Characterization of groups using composite kernels and multi-source fMRI analysis data: application to schizophrenia. *Neuroimage* 58, 526-536.
- Cetin, M.S., Christensen, F., Abbott, C.C., Stephen, J.M., Mayer, A.R., Canive, J.M., Bustillo, J.R., Pearlson, G.D., Calhoun, V.D., 2014. Thalamus and posterior temporal lobe show greater inter-network connectivity at rest and across sensory paradigms in schizophrenia. *Neuroimage*.
- Chen, S., Cowan, C.F.N., Grant, P.M., 1991. Orthogonal Least-Squares Learning Algorithm for Radial Basis Function Networks. *Ieee Transactions on Neural Networks* 2, 302-309.
- Christova, P., Lewis, S.M., Jerde, T.A., Lynch, J.K., Georgopoulos, A.P., 2011. True associations between resting fMRI time series based on innovations. *Journal of neural engineering* 8, 046025.
- Cordes, D., Haughton, V., Carew, J.D., Arfanakis, K., Maravilla, K., 2002. Hierarchical clustering to measure connectivity in fMRI resting-state data. *Magn Reson Imaging* 20, 305-317.
- Cordes, D., Haughton, V.M., Arfanakis, K., Carew, J.D., Turski, P.A., Moritz, C.H., Quigley, M.A., Meyerand, M.E., 2001a. Frequencies contributing to functional connectivity in the cerebral cortex in "resting-state" data. *AJNR Am J Neuroradiol* 22, 1326-1333.

- Cordes, D., Haughton, V.M., Arfanakis, K., Carew, J.D., Turski, P.A., Moritz, C.H., Quigley, M.A., Meyerand, M.E., 2001b. Frequencies contributing to functional connectivity in the cerebral cortex in "resting-state" data. *AJNR. American journal of neuroradiology* 22, 1326-1333.
- Cordes, D., Haughton, V.M., Arfanakis, K., Wendt, G.J., Turski, P.A., Moritz, C.H., Quigley, M.A., Meyerand, M.E., 2000. Mapping functionally related regions of brain with functional connectivity MR imaging. *AJNR Am J Neuroradiol* 21, 1636-1644.
- Cortes, C., Vapnik, V., 1995. Support-Vector Networks. *Machine Learning* 20, 273-297.
- Cover, T.M., Hart, P.E., 1967. Nearest Neighbor Pattern Classification. *Ieee Transactions on Information Theory* 13, 21-+.
- Csernansky, J.G., Schindler, M.K., Splinter, N.R., Wang, L., Gado, M., Selemon, L.D., Rastogi-Cruz, D., Posener, J.A., Thompson, P.A., Miller, M.I., 2004. Abnormalities of thalamic volume and shape in schizophrenia. *The American journal of psychiatry* 161, 896-902.
- Damaraju, E., Phillips, J.R., Lowe, J.R., Ohls, R., Calhoun, V.D., Caprihan, A., 2010. Resting-state functional connectivity differences in premature children. *Front Syst Neurosci* 4.
- Damoiseaux, J.S., Rombouts, S.A., Barkhof, F., Scheltens, P., Stam, C.J., Smith, S.M., Beckmann, C.F., 2006. Consistent resting-state networks across healthy subjects. *Proceedings of the National Academy of Sciences of the United States of America* 103, 13848-13853.
- Davatzikos, C., Shen, D., Gur, R.C., Wu, X., Liu, D., Fan, Y., Huggett, P., Turetsky, B.I., Gur, R.E., 2005. Whole-brain morphometric study of schizophrenia revealing a spatially complex set of focal abnormalities. *Archives of general psychiatry* 62, 1218-1227.
- Davey, C.E., Grayden, D.B., Egan, G.F., Johnston, L.A., 2013. Filtering induces correlation in fMRI resting state data. *Neuroimage* 64, 728-740.
- Davis, C.E., Jeste, D.V., Eyler, L.T., 2005. Review of longitudinal functional neuroimaging studies of drug treatments in patients with schizophrenia. *Schizophrenia research* 78, 45-60.
- Demirci, O., Clark, V.P., Calhoun, V.D., 2008a. A projection pursuit algorithm to classify individuals using fMRI data: Application to schizophrenia. *Neuroimage* 39, 1774-1782.
- Demirci, O., Clark, V.P., Magnotta, V.A., Andreasen, N.C., Lauriello, J., Kiehl, K.A., Pearlson, G.D., Calhoun, V.D., 2008b. A Review of Challenges in the Use of fMRI for Disease Classification / Characterization and A Projection Pursuit Application from Multi-site fMRI Schizophrenia Study. *Brain imaging and behavior* 2, 147-226.
- Domingos, P., Pazzani, M., 1997. On the optimality of the simple Bayesian classifier under zero-one loss. *Machine Learning* 29, 103-130.
- Dosenbach, N.U., Nardos, B., Cohen, A.L., Fair, D.A., Power, J.D., Church, J.A., Nelson, S.M., Wig, G.S., Vogel, A.C., Lessov-Schlaggar, C.N., Barnes, K.A., Dubis, J.W., Feczko, E., Coalson, R.S., Pruett, J.R., Jr., Barch, D.M., Petersen, S.E., Schlaggar, B.L., 2010. Prediction of individual brain maturity using fMRI. *Science* 329, 1358-1361.

- Du, W., Calhoun, V.D., Li, H., Ma, S., Eichele, T., Kiehl, K.A., Pearlson, G.D., Adali, T., 2012. High classification accuracy for schizophrenia with rest and task fMRI data. *Frontiers in human neuroscience* 6, 145.
- Duda, R.O., Hart, P.E., Stork, D.G., 2001. *Pattern classification*, 2nd ed. Wiley, New York ; Chichester England.
- Duin, R.P.W., Juszczak, P., de Ridder, D., Paclik, P., Pekalska, E., Tax, D.M.J., Verzakov, S., 2007. *PRTools, a Matlab toolbox for pattern recognition*. Delft University of technology.
- Durbin, J., Watson, G.S., 1950. Testing for Serial Correlation in Least Squares Regression .1. *Biometrika* 37, 409-428.
- Durbin, J., Watson, G.S., 1951. Testing for Serial Correlation in Least Squares Regression .2. *Biometrika* 38, 159-178.
- Erhardt, E.B., Rachakonda, S., Bedrick, E.J., Allen, E.A., Adali, T., Calhoun, V.D., 2011. Comparison of multi-subject ICA methods for analysis of fMRI data. *Hum Brain Mapp* 32, 2075-2095.
- Esposito, F., Scarabino, T., Hyvarinen, A., Himberg, J., Formisano, E., Comani, S., Tedeschi, G., Goebel, R., Seifritz, E., Di Salle, F., 2005. Independent component analysis of fMRI group studies by self-organizing clustering. *Neuroimage* 25, 193-205.
- Fan, Y., Rao, H., Hurt, H., Giannetta, J., Korczykowski, M., Shera, D., Avants, B.B., Gee, J.C., Wang, J., Shen, D., 2007a. Multivariate examination of brain abnormality using both structural and functional MRI. *Neuroimage* 36, 1189-1199.
- Fan, Y., Shen, D., Davatzikos, C., 2005. Classification of structural images via high-dimensional image warping, robust feature extraction, and SVM. *Medical image computing and computer-assisted intervention : MICCAI ... International Conference on Medical Image Computing and Computer-Assisted Intervention* 8, 1-8.
- Fan, Y., Shen, D., Gur, R.C., Gur, R.E., Davatzikos, C., 2007b. COMPARE: classification of morphological patterns using adaptive regional elements. *IEEE transactions on medical imaging* 26, 93-105.
- Finger, S., 1994. *Origins of neuroscience : a history of explorations into brain function*. Oxford University Press, New York ; Oxford.
- First, M.B., Spitzer, R.L., Gibbon, M., Williams, J.B.W., 1995. The Structured Clinical Interview for Dsm-Iii-R Personality-Disorders (Scid-Ii) .1. Description. *Journal of Personality Disorders* 9, 83-91.
- Fisher, R.A., 1914. Frequency distribution of the values of the correlation coefficient in samples from an indefinitely large population. *Biometrika* 10, 507-521.
- Ford, J., Shen, L., Makedon, F., Flashman, L.A., Saykin, A.J., 2002. A combined structural-functional classification of schizophrenia using hippocampal volume plus fMRI activation In *Second joint EMBS/BMES conference*, Houston, TX.
- Ford, J.M., Johnson, M.B., Whitfield, S.L., Faustman, W.O., Mathalon, D.H., 2005. Delayed hemodynamic responses in schizophrenia. *Neuroimage* 26, 922-931.
- Fox, M.D., Greicius, M., 2010. Clinical applications of resting state functional connectivity. *Front Syst Neurosci* 4, 19.



- Fox, M.D., Snyder, A.Z., Vincent, J.L., Corbetta, M., Van Essen, D.C., Raichle, M.E., 2005. The human brain is intrinsically organized into dynamic, anticorrelated functional networks. *Proc Natl Acad Sci U S A* 102, 9673-9678.
- Franco, A.R., Pritchard, A., Calhoun, V.D., Mayer, A.R., 2009. Interrater and intermethod reliability of default mode network selection. *Hum Brain Mapp* 30, 2293-2303.
- Fransson, P., 2006. How default is the default mode of brain function? Further evidence from intrinsic BOLD signal fluctuations. *Neuropsychologia* 44, 2836-2845.
- Fransson, P., Marrelec, G., 2008. The precuneus/posterior cingulate cortex plays a pivotal role in the default mode network: Evidence from a partial correlation network analysis. *Neuroimage* 42, 1178-1184.
- Friston, K., 2002. Beyond phrenology: what can neuroimaging tell us about distributed circuitry? *Annual review of neuroscience* 25, 221-250.
- Friston, K., Jezzard, P., Turner, R., 1994. Analysis of functional MRI time-series. *Hum. Brain Mapp.* 1, 153-171.
- Friston, K.J., 2011. Functional and effective connectivity: a review. *Brain Connect* 1, 13-36.
- Friston, K.J., Frith, C.D., 1995. Schizophrenia: a disconnection syndrome? *Clinical neuroscience* 3, 89-97.
- Friston, K.J., Holmes, A.P., Poline, J.B., Grasby, P.J., Williams, S.C., Frackowiak, R.S., Turner, R., 1995. Analysis of fMRI time-series revisited. *Neuroimage* 2, 45-53.
- Friston, K.J., Josephs, O., Zarahn, E., Holmes, A.P., Rouquette, S., Poline, J., 2000. To smooth or not to smooth? Bias and efficiency in fMRI time-series analysis. *Neuroimage* 12, 196-208.
- Friston, K.J., Williams, S., Howard, R., Frackowiak, R.S., Turner, R., 1996. Movement-related effects in fMRI time-series. *Magn Reson Med* 35, 346-355.
- Frith, C.D., Friston, K.J., Herold, S., Silbersweig, D., Fletcher, P., Cahill, C., Dolan, R.J., Frackowiak, R.S., Liddle, P.F., 1995. Regional brain activity in chronic schizophrenic patients during the performance of a verbal fluency task. *The British journal of psychiatry : the journal of mental science* 167, 343-349.
- Fukunaga, M., Horowitz, S.G., van Gelderen, P., de Zwart, J.A., Jansma, J.M., Ikonomidou, V.N., Chu, R.X., Deckers, R.H.R., Leopold, D.A., Duyn, J.H., 2006. Large-amplitude, spatially correlated fluctuations in BOLD fMRI signals during extended rest and early sleep stages. *Magn Reson Imaging* 24, 979-992.
- Gard, T., Taquet, M., Dixit, R., Holzel, B.K., de Montjoye, Y.A., Brach, N., Salat, D.H., Dickerson, B.C., Gray, J.R., Lazar, S.W., 2014. Fluid intelligence and brain functional organization in aging yoga and meditation practitioners. *Front Aging Neurosci* 6, 76.
- Garrity, A.G., Pearlson, G.D., McKiernan, K., Lloyd, D., Kiehl, K.A., Calhoun, V.D., 2007a. Aberrant "default mode" functional connectivity in schizophrenia. *The American journal of psychiatry* 164, 450-457.
- Garrity, A.G., Pearlson, G.D., McKiernan, K., Lloyd, D., Kiehl, K.A., Calhoun, V.D., 2007b. Aberrant "default mode" functional connectivity in schizophrenia. *The American journal of psychiatry* 164, 450-457.
- Gautama, T., Van Hulle, M.M., 2004. Optimal spatial regularisation of autocorrelation estimates in fMRI analysis. *Neuroimage* 23, 1203-1216.

- Genovese, C.R., Lazar, N.A., Nichols, T., 2002. Thresholding of statistical maps in functional neuroimaging using the false discovery rate. *Neuroimage* 15, 870-878.
- Georgopoulos, A.P., Karageorgiou, E., Leuthold, A.C., Lewis, S.M., Lynch, J.K., Alonso, A.A., Aslam, Z., Carpenter, A.F., Georgopoulos, A., Hemmy, L.S., Koutlas, I.G., Langheim, F.J., McCarten, J.R., McPherson, S.E., Pardo, J.V., Pardo, P.J., Parry, G.J., Rottunda, S.J., Segal, B.M., Sponheim, S.R., Stanwyck, J.J., Stephane, M., Westermeyer, J.J., 2007. Synchronous neural interactions assessed by magnetoencephalography: a functional biomarker for brain disorders. *Journal of neural engineering* 4, 349-355.
- Georgopoulos, A.P., Mahan, M.Y., 2013. Fmri Data Analysis: State of Affairs and Challenges. *Quarterly Review of Biology* 88, 121-124.
- Goghari, V.M., Rehm, K., Carter, C.S., MacDonald, A.W., 3rd, 2007. Regionally specific cortical thinning and gray matter abnormalities in the healthy relatives of schizophrenia patients. *Cerebral cortex* 17, 415-424.
- Granger, C.W.J., Morris, M.J., 1976. Time-Series Modeling and Interpretation. *Journal of the Royal Statistical Society Series a-Statistics in Society* 139, 246-257.
- Granger, C.W.J., Newbold, P., 1974. Spurious regressions in econometrics. *Journal of Econometrics* 2, 111-120.
- Greicius, M., 2008. Resting-state functional connectivity in neuropsychiatric disorders. *Curr Opin Neurol* 21, 424-430.
- Greicius, M.D., Krasnow, B., Reiss, A.L., Menon, V., 2003. Functional connectivity in the resting brain: a network analysis of the default mode hypothesis. *Proc Natl Acad Sci U S A* 100, 253-258.
- Hahn, G.J., Shapiro, S.S., 1967. *Statistical models in engineering*. Wiley, New York.
- Hampson, M., Olson, I.R., Leung, H.C., Skudlarski, P., Gore, J.C., 2004. Changes in functional connectivity of human MT/V5 with visual motion input. *Neuroreport* 15, 1315-1319.
- Hampson, M., Peterson, B.S., Skudlarski, P., Gatenby, J.C., Gore, J.C., 2002. Detection of functional connectivity using temporal correlations in MR images. *Hum Brain Mapp* 15, 247-262.
- Harrison, B.J., Pujol, J., Lopez-Sola, M., Hernandez-Ribas, R., Deus, J., Ortiz, H., Soriano-Mas, C., Yucel, M., Pantelis, C., Cardoner, N., 2008. Consistency and functional specialization in the default mode brain network. *Proc Natl Acad Sci U S A* 105, 9781-9786.
- Hasson, U., Nusbaum, H.C., Small, S.L., 2009. Task-dependent organization of brain regions active during rest. *Proc Natl Acad Sci U S A* 106, 10841-10846.
- Haugh, L.D., 1976. Checking Independence of 2 Covariance-Stationary Time-Series - Univariate Residual Cross-Correlation Approach. *Journal of the American Statistical Association* 71, 378-385.
- Havlicek, M., Jan, J., Brazdil, M., Calhoun, V.D., 2010. Dynamic Granger causality based on Kalman filter for evaluation of functional network connectivity in fMRI data. *Neuroimage* 53, 65-77.
- Heinrichs, R.W., Zakzanis, K.K., 1998. Neurocognitive deficit in schizophrenia: a quantitative review of the evidence. *Neuropsychology* 12, 426-445.

- Himberg, J., Hyvarinen, A., Esposito, F., 2004. Validating the independent components of neuroimaging time series via clustering and visualization. *Neuroimage* 22, 1214-1222.
- Honea, R., Crow, T.J., Passingham, D., Mackay, C.E., 2005. Regional deficits in brain volume in schizophrenia: a meta-analysis of voxel-based morphometry studies. *The American journal of psychiatry* 162, 2233-2245.
- Hyvarinen, A., Oja, E., 1997. A fast fixed-point algorithm for independent component analysis. *Neural Computation* 9, 1483-1492.
- Hyvarinen, A., Oja, E., 2000. Independent component analysis: algorithms and applications. *Neural Netw* 13, 411-430.
- Jafri, M.J., Pearlson, G.D., Stevens, M., Calhoun, V.D., 2008. A method for functional network connectivity among spatially independent resting-state components in schizophrenia. *Neuroimage* 39, 1666-1681.
- Jang, J.H., Jung, W.H., Choi, J.S., Choi, C.H., Kang, D.H., Shin, N.Y., Hong, K.S., Kwon, J.S., 2011. Reduced prefrontal functional connectivity in the default mode network is related to greater psychopathology in subjects with high genetic loading for schizophrenia. *Schizophrenia research* 127, 58-65.
- Josin, G.M., Liddle, P.F., 2001. Neural network analysis of the pattern of functional connectivity between cerebral areas in schizophrenia. *Biological cybernetics* 84, 117-122.
- Kandel, E.R., Schwartz, J.H., Jessell, T.M., 2000. Principles of neural science, 4th ed. McGraw-Hill, Health Professions Division, New York.
- Kanizsa, G., 1979. Organization in vision : essays on gestalt perception. Praeger, New York.
- Karlsgodt, K.H., Sun, D.Q., Cannon, T.D., 2010. Structural and Functional Brain Abnormalities in Schizophrenia. *Current Directions in Psychological Science* 19, 226-231.
- Kawasaki, Y., Suzuki, M., Kherif, F., Takahashi, T., Zhou, S.Y., Nakamura, K., Matsui, M., Sumiyoshi, T., Seto, H., Kurachi, M., 2007. Multivariate voxel-based morphometry successfully differentiates schizophrenia patients from healthy controls. *Neuroimage* 34, 235-242.
- Kelly, R.E., Wang, Z., Alexopoulos, G.S., Gunning, F.M., Murphy, C.F., Morimoto, S.S., Kanellopoulos, D., Jia, Z., Lim, K.O., Hoptman, M.J., 2010. Hybrid ICA-Seed-Based Methods for fMRI Functional Connectivity Assessment: A Feasibility Study. *Int J Biomed Imaging* 2010.
- Kiehl, K.A., Liddle, P.F., 2001. An event-related functional magnetic resonance imaging study of an auditory oddball task in schizophrenia. *Schizophrenia research* 48, 159-171.
- Kiehl, K.A., Stevens, M.C., Laurens, K.R., Pearlson, G., Calhoun, V.D., Liddle, P.F., 2005. An adaptive reflexive processing model of neurocognitive function: supporting evidence from a large scale (n=100) MRI study of an auditory oddball task. *Neuroimage* 25, 899-915.
- Kingsley, P.B., 2006. Introduction to diffusion tensor imaging mathematics: Part II. Anisotropy, diffusion-weighting factors, and gradient encoding schemes. *Concepts in Magnetic Resonance Part A* 28A, 123-154.

- Konick, L.C., Friedman, L., 2001. Meta-analysis of thalamic size in schizophrenia. *Biological psychiatry* 49, 28-38.
- Krugel, F., Pelegrini-Issac, M., Benali, H., 2002. Estimating the effective degrees of freedom in univariate multiple regression analysis. *Medical image analysis* 6, 63-75.
- Kubicki, M., McCarley, R., Westin, C.F., Park, H.J., Maier, S., Kikinis, R., Jolesz, F.A., Shenton, M.E., 2007. A review of diffusion tensor imaging studies in schizophrenia. *Journal of psychiatric research* 41, 15-30.
- Laird, A.R., Eickhoff, S.B., Li, K., Robin, D.A., Glahn, D.C., Fox, P.T., 2009. Investigating the functional heterogeneity of the default mode network using coordinate-based meta-analytic modeling. *J Neurosci* 29, 14496-14505.
- Lee, K., Yoshida, T., Kubicki, M., Bouix, S., Westin, C.F., Kindlmann, G., Niznikiewicz, M., Cohen, A., McCarley, R.W., Shenton, M.E., 2009. Increased diffusivity in superior temporal gyrus in patients with schizophrenia: a Diffusion Tensor Imaging study. *Schizophrenia research* 108, 33-40.
- Lenoski, B., Baxter, L.C., Karam, L.J., Maisog, J., Debbins, J., 2008. On the Performance of Autocorrelation Estimation Algorithms for fMRI Analysis. *Ieee Journal of Selected Topics in Signal Processing* 2, 828-838.
- Levenberg, K., 1944. A method for the solution of certain problems in least squares. *Quart. Appl. Math.* 2, 164-168.
- Li, Y.O., Adali, T., Calhoun, V.D., 2007. Estimating the number of independent components for functional magnetic resonance imaging data. *Hum Brain Mapp* 28, 1251-1266.
- Liang, M., Zhou, Y., Jiang, T., Liu, Z., Tian, L., Liu, H., Hao, Y., 2006. Widespread functional disconnectivity in schizophrenia with resting-state functional magnetic resonance imaging. *Neuroreport* 17, 209-213.
- Lowe, M.J., Mock, B.J., Sorenson, J.A., 1998. Functional connectivity in single and multislice echoplanar imaging using resting-state fluctuations. *Neuroimage* 7, 119-132.
- Lui, S., Li, T., Deng, W., Jiang, L., Wu, Q., Tang, H., Yue, Q., Huang, X., Chan, R.C., Collier, D.A., Meda, S.A., Pearlson, G., Mechelli, A., Sweeney, J.A., Gong, Q., 2010. Short-term effects of antipsychotic treatment on cerebral function in drug-naive first-episode schizophrenia revealed by "resting state" functional magnetic resonance imaging. *Archives of general psychiatry* 67, 783-792.
- Lund, T.E., Madsen, K.H., Sidaros, K., Luo, W.L., Nichols, T.E., 2006. Non-white noise in fMRI: does modelling have an impact? *Neuroimage* 29, 54-66.
- McGlashan, T.H., 1998. Early detection and intervention of schizophrenia: rationale and research. *The British journal of psychiatry. Supplement* 172, 3-6.
- McKeown, M.J., Makeig, S., Brown, G.G., Jung, T.P., Kindermann, S.S., Bell, A.J., Sejnowski, T.J., 1998. Analysis of fMRI data by blind separation into independent spatial components. *Hum Brain Mapp* 6, 160-188.
- Meda, S.A., Gill, A., Stevens, M.C., Lorenzoni, R.P., Glahn, D.C., Calhoun, V.D., Sweeney, J.A., Tamminga, C.A., Keshavan, M.S., Thaker, G., Pearlson, G.D., 2012. Differences in resting-state functional magnetic resonance imaging functional network connectivity between schizophrenia and psychotic bipolar

- probands and their unaffected first-degree relatives. *Biological psychiatry* 71, 881-889.
- Melgani, F., Bruzzone, L., 2004. Classification of hyperspectral remote sensing images with support vector machines. *Ieee Transactions on Geoscience and Remote Sensing* 42, 1778-1790.
- Meyer-Lindenberg, A.S., Olsen, R.K., Kohn, P.D., Brown, T., Egan, M.F., Weinberger, D.R., Berman, K.F., 2005a. Regionally specific disturbance of dorsolateral prefrontal-hippocampal functional connectivity in schizophrenia. *Archives of general psychiatry* 62, 379-386.
- Meyer-Lindenberg, A.S., Olsen, R.K., Kohn, P.D., Brown, T., Egan, M.F., Weinberger, D.R., Berman, K.F., 2005b. Regionally specific disturbance of dorsolateral prefrontal-hippocampal functional connectivity in schizophrenia. *Archives of general psychiatry* 62, 379-386.
- Michael, A.M., Calhoun, V.D., Andreasen, N.C., Baum, S.A., 2008. A method to classify schizophrenia using inter-task spatial correlations of functional brain images. *Conf Proc IEEE Eng Med Biol Soc* 2008, 5510-5513.
- Mikula, S., Niebur, E., 2006. A novel method for visualizing functional connectivity using principal component analysis. *International Journal of Neuroscience* 116, 419-+.
- Mingoia, G., Wagner, G., Langbein, K., Maitra, R., Smesny, S., Dietzek, M., Burmeister, H.P., Reichenbach, J.R., Schlosser, R.G., Gaser, C., Sauer, H., Nenadic, I., 2012. Default mode network activity in schizophrenia studied at resting state using probabilistic ICA. *Schizophrenia research* 138, 143-149.
- Monti, M.M., 2011. Statistical Analysis of fMRI Time-Series: A Critical Review of the GLM Approach. *Front Hum Neurosci* 5, 28.
- Morgan, V.L., Price, R.R., 2004. The effect of sensorimotor activation on functional connectivity mapping with MRI. *Magn Reson Imaging* 22, 1069-1075.
- Muller, J.L., Deuticke, C., Putzhammer, A., Roder, C.H., Hajak, G., Winkler, J., 2003. Schizophrenia and Parkinson's disease lead to equal motor-related changes in cortical and subcortical brain activation: an fMRI fingertapping study. *Psychiatry and clinical neurosciences* 57, 562-568.
- Nakamura, K., Kawasaki, Y., Suzuki, M., Hagino, H., Kurokawa, K., Takahashi, T., Niu, L., Matsui, M., Seto, H., Kurachi, M., 2004. Multiple structural brain measures obtained by three-dimensional magnetic resonance imaging to distinguish between schizophrenia patients and normal subjects. *Schizophr Bull* 30, 393-404.
- Narr, K.L., Hageman, N., Woods, R.P., Hamilton, L.S., Clark, K., Phillips, O., Shattuck, D.W., Asarnow, R.F., Toga, A.W., Nuechterlein, K.H., 2009. Mean diffusivity: a biomarker for CSF-related disease and genetic liability effects in schizophrenia. *Psychiatry research* 171, 20-32.
- Nir, Y., Hasson, U., Levy, I., Yeshurun, Y., Malach, R., 2006. Widespread functional connectivity and fMRI fluctuations in human visual cortex in the absence of visual stimulation. *Neuroimage* 30, 1313-1324.
- Ogawa, S., Lee, T.M., Kay, A.R., Tank, D.W., 1990. Brain magnetic resonance imaging with contrast dependent on blood oxygenation. *Proc Natl Acad Sci U S A* 87, 9868-9872.

- Omori, M., Koshino, Y., Murata, T., Murata, I., Nishio, M., Sakamoto, K., Horie, T., Isaki, K., 1995. Quantitative EEG in never-treated schizophrenic patients. *Biological psychiatry* 38, 305-309.
- Orliac, F., Naveau, M., Joliot, M., Delcroix, N., Razafimandimby, A., Brazo, P., Dollfus, S., Delamillieure, P., 2013. Links among resting-state default-mode network, salience network, and symptomatology in schizophrenia. *Schizophrenia research*.
- Pardo, P.J., Georgopoulos, A.P., Kenny, J.T., Stuve, T.A., Findling, R.L., Schulz, S.C., 2006. Classification of adolescent psychotic disorders using linear discriminant analysis. *Schizophrenia research* 87, 297-306.
- Pearlson, G., 2009. Multisite collaborations and large databases in psychiatric neuroimaging: advantages, problems, and challenges. *Schizophrenia bulletin* 35, 1-2.
- Pearlson, G.D., Calhoun, V.D., 2009. Convergent approaches for defining functional imaging endophenotypes in schizophrenia. *Frontiers in human neuroscience* 3, 37.
- Purdon, P.L., Weisskoff, R.M., 1998. Effect of temporal autocorrelation due to physiological noise and stimulus paradigm on voxel-level false-positive rates in fMRI. *Hum Brain Mapp* 6, 239-249.
- Quinlan, J.R., 1987. Simplifying Decision Trees. *International Journal of Man-Machine Studies* 27, 221-234.
- Quinlan, J.R., 1993. *C4.5 : programs for machine learning*. Morgan Kaufmann Publishers, San Mateo, Calif.
- Raichle, M.E., MacLeod, A.M., Snyder, A.Z., Powers, W.J., Gusnard, D.A., Shulman, G.L., 2001. A default mode of brain function. *Proc Natl Acad Sci U S A* 98, 676-682.
- Raichle, M.E., Snyder, A.Z., 2007. A default mode of brain function: a brief history of an evolving idea. *Neuroimage* 37, 1083-1090; discussion 1097-1089.
- Rajapakse, J.C., Kruggel, F., Maisog, J.M., von Cramon, D.Y., 1998. Modeling hemodynamic response for analysis of functional MRI time-series. *Hum Brain Mapp* 6, 283-300.
- Rice, D.P., 1999. The economic impact of schizophrenia. *The Journal of clinical psychiatry* 60 Suppl 1, 4-6; discussion 28-30.
- Rish, I., 2001. An Empirical Study of the Naive Bayes Classifier. *IJCAI-01 Workshop on Empirical Methods in AI*.
- Rogowska, J., Gruber, S.A., Yurgelun-Todd, D.A., 2004. Functional magnetic resonance imaging in schizophrenia: cortical response to motor stimulation. *Psychiatry research* 130, 227-243.
- Rosenblatt, F., 1958. The Perceptron - a Probabilistic Model for Information-Storage and Organization in the Brain. *Psychological Review* 65, 386-408.
- Rubia, K., Russell, T., Bullmore, E.T., Soni, W., Brammer, M.J., Simmons, A., Taylor, E., Andrew, C., Giampietro, V., Sharma, T., 2001. An fMRI study of reduced left prefrontal activation in schizophrenia during normal inhibitory function. *Schizophrenia research* 52, 47-55.
- Salvador, R., Sarro, S., Gomar, J.J., Ortiz-Gil, J., Vila, F., Capdevila, A., Bullmore, E., McKenna, P.J., Pomarol-Clotet, E., 2010. Overall brain connectivity maps show cortico-subcortical abnormalities in schizophrenia. *Hum Brain Mapp* 31, 2003-2014.

- Salvador, R., Suckling, J., Coleman, M.R., Pickard, J.D., Menon, D., Bullmore, E., 2005. Neurophysiological architecture of functional magnetic resonance images of human brain. *Cerebral cortex* 15, 1332-1342.
- Seewald, A.K., 2007. An evaluation of Naive Bayes variants in content-based learning for spam filtering. *Intelligent Data Analysis* 11, 497-524.
- Shehzad, Z., Kelly, A.M., Reiss, P.T., Gee, D.G., Gotimer, K., Uddin, L.Q., Lee, S.H., Margulies, D.S., Roy, A.K., Biswal, B.B., Petkova, E., Castellanos, F.X., Milham, M.P., 2009. The resting brain: unconstrained yet reliable. *Cereb Cortex* 19, 2209-2229.
- Shen, H., Wang, L., Liu, Y., Hu, D., 2010. Discriminative analysis of resting-state functional connectivity patterns of schizophrenia using low dimensional embedding of fMRI. *Neuroimage* 49, 3110-3121.
- Shenton, M.E., Dickey, C.C., Frumin, M., McCarley, R.W., 2001. A review of MRI findings in schizophrenia. *Schizophrenia research* 49, 1-52.
- Shirer, W.R., Ryali, S., Rykhlevskaia, E., Menon, V., Greicius, M.D., 2012. Decoding subject-driven cognitive states with whole-brain connectivity patterns. *Cereb Cortex* 22, 158-165.
- Smith, S.M., 2004. Overview of fMRI analysis. *Br J Radiol* 77 Spec No 2, S167-175.
- Smith, S.M., Fox, P.T., Miller, K.L., Glahn, D.C., Fox, P.M., Mackay, C.E., Filippini, N., Watkins, K.E., Toro, R., Laird, A.R., Beckmann, C.F., 2009a. Correspondence of the brain's functional architecture during activation and rest. *Proc Natl Acad Sci U S A* 106, 13040-13045.
- Smith, S.M., Fox, P.T., Miller, K.L., Glahn, D.C., Fox, P.M., Mackay, C.E., Filippini, N., Watkins, K.E., Toro, R., Laird, A.R., Beckmann, C.F., 2009b. Correspondence of the brain's functional architecture during activation and rest. *Proceedings of the National Academy of Sciences of the United States of America* 106, 13040-13045.
- Stein, T., Moritz, C., Quigley, M., Cordes, D., Haughton, V., Meyerand, E., 2000. Functional connectivity in the thalamus and hippocampus studied with functional MR imaging. *AJNR Am J Neuroradiol* 21, 1397-1401.
- Stevens, M.C., Kiehl, K.A., Pearlson, G.D., Calhoun, V.D., 2007. Functional neural networks underlying response inhibition in adolescents and adults. *Behav Brain Res* 181, 12-22.
- Stevens, M.C., Kiehl, K.A., Pearlson, G.D., Calhoun, V.D., 2009. Brain network dynamics during error commission. *Hum Brain Mapp* 30, 24-37.
- Sui, J., He, H., Yu, Q., Chen, J., Rogers, J., Pearlson, G.D., Mayer, A., Bustillo, J., Canive, J., Calhoun, V.D., 2013. Combination of Resting State fMRI, DTI, and sMRI Data to Discriminate Schizophrenia by N-way MCCA + jICA. *Front Hum Neurosci* 7, 235.
- Sui, J., Pearlson, G., Caprihan, A., Adali, T., Kiehl, K.A., Liu, J., Yamamoto, J., Calhoun, V.D., 2011. Discriminating schizophrenia and bipolar disorder by fusing fMRI and DTI in a multimodal CCA+ joint ICA model. *Neuroimage* 57, 839-855.
- Sun, D., van Erp, T.G., Thompson, P.M., Bearden, C.E., Daley, M., Kushan, L., Hardt, M.E., Nuechterlein, K.H., Toga, A.W., Cannon, T.D., 2009. Elucidating a magnetic resonance imaging-based neuroanatomic biomarker for psychosis:

- classification analysis using probabilistic brain atlas and machine learning algorithms. *Biological psychiatry* 66, 1055-1060.
- Sun, F.T., Miller, L.M., D'Esposito, M., 2004. Measuring interregional functional connectivity using coherence and partial coherence analyses of fMRI data. *Neuroimage* 21, 647-658.
- Szeszko, P.R., Robinson, D.G., Ashtari, M., Vogel, J., Betensky, J., Sevy, S., Ardekani, B.A., Lencz, T., Malhotra, A.K., McCormack, J., Miller, R., Lim, K.O., Gunduz-Bruce, H., Kane, J.M., Bilder, R.M., 2008. Clinical and neuropsychological correlates of white matter abnormalities in recent onset schizophrenia. *Neuropsychopharmacology : official publication of the American College of Neuropsychopharmacology* 33, 976-984.
- Takahashi, H., Koeda, M., Oda, K., Matsuda, T., Matsushima, E., Matsuura, M., Asai, K., Okubo, Y., 2004. An fMRI study of differential neural response to affective pictures in schizophrenia. *Neuroimage* 22, 1247-1254.
- Takayanagi, Y., Kawasaki, Y., Nakamura, K., Takahashi, T., Orikabe, L., Toyoda, E., Mozue, Y., Sato, Y., Itokawa, M., Yamasue, H., Kasai, K., Kurachi, M., Okazaki, Y., Matsushita, M., Suzuki, M., 2010. Differentiation of first-episode schizophrenia patients from healthy controls using ROI-based multiple structural brain variables. *Progress in neuro-psychopharmacology & biological psychiatry* 34, 10-17.
- Takayanagi, Y., Takahashi, T., Orikabe, L., Mozue, Y., Kawasaki, Y., Nakamura, K., Sato, Y., Itokawa, M., Yamasue, H., Kasai, K., Kurachi, M., Okazaki, Y., Suzuki, M., 2011. Classification of first-episode schizophrenia patients and healthy subjects by automated MRI measures of regional brain volume and cortical thickness. *PloS one* 6, e21047.
- Thomas, C.G., Harshman, R.A., Menon, R.S., 2002. Noise reduction in BOLD-based fMRI using component analysis. *NeuroImage* 17, 1521-1537.
- Tononi, G., Edelman, G.M., 1998. Consciousness and complexity. *Science* 282, 1846-1851.
- Tononi, G., Edelman, G.M., Sporns, O., 1998. Complexity and coherency: integrating information in the brain. *Trends Cogn Sci* 2, 474-484.
- Tregellas, J.R., Davalos, D.B., Rojas, D.C., Waldo, M.C., Gibson, L., Wylie, K., Du, Y.P., Freedman, R., 2007. Increased hemodynamic response in the hippocampus, thalamus and prefrontal cortex during abnormal sensory gating in schizophrenia. *Schizophrenia research* 92, 262-272.
- Treisman, A., 1996. The binding problem. *Curr Opin Neurobiol* 6, 171-178.
- Turner, G.H., Twieg, D.B., 2005. Study of temporal stationarity and spatial consistency of fMRI noise using independent component analysis. *IEEE transactions on medical imaging* 24, 712-718.
- van de Ven, V.G., Formisano, E., Prvulovic, D., Roeder, C.H., Linden, D.E., 2004. Functional connectivity as revealed by spatial independent component analysis of fMRI measurements during rest. *Hum Brain Mapp* 22, 165-178.
- Van Dijk, K.R., Hedden, T., Venkataraman, A., Evans, K.C., Lazar, S.W., Buckner, R.L., 2010. Intrinsic functional connectivity as a tool for human connectomics: theory, properties, and optimization. *J Neurophysiol* 103, 297-321.



- Venkataraman, A., Whitford, T.J., Westin, C.F., Golland, P., Kubicki, M., 2012. Whole brain resting state functional connectivity abnormalities in schizophrenia. *Schizophr Res* 139, 7-12.
- Vincent, J.L., Patel, G.H., Fox, M.D., Snyder, A.Z., Baker, J.T., Van Essen, D.C., Zempel, J.M., Snyder, L.H., Corbetta, M., Raichle, M.E., 2007. Intrinsic functional architecture in the anaesthetized monkey brain. *Nature* 447, 83-86.
- Wang, J., Zuo, X., He, Y., 2010. Graph-based network analysis of resting-state functional MRI. *Front Syst Neurosci* 4, 16.
- Wang, K., Liang, M., Wang, L., Tian, L., Zhang, X., Li, K., Jiang, T., 2007. Altered functional connectivity in early Alzheimer's disease: a resting-state fMRI study. *Hum Brain Mapp* 28, 967-978.
- Wenz, F., Schad, L.R., Knopp, M.V., Baudendistel, K.T., Flomer, F., Schroder, J., van Kaick, G., 1994. Functional magnetic resonance imaging at 1.5 T: activation pattern in schizophrenic patients receiving neuroleptic medication. *Magnetic resonance imaging* 12, 975-982.
- Werbos, P.J., 1990. Backpropagation through Time - What It Does and How to Do It. *Proceedings of the Ieee* 78, 1550-1560.
- Williams, R.W., Herrup, K., 1988. The control of neuron number. *Annual review of neuroscience* 11, 423-453.
- Wilson, E.B., 1927. Probable inference, the law of succession, and statistical inference. *Journal of the American Statistical Association* 22, 209-212.
- Wood, I.A., Visscher, P.M., Mengersen, K.L., 2007. Classification based upon gene expression data: bias and precision of error rates. *Bioinformatics* 23, 1363-1370.
- Woolrich, M.W., Ripley, B.D., Brady, M., Smith, S.M., 2001. Temporal autocorrelation in univariate linear modeling of FMRI data. *Neuroimage* 14, 1370-1386.
- Worsley, K.J., Liao, C.H., Aston, J., Petre, V., Duncan, G.H., Morales, F., Evans, A.C., 2002. A general statistical analysis for fMRI data. *Neuroimage* 15, 1-15.
- Wyatt, R.J., Henter, I., Leary, M.C., Taylor, E., 1995. An economic evaluation of schizophrenia--1991. *Social psychiatry and psychiatric epidemiology* 30, 196-205.
- Xiong, J., Parsons, L.M., Gao, J.H., Fox, P.T., 1999. Interregional connectivity to primary motor cortex revealed using MRI resting state images. *Human brain mapping* 8, 151-156.
- Yang, H., Liu, J., Sui, J., Pearlson, G., Calhoun, V.D., 2010. A Hybrid Machine Learning Method for Fusing fMRI and Genetic Data: Combining both Improves Classification of Schizophrenia. *Frontiers in human neuroscience* 4, 192.
- Ylipavalniemi, J., Vigario, R., 2008. Analyzing consistency of independent components: An fMRI illustration. *Neuroimage* 39, 169-180.
- Yoon, U., Lee, J.M., Im, K., Shin, Y.W., Cho, B.H., Kim, I.Y., Kwon, J.S., Kim, S.I., 2007. Pattern classification using principal components of cortical thickness and its discriminative pattern in schizophrenia. *Neuroimage* 34, 1405-1415.
- Young, K.A., Manaye, K.F., Liang, C., Hicks, P.B., German, D.C., 2000. Reduced number of mediodorsal and anterior thalamic neurons in schizophrenia. *Biological psychiatry* 47, 944-953.

- Yu, Q., Allen, E.A., Sui, J., Arbabshirani, M.R., Pearlson, G., Calhoun, V.D., 2012. Brain connectivity networks in schizophrenia underlying resting state functional magnetic resonance imaging. *Curr Top Med Chem* 12, 2415-2425.
- Zarahn, E., Aguirre, G.K., D'Esposito, M., 1997. Empirical analyses of BOLD fMRI statistics. I. Spatially unsmoothed data collected under null-hypothesis conditions. *Neuroimage* 5, 179-197.
- Zeki, S., 1990. Parallelism and functional specialization in human visual cortex. *Cold Spring Harb Symp Quant Biol* 55, 651-661.
- Zeki, S., Watson, J.D., Lueck, C.J., Friston, K.J., Kennard, C., Frackowiak, R.S., 1991. A direct demonstration of functional specialization in human visual cortex. *J Neurosci* 11, 641-649.
- Zhong, Y., Wang, H., Lu, G., Zhang, Z., Jiao, Q., Liu, Y., 2009. Detecting functional connectivity in fMRI using PCA and regression analysis. *Brain Topogr* 22, 134-144.
- Zhou, Y., Liang, M., Jiang, T., Tian, L., Liu, Y., Liu, Z., Liu, H., Kuang, F., 2007. Functional dysconnectivity of the dorsolateral prefrontal cortex in first-episode schizophrenia using resting-state fMRI. *Neurosci Lett* 417, 297-302.
- Zuo, X.N., Di Martino, A., Kelly, C., Shehzad, Z.E., Gee, D.G., Klein, D.F., Castellanos, F.X., Biswal, B.B., Milham, M.P., 2010. The oscillating brain: complex and reliable. *Neuroimage* 49, 1432-1445.